SURFACE STUDIES ON THE STRUCTURE AND FUNCTIONALITY OF BIOACTIVE MATERIALS

by

Yuwei Liu

A dissertation submitted in partial fulfillment
of the requirements for the degree of
Doctor of Philosophy
(Chemistry)
in the University of Michigan
2014

Doctoral Committee:

Professor Zhan Chen, Chair
Associate Professor Kenichi Kuroda
Professor E. Neil G. Marsh
Associate Professor Anne J. McNeil

I would like to dedicate my thesis to my beloved parents, my husband for their love and support, and to my daughter because Mommy loves you

ACKNOWLEDGEMENTS

I would never have been able to finish my dissertation without the guidance of my research advisor and my committee members, help from friends, and support from my family and husband, to only some of whom it is possible to give particular mention here.

I would like to express my sincere gratitude to my advisor, Professor Zhan Chen, for his excellent guidance, motivation, patience, and providing me with an excellent atmosphere for doing research. His guidance has helped me through my entire PhD life from the difficult days when I first came to the study abroad to the writing of this thesis. I have had many opportunities presented to me because of my participation in Professor Chen's lab, including authorship of scholarly articles and reviews, travel for conferences, teaching opportunities, and a multitude of other experiences.

I would like to thank Professor Marsh, Professor McNeil and Professor Kuroda for serving on my thesis committee and for providing beneficial feedback and suggestions for my research. I would specially thank Professor Marsh for his willingness to participate in my final data meeting and defense at the last moment and to commit time and resources and to provide insightful advice to some of the work presented in this dissertation.

None of these chapters would have been possible without the many collaborators I have had the privilege of working with. I would like to acknowledge Dr. Bret Chisholm, Dr. Shane Stafslien and Dr. Partha Majumdar from North Dakota State University for their contribution in Chapter 2. Dr. Charlene Mello from US Army Natick Soldier

Research, Development, and Engineering Center, Dr. Chuanwu Xi and Dr. Jianfeng Wu from School of Public Health were collaborators for the work presented in Chapter 3. Dr. Neil Marsh and his students Tadeusz Ogorzalek collaborated with me in the work presented in Chapter 4. Dr. Shuai Wei from Dr. Charles Brooks' Lab collaborated with me for all the MD simulation studies. Dr. Xiaopei Deng and Kenneth Cheng from Dr. Joerg Lahann's lab provided all the CVD polymer samples.

My labmates in the Chen Lab are a valuable asset in my graduate career. It would have been a lonely lab without the support and friendship from everyone in the lab. The stimulating discussions, the great work we have accomplished and fun time we have had together fulfill my PhD life. I take this opportunity to specially thank Dr. Xiaofeng Han for introducing me to the background and techniques used in the lab and for building some of the fundamental knowledge of this dissertation.

I would like to acknowledge the financial support from the Office of Naval Research for Chapter 2, Multidisciplinary University Research Initiative (MURI) for Chapter 3, and MURI as well as Defense Threat Reduction Agency (DTRA) for Chapter 4. I thank the Chemistry Department and the Rackham School for providing fellowship opportunities. I am also deeply grateful to have been working with all the extraordinary scientists and engineers in the MURI group.

In the grand scheme of my training as a scientist, graduate school was the culmination of a long process, and I would never have come to this point without those people who set me on this path. I am grateful to my undergraduate advisors Professor Hanying Zhao and Professor Li Liu for enlightening me the first glance of research.

I could never have made it through this experience without the support of my friends. Being pregnant in the last year of graduate school was stressful at the very beginning; but thanks to a support group for Chinese expecting mothers in the US initiated by Jing Fan, I was able to get through the difficult times both before and after giving birth by accompanying and sharing with each other.

Finally, I would like to thank my family. My parents, Jinming Liu and Aying Xiangli and my mother-in-law Weimin Zhao, were always supporting me most generously and encouraging me with their best wishes throughout my life. Last but not least, I want to thank my husband Qia Yang who has always been there cheering me up and standing by me celebrating me at my best and supporting me at my worst.

Section 1.2 was partially adapted from work published by the American Chemical Society (*Langmuir*, **2012**, *28*, 2113–2121) who holds the copyright thereto. Chapter 2 was adapted from work published by the American Chemical Society (*Langmuir*, **2013**, *29*, 2897−2905) who will hold the copyright thereto upon final publication therein. Section 3.4 was partially adapted from work published by the American Chemical Society (*J. Phys. Chem. B*, **2014**, *118*, 2904−2912) who holds the copyright thereto. Chapter 4 was partially adapted from work published by the American Chemical Society (*J. Am. Chem. Soc.*, **2013**, *135*, 12660−12669) who will hold the copyright thereto upon final publication.

TABLE OF CONTENTS

DEDICATION……..……..ii

ACKNOWLEDGEMENTS iii

LIST OF FIGURES..... viii

LIST OF TABLES..... xiii

ABSTRACT xiv

CHAPTER 1 INTRODUCTION..... 1

1.1 BIOACTIVE MATERIALS..... 1

1.2 THE IMPORTANCE OF SURFACE/INTERFACE ANALYSIS..... 2

1.3 SUM FREQUENCY GENERATION VIBRATIONAL SPECTROSCOPY 3

1.3.1 Overview 3

1.3.2 Basic Theory..... 5

1.3.3 Experimental System..... 9

1.3.4 Experimental Setup 13

1.4 OBJECTIVES AND PRESENTED RESEARCH 15

1.5 REFERENCES..... 18

CHAPTER 2 ANTIBIOFOULING MECHANISM STUDIES ON PDMS INCORPORATED WITH QAS MOLECULES 22

2.1 INTRODUCTION..... 22

2.2 EXPERIMENTAL 25

2.2.1 Materials..... 25

2.2.2 Instrumentation..... 28

2.3 RESULTS AND DISCUSSION..... 29

2.3.1 QAS-tethered PDMS coatings..... 29

2.3.2 Q-POSS incorporated PDMS coatings..... 34

2.4 CONCLUSION 40

2.5 REFERENCES..... 42

CHAPTER 3 ANTIMICROBIAL SURFACE STUDIES—ANTIMICROBIAL PEPTIDE (AMP) IMMOBILIZATION TO DIFFERENT SURFACES 46

3.1 INTRODUCTION..... 46

3.2 EXPERIMENTAL 49

3.2.1 Materials and Sample Preparation 49
3.2.2 Instrumentation and Experimental Setup 52
3.3 RESULTS AND DISCUSSION 53
3.3.1 Immobilization Of AMP to Maleimide Functionalized Polystyrene (PS-MA) Surface 53
3.3.2 Immobilization of CP1 to SAM Surfaces 63
3.3.3 Immobilization of CP1 to Polymer Prepared by Chemical Vapor Deposition (CVD) Polymer 70
3.4 SUMMARY 75
3.5 REFERENCES 77
CHAPTER 4 ENZYME IMMOBILIZATION THROUGH DIFFERENT ATTACHMENT SITES 81
4.1 INTRODUCTION 81
4.2 EXPERIMENTAL 83
4.2.1 Materials and Methods 83
4.2.2 Synthesis of Model Enzymes with Cysteine at Selected Sites 83
4.2.3 Functionalization of Substrates 84
4.2.4 Instrumentation and Setup 85
4.3 RESULTS AND DISCUSSION 88
4.3.1 Molecular Orientation of Enzymes Attached to Surfaces through Defined Chemical Linkages 88
4.3.2 SFG and ATR-FTIR experiments and data analysis for β-Gal on Mal-EG4 SAM 89
4.3.3 Activity of Surface-immobilized β-Gal 100
4.3.4 Variation of Immobilization Sites on Enzyme Structure and Orientation 102
4.4 SUMMARY 108
4.5 REFERENCES 110
CHAPTER 5 CONCLUSIONS AND OUTLOOK 115

LIST OF FIGURES

Figure 1.1 The SFG process. 4

Figure 1.2 Energy level diagram of the SFG process. 5

Figure 1.3 Layout of the EKSPLA SFG laser spectrometer.[65] 10

Figure 1.4 The SFG sample experimental geometry. Left: window face-down geometry; Right: prism geometry (can be used for the near total reflection geometry). 15

Figure 2.1 Chemical structures of the QAS incorporated PDMS systems (A: QAS-tethered system; B: Q-POSS-incorporated PDMS system) 27

Figure 2.2 SFG experimental face-down sample geometry 29

Figure 2.3 SFG ssp spectra collected from QAS-tethered PDMS systems in (a) air, (b) water, and (c) ASW. The four samples studied are: (A) 49K-PDMS, C18-TMS; (B) 49K-PDMS, C18-TES; (C) 18K-PDMS, C18-TMS; (D) 18K-PDMS, C18-TES. 33

Figure 2.4 Illustration showing the surface structures of QAS-tethered PDMS system in aqueous environment. Different head groups of QAS lead to different alkyl chain ordering of the system. 34

Figure 2.5 SFG ssp spectra collected from Q-POSS-incorporated PDMS materials in (a) air, (b) water, and (c) ASW. The four samples are (E) R=$C_{16}H_{33}$-, high extent of quaternization; (F) R=$C_{16}H_{33}$-, low extent of quaternization; (G) R=$C_{18}H_{37}$-, high extent of quaternization; (H) R=$C_{18}H_{37}$-, low extent of quaternization. 39

Figure 2.6 Schematic showing the surface structures of Q-POSS-incorporated PDMS systems in aqueous environment. Different extents of quaternization result in different mobility of the alkyl chains. 40

Figure 3.1 Molecular formula of PS-MA. 50

Figure 3.2 Molecular formula of maleimide-EG4-silane 50

Figure 3.3 Molecular formula of PPX-dibromomaleimide. 52

Figure 3.4 Schematics showing SFG experimental setup for immobilized peptides on surfaces 53

Figure 3.5 SFG time-dependent signal collected at 1650 cm^{-1} for CA-ME (left) and SMAP (right) when contacting PS-MA surfaces in different solvent composition (Black: 100% PB; Red: 25% TFE in PB; Blue: 50% TFE in PB; Pink: 75% TFE in PB) 54

Figure 3.6 SFG ssp (red, filled squares) and ppp (blue, open squares) spectra collected from the immobilized CA-ME at the PS-MA/solution interface with different solvent compositions. Squares: experimental data; lines: fitting results. .. 56

Figure 3.7 SFG ssp (red, filled squares) and ppp (blue, open squares) spectra collected from the immobilized SMAP at the PS-MA/solution interface with different solvent compositions. Squares: experimental data; lines: fitting results. .. 57

Figure 3.8 Relations between the SFG susceptibility tensor component ratio χ_{ppp}/χ_{ssp} and the orientation angle for CA-ME (left) and SMAP (right) assuming a delta orientation distribution. The colored plots showed the deduced orientations for AMPs immobilized in different solvent compositions (Black: 100% PB; Red: 25% TFE in PB; Blue: 50% TFE in PB; Pink: 75% TFE in PB) 58

Figure 3.9 Time-dependent SFG signal at 1650 cm^{-1} collected from CA-ME (left) and SMAP (right) at the PS-MA/solution (with different peptide concentrations) interface. A: in PB without TFE; B: in PB with 50% TFE. 59

Figure 3.10 (a) SFG spectra of the Mal-EG4/CP1c PB interface. (b) SFG spectra of the Mal-EG4 SAM immobilized with CP1c in contact with a PB solution after PB wash. 65

Figure 3.11 (a) SFG spectra of the Mal-EG4/PB solution interface (solid circle) and the Mal-EG4 SAM/cCP1 PB solution interface (open circle) (b) SFG spectrum of Mal-EG4 SAM immobilized with cCP1 in contact with a PB solution after PB wash. (c) SFG spectra of Mal-EG4 SAM immobilized with cCP1 in contact with a TFE-PB 50%−50% mixture solution (ppp and ssp). (d) Schematic of cCP1 conformation change at different interface conditions: contacting with PB or TFE-PB solution. . 67

Figure 3.12 Representative fluorescence micrographs showing comparison of Mal-EG4 immobilized with (a) CP1c and (b) cCP1 after soaking in 10^5 CFU/mL *E. coli* containing 50 mM GSH for 18 h at 37.5 ℃. Bacterial cells were stained with Bacterial LIVE/DEAD staining dyes, and viable cells show green while dead or membrane damaged cells show red fluorescence in the images. Images shown in the left column contain a composite image of both alive and dead cells, whereas the right images contain only the dead cells from the corresponding images on the left. Scale bar represents 20 μm in length and applies to all images. 69

Figure 3.13 SFG time-dependent signal collected from CP1c immobilized at the PPX-dibromomaleimide/CP1c PB solution interface. A. after the addition of CP1c to the PB buffer; B. after washing the CP1c-immobilized surface with PB; C. after the addition of excessive amount of TCEP to PB; D: after final washing of the surface. 72

Figure 3.14 SFG ssp and ppp spectra collected from PPX-dibromomaleimide/PB interfaces with immobilization of A. CP1c; B. cCP1 and C. Stable cCP1. 75

Figure 4.1 A: Molecular formulas for Mal-EG4 and OTS. B: SFG experimental geometry used in this study. This is a near-total-reflection geometry. The sample surface is in contact with a reservoir of buffer solution containing enzyme molecules. C: Crystal structure of β-Gal-V152C. The cysteine group can bind to the maleimide group on Mal-EG4 SAM to immobilize β-Gal to the surface. The binding site is opposite to the enzyme active site. 85

Figure 4.2 SFG ssp spectra collected from the Mal-EG4/PB solution interface before (black, filled squares) and after (red, open squares) introducing "no cysteine" β-Gal to the buffer solution in the amide I (left) and C-H/O-H stretching frequency regions. 89

Figure 4.3 SFG ssp spectra collected from the Mal-EG4 SAM/buffer solution interface before (black, squares) and after (red, circles) the addition of β-Gal-V152C. Strong SFG signal was observed after the addition of β-Gal-V152C, indicating the surface immobilization. SFG signal remains the same (blue, triangles) after washing the interface with buffer, showing that the chemical immobilization occurred. 91

Figure 4.4. A: SFG ssp (red, filled squares) and ppp (blue, open squares) spectra collected from the immobilized β-Gal-V152C at the Mal-EG4 SAM/solution interface. Squares: experimental data; lines: fitting results. B: The orientation of β-Gal with tilt angle = 0, twist angle = 0. The cysteine functionalized site is shown in red. SAM is shown as a blue plane. C: Top: Dependence of the SFG χ_{zzz}/χ_{xxz} ratio on the tilt/twist angles of β-Gal calculated using the newly developed computer package.[56] Bottom: Possible orientation angle regions deduced based on the experimentally measured χ_{zzz}/χ_{xxz} ratio of β-Gal-V152C. Colors indicate the quality of the match (1=exact). 93

Figure 4.5 A: ATR–FTIR spectra collected from the immobilized β-Gal-V152C at the Mal-EG4 SAM/solution interface using p (blue, open squares) and s (red, filled squares) polarizations. Squares: experimental data; lines: fitting results. B: Dependence of the ATR–FTIR dichroic ratio R^{ATR} on the tilt/twist angles of β-Gal

calculated using the newly developed computer package.[56] Right: Possible orientation angle regions deduced based on the experimentally measured R^{ATR} ratio of β-Gal-V152C. Colors indicate the quality of the match (1=exact). 95

Figure 4.6 Possible orientation angle regions deduced based on both the SFG and ATR – FTIR measurements. Colors indicate the quality of the match (100%=exact). The right figure plotted the possible orientation angles with probability ⩾ 90% in red. 97

Figure 4.7 Possible orientations of immobilized β-Gal shown in format of (tilt angle, twist angle). The most likely orientations are a. (14°, 75°) and b. (25°, 130°) because they are well correlated to the designed orientations. 97

Figure 4.8 Top: SFG spectra collected from the OTS SAM/buffer solution before (black) and after (red) the addition of β-Gal-V152C to the buffer. After washing, SFG signal (blue) decreased, showing some loosely adsorbed enzyme molecules were washed off. Bottom: ssp (red, filled squares) and ppp (blue, open squares) SFG spectra collected from the OTS SAM/buffer solution after the addition of β-Gal-V152C to the buffer. Squares: experimental data; lines: fitting results. 99

Figure 4.9 Activity of the β-Gal free in solution (blue), covalently tethered to the EG4-Mal SAM via the single engineered cysteine at position 153 (red), and physically adsorbed to the hydrophobic OTS SAM (green). In each case, 10 pmol of β-Gal-V152C was added to 1 mL of solution..... 101

Figure 4.10 Left: SFG ssp (red, filled squares) and ppp (blue, open squares) spectra collected from the immobilized β-Gal-E147C at the Mal-EG4 SAM/solution interface. Squares: experimental data; lines: fitting results. Right: Possible orientation angle regions deduced based on the experimentally measured χ_{zzz}/χ_{xxz} ratio of β-Gal-E147C. Colors indicate the quality of the match (1=exact). 103

Figure 4.11 Left: ATR–FTIR spectra collected from the immobilized β-Gal-E147C at the Mal-EG4 SAM/solution interface using p (blue, open squares) and s (red, filled squares) polarizations. Squares: experimental data; lines: fitting results. Right: Possible orientation angle regions deduced based on the experimentally measured R^{ATR} ratio of β-Gal-E152C. Colors indicate the quality of the match (1=exact). ... 104

Figure 4.12 Possible orientation angle regions deduced based on both the SFG and ATR–FTIR measurements for β-Gal-E147C. Colors indicate the quality of the match (100%=exact). The right figure plotted the possible orientation angles with probability ⩾ 90% in red. 105

Figure 4.13 Crystal structure of β-Gal-E147C on the left and β-Gal-E227C on the right 105

Figure 4.14 SFG ssp spectra collected from the Mal-EG4/PB solution interface before (black, filled squares) and after (red, open squares) introducing β-Gal-E227C to the buffer solution in the amide I (left) and C-H/O-H stretching frequency regions. 106

Figure 4.15 Left plot shows the dependence of the SFG χ_{xxz} on the tilt/twist angles of β-Gal calculated using the computer package.[56] Two representative orientations of β-Gal that would generate different SFG intensities are shown on the right. The top enzyme is β-Gal-E227C, the lower enzyme is β-Gal-E147C. 108

Figure 4.16 Red circles show the possible orientations calculated by MD simulation for β-Gal-E227C which is in agreement with our SFG analysis..... 108

LIST OF TABLES

Table 1.1 Summary of wavelengths generated and used in SFG laser setup. 12

Table 2.1 Compositions of the PDMS coatings incorporated with QAS (all values are in grams) 26

Table 2.2 Q-POSS molecules studied (30 wt% in THF) 26

Table 3.1 χ_{ppp}/χ_{ssp} comparisons for immobilized CA-ME in different solvent compositions 62

Table 3.2 χ_{ppp}/χ_{ssp} comparisons for immobilized SMAP in different solvent compositions 62

Table 4.1. SFG fitting parameters 92

Table 4.2. ATR-FTIR fitting parameters 95

ABSTRACT

Surface Studies on the Structure and Functionality of Bioactive Materials

by

Yuwei Liu

Chair: Professor Zhan Chen

Bioactive materials are critical in many applications in the fields ranging from antibiofouling coatings to tissue engineering to biosensing devices because of their ability in inducing and regulating biological activities and functions. The construction of bioactive materials generally involves dispersion of bioactive components such as biocides, peptides or proteins in organic or inorganic matrices. However, when these bioactive components are incorporated to such matrices, their functionalities may be significantly hindered. As a result, it has spurred great attention seeking guidelines for future rational design and development of bioactive materials with optimal functionalities. In this thesis, optimization strategies are proposed by investigating interfacial molecular interactions of various bioactive materials *in situ* using surface specific spectroscopies and correlating the structural and orientational information to their activity tests.

Firstly, two biocide-incorporated antifouling polymeric materials are characterized using sum frequency generations vibrational spectroscopy at solid/liquid interfaces. The interaction mechanism is unraveled by varying both biocidal components and the

polymer components of the system. The structure of the alkyl chains from the biocidal components is determined and by comparing to their antifouling performance, it is concluded that the protruding-out state offers the best antifouling activity. Factors that affect the extension state of the biocidal components are carefully examined. Secondly, antimicrobial peptides (AMPs) are immobilized to various surface platforms. The immobilization processes are thoroughly monitored and the final immobilized peptide structures and orientations are determined using spectroscopic technique. The immobilization environment, the location of the attachment point and the peptide sequence all play important roles in determining the immobilization process and the final state of the immobilized AMPs. Finally, a model enzyme is immobilized to solid surfaces and characterized by using combined spectroscopic measurements. These results are further correlated to the enzymatic activities and confirmed by molecular dynamics simulations performed by our collaborators. It is concluded that the surface properties, the location of the attachment point, the secondary structure of the attachment point are factors influencing the immobilized enzyme structure and further determining the activity and stability of the immobilized enzyme. In all, this thesis provides systematic understanding how structural differences are related to the difference in the functionality of the bioactive materials under study based on which the optimization designing rules are proposed.

CHAPTER 1

INTRODUCTION

1.1 BIOACTIVE MATERIALS

Bioactive materials are designed to induce or regulate biological activities and functions. These materials have been applied extensively in fields ranging from antibiofouling coatings, tissue engineering to biosensing devices.[1-6] The induction and regulation of such materials usually involve incorporation of bioactive components such as peptides and proteins. To tailor the performance of these materials, it is crucial to understand how the bioactive components behave upon interacting with target molecules under biologically-relevant environments. The bioactive components involved in these materials are varied based on specific applications.

When bioactive components are incorporated into material matrices, their functionalities are affected. Some show improved activity while others show reduced activity.[7-10] Effort has been put to rationalize the scenario. It has been demonstrated that the macroscopic topography of materials as well as the microscopic chemistry play important roles in regulating the activity of designed bioactive materials.[11-13] To push forward the development of these materials, it is essential to understand how the bioactive components interact with target molecules and factors that govern the favorable interactions.

In this dissertation, I mainly focus on three types of bioactive components. They are a) quartenary ammonium salts which are used for antibiofouling applications based on

their biocidal property; b) antimicrobial peptide molecules which are membrane active and form α-helical structure when functioning; c) enzyme molecules which are models for large proteins yet whose activity is easier to measure.

1.2 THE IMPORTANCE OF SURFACE/INTERFACE ANALYSIS

The interactions between bioactive components and their target molecules occur at their interfaces upon contact. On the interaction interface of bioactive materials, there are organic or inorganic matrices of the materials, bioactive components that were incorporated to the materials for biofunctionality and biomolecules in contact with the materials. It has been shown that the interfacial properties of these molecules are of great importance in determining the performance of the materials[14-20] and hence forth attention has been applied to interfacial properties in a variety of research fields. [21-23] One of the research aspects is the microscopic structure and orientation of the interfacial molecules which have been proven to regulate the effectiveness of the functions of materials.

A variety of surface sensitive analytical techniques and methodologies have been applied to explore conformation, ordering and orientation behaviors of the interfacial molecules. Examples are ellipsometry and surface plasmon resonance (SPR) which mostly probe the adsorption/desorption behavior of biomolecules on substrate surfaces.[24-26] Secondary ion mass spectrometry (SIMS) and x-ray photoelectron spectroscopy (XPS) have been employed to monitor structural changes of peptides and proteins on surfaces by analyzing the surface species.[27-30] Atomic force microscopy (AFM) is important in investigating protein packing and ordering states.[31, 32] In addition, many techniques focus on using intrinsic vibrational modes of various chemical species to determine compositions and orientations of biomolecules. Using different-polarized incident light,

Attenuated Total Reflectance-Fourier Transform Infrared (ATR-FTIR) spectroscopy can be used to study orientation of interfacial peptide/proteins.[33-36] Surface-enhanced Raman Spectroscopy (SERS) is another useful spectroscopic technique which is exceptionally sensitive and has been used to track structural changes in various biological processes.[37] These experimental tools have the ability to acquire a qualitative and quantitative understanding at the molecular-level of interfacial peptides/proteins and their functions. However, it is still very difficult to probe molecular level structural information of peptides and proteins *in situ* (e.g., at the solid/liquid interface) with a monolayer surface sensitivity. As a result, further investigations of these molecular interactions still require more accurate *in situ* measurements.

1.3 SUM FREQUENCY GENERATION VIBRATIONAL SPECTROSCOPY

Sum frequency generation vibrational spectroscopy (SFG) is a highly useful and unique technique that has emerged as a valuable tool to study surfaces and interfaces *in situ* at the molecular level.[38-52] It combines two other well-known spectroscopic techniques, infrared (IR) and Raman processes to yield a new technique that is capable of looking at very specialized aspects of chemical systems. As it is a laser technique, any surface or interface that is accessible by light can be probed using SFG, making it an ideal tool for investigating the interfacial molecular structures in this study.

1.3.1 Overview

Optical SFG describes the process in which two input laser beams of frequencies ω_1 and ω_2 overlap in a medium, which then generates an output beam with frequency at the sum of the two input frequencies ($\omega_{SF} = \omega_1 + \omega_2$).[53, 54] This process is diagrammed below in Figure 1.1 where ω_1 describes the input visible beam, which is maintained at a fixed frequency, and ω_2 describes the tunable input IR beam. When ω_2 is scanned over the

vibrational resonances of the molecules of the material under study, the SFG signal becomes resonantly enhanced, thus generating a vibrational spectrum of the sample. Figure 1.2, depicts a schematic energy level diagram for the IR-visible SFG process. It is a combination of an IR absorption process and an anti-stokes Raman scattering process. Only those vibrational modes that are both IR-active and Raman active will be SFG-active.

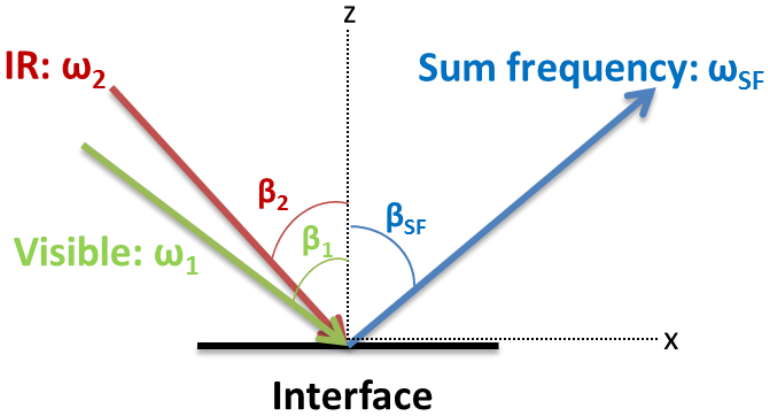

Figure 1.1 The SFG process.

Sum frequency generation is a second-order nonlinear optical process, and under the electric-dipole approximation, SFG is forbidden in media that possess inversion symmetry. Most bulk material, such as polymers or pure liquid samples are centrosymmetric and therefore do not exhibit an SFG signal. However, at interfaces between sample layers, or at sample surfaces, the symmetry of the bulk is broken and an SFG signal can be detected. SFG is also known to be submonolayer surface-sensitive, a determination that was made based on both theoretical calculations and experimental evidence.[39, 40, 53] In addition, the orientation and orientational distribution of functional

groups on the sample surface can be deduced by collecting SFG spectra using different polarization combinations of the three input and output beams.

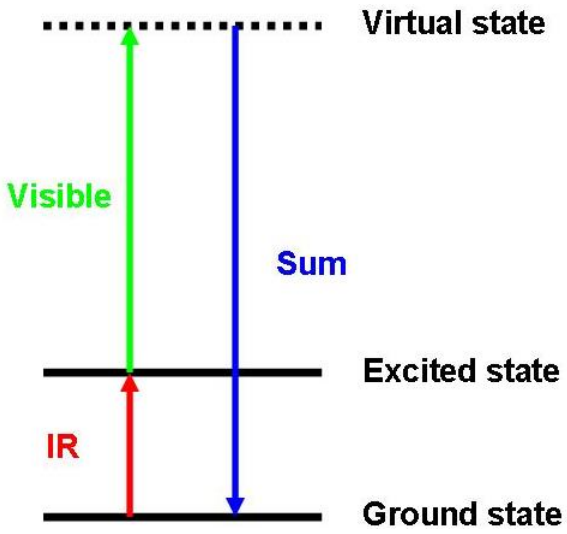

Figure 1.2 Energy level diagram of the SFG process.

1.3.2 Basic Theory

When a molecule is placed in a weak electric field, the polarization P, also called the oscillating dipoles per unit volume of molecule, is proportional to the strength of the electric field E. This relationship is described by

$$P = \chi^{(1)}E \tag{1.1}$$

where $\chi^{(1)}$ is the linear susceptibility. In the intense laser light, the external electric field becomes comparable to the fields experienced by an electron in a molecule, and the linear polarization of matter is no longer an appropriate approximation. Higher order terms must then be taken into account. Using the electric dipole approximation, the total polarization can be described by

$$P = P^{(1)} + P^{(2)} + P^{(3)} + ... = \chi^{(1)}E + \chi^{(2)} : EE + \chi^{(3)} : EEE + ... \quad (1.2)$$

where the second-order nonlinear susceptibility, $\chi^{(2)}$, is a third-rank tensor, the third-order susceptibility, $\chi^{(3)}$, is a fourth-rank tensor, as so on.[55] The SFG intensity, I, of the emitted light depends on $\left|P^{(2)}\right|^2$. So, for SFG:

$$I(\omega_{SF}) \propto \left|\chi^{(2)}\right|^2 I(\omega_1)I(\omega_2) \quad (1.3)$$

Under the electric dipole approximation, when inversion symmetry is broken (as occurs at surfaces and interfaces), $\chi^{(2)}$ is nonzero and consequently SFG signal can be detected. The majority of bulk phases, on the other hand, are centrosymmetric, generating no SFG signal

In addition to the symmetry constraints, it is necessary that the two input beams also overlap spatially and temporally to attain an SFG signal. SFG is a coherent process and accordingly, the generated light has a definite direction.

In the reflected direction, the intensity of the sum frequency is given by

$$I(\omega_{SF}) = \frac{8\pi_3\omega_2 \sec^2\beta_{SF}}{c^3 n_1(\omega_{SF})n_1(\omega_1)n_1(\omega_2)}\left|\chi^{(2)}_{eff}\right|^2 I_1(\omega_1)I_2(\omega_2) \quad (1.4)$$

where $n_i(\Omega)$ is the refractive index of medium i at frequency Ω, β_{SF} is the reflection angle of the sum frequency field, and $I_1(\omega_1)$ and $I_2(\omega_2)$ are the intensities of the two input beams. The effective second-order nonlinear susceptibility tensor, $\chi^{(2)}_{eff}$, of the surface is related to the second order nonlinear susceptibility tensor, $\chi^{(2)}$, in the lab coordinate system and takes the form

$$\chi_{eff}^{(2)} = [\hat{e}(\omega SF) \cdot L(\omega SF)] \cdot \chi^{(2)} : [L(\omega_1) \cdot \hat{e}(\omega_1)][L(\omega_2) \cdot \hat{e}(\omega_2)] \quad (1.5)$$

with $\hat{e}(\Omega)$ being the unit polarization vector and $L(\Omega)$ being the Fresnel factor at frequency Ω. Therefore, different tensor components of $\chi^{(2)}$ can be elucidated from different components of $\chi_{eff}^{(2)}$.[56] The different components of $\chi_{eff}^{(2)}$ can be probed using different polarization combinations of the input and output light beams in the SFG measurement.

For IR-visible SFG when the IR frequency (ω_2) is near a vibrational resonance $\chi^{(2)}$ can be written as

$$\chi^{(2)} = \chi_{NR}^{(2)} + \sum_q \frac{\chi_q}{\omega_2 - \omega_q + i\Gamma_q} \quad (1.6)$$

where the subscript NR designates the nonresonant contribution, χ_q, ω_q, and Γ_q denote the strength, resonant frequency, and damping constant of the q^{th} vibrational mode, respectively. By obtaining different $(\chi_q)_{ijk}$ components from the resonant vibrational features associated with any particular molecule or chemical group on the surface in the SFG spectra collected using different polarization combinations of the input and output beams, the average orientation of that moiety can be determined.

As an example, a common application of this method in this lab is to use the above information to determine the orientation of α-helical component in peptide molecules on a surface. The orientation information can be obtained by using group theory and projection operators when analyzing the SFG spectra collected with different polarization combinations of the laser beams.[57] It has been shown that both amide I A mode and

amide I E_1 mode are SFG active.[57-60] Using the near-total-reflection geometry (shown in Figure 1A), *ssp* (s-polarized sum frequency signal beam, s-polarized input visible beam, p-polarized input IR beam) and *ppp* spectra of the amide I band can be collected corresponding to the χ_{yyz} and χ_{zzz} second order nonlinear optical susceptibility components respectively.[58] The dependence of χ_{yyz} and χ_{zzz} susceptibility components on the molecular hyperpolarizability is described by the following equations:[58]

For the A mode,

$$\begin{aligned}\chi_{A,xxz} &= \chi_{A,yyz} = \frac{1}{2} N_s \left[(1+r)\langle\cos\theta\rangle - (1-r)\langle\cos^3\theta\rangle\right]\beta_{ccc} \\ \chi_{A,zzz} &= N_s \left[r\langle\cos\theta\rangle + (1-r)\langle\cos^3\theta\rangle\right]\beta_{ccc}\end{aligned} \tag{1.7}$$

where $r = \beta_{aac}/\beta_{ccc}$

For the E1 mode,

$$\begin{aligned}\chi_{E_1,xxz} &= \chi_{E_1,yyz} = -N_s \left[\langle\cos\theta\rangle - \langle\cos^3\theta\rangle\right]\beta_{aca} \\ \chi_{E_1,zzz} &= 2N_s \left[\langle\cos\theta\rangle - \langle\cos^3\theta\rangle\right]\beta_{aca}\end{aligned} \tag{1.8}$$

where β_{ccc} and β_{aca} are the molecular hyperpolarizability elements, N_s is the number density of an ideal α-helix, and "< >" means average. The A mode and E_1 mode cannot be resolved in the frequency domain because of the limitation of the SFG spectral resolution. The total susceptibility is often assumed to be the sum of the susceptibilities from these two modes.[58] The hyperpolarizability elements of an α-helix are the product of the components of the Raman polarizability and IR transition dipole moment. Theoretically, we deduced the ratios r= $\beta_{aac}/\beta_{ccc} = 0.59$ and $\beta_{aca}/\beta_{ccc} = 0.31$.[58] Also, if

we assume all α-helical structures at the surface/interface adopt the same orientation, <cos θ> and <cos^3 θ> can be substituted by cos θ and cos^3 θ. Therefore, we can deduce a function relating χ_{yyz} / χ_{zzz} with the orientation angle for an ideal α-helix. Experimentally, χ_{yyz} / χ_{zzz} can be measured. Combining these values and the equations above, the orientation angle θ of an α-helix on a surface or at an interface should be able to be deduced.

There are some deviations from this ideal situation.[58] First of all, the calculation model discussed above is perfect α-helical structure which either has a unit cell with 18 peptide units or is infinitely long. In nature, it is not always the case. To address this problem, we have done a thorough discussion in previous publications and have shown that "extra" or "missing" amino acid residues from the 18 (or multiple of 18)-unit cell play minimal role in data analysis. Also the deviations from an ideal helix can be corrected by considering the helix length in the orientation analysis.[58] On the other hand, one peptide or protein may have more α-helical segments pointing at different directions. We have successfully calculated the overall hyperpolarizability of such bent helical components, which can be used to determine the orientation of entire proteins.[61] Finally, peptides or proteins do not necessarily adopt a single orientation in biological systems; they can stay in multiple orientations. For this situation, the maximum entropy function has been introduced to calculate the orientation distribution of the target peptide or protein in combination of both SFG and ATR-FTIR orientation analysis results.[59, 60]

1.3.3 Experimental System

A schematic diagram of the SFG laser system used in this lab is displayed below in Figure 1.3. It is a custom-designed EKSPLA SFG spectrometer. The 20 picosecond

mode-locked Nd:YAG laser has a fundamental output of 1064 nm and a repetition rate of 20 Hz. The fundamental beam from the laser is directed to the harmonics unit, where two K*DP nonlinear crystals produce the second and third harmonics, which are at 532 nm and 355 nm, respectively. The 532 nm beam serves as the visible beam for the SFG experiment. The 355 nm beam, along with the fundamental 1064 nm beam pump the optical parametric generation/amplification and difference frequency generation system (OPG/OPA/DFG) which is based on LBO and $AgGaS_2$ crystals. The IR beam generated from the OPG/OPA/DFG is tunable from 2.3 to 10 μm (4300 to 1000 cm^{-1}).[62-64]

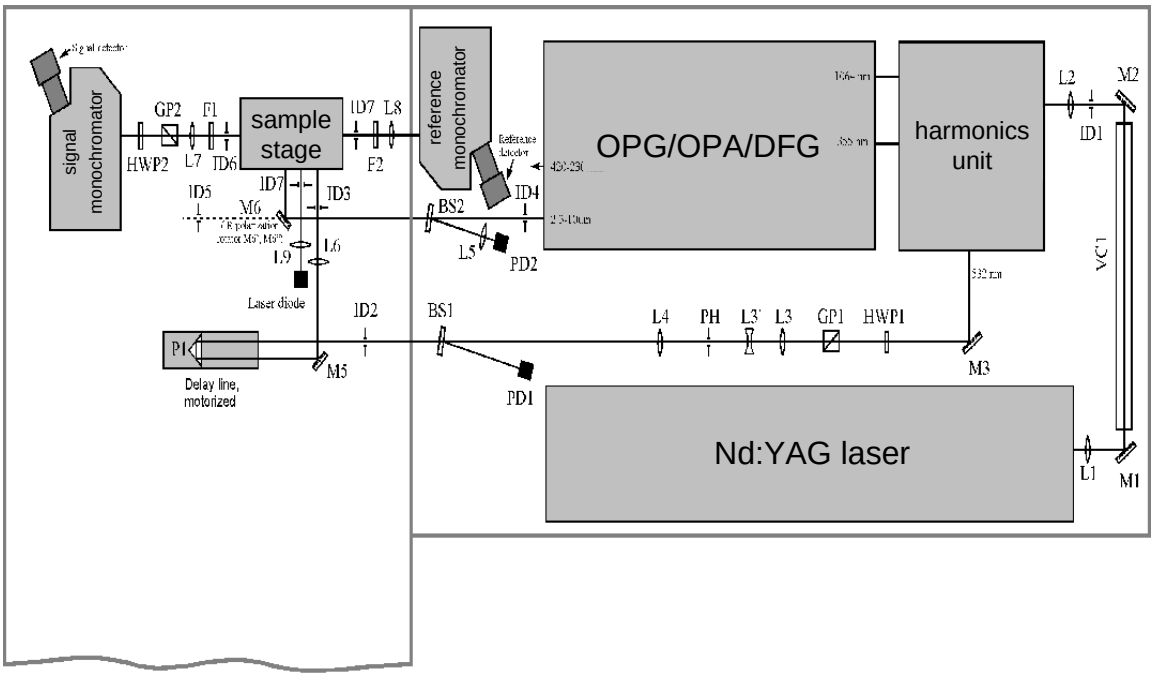

Figure 1.3 Layout of the EKSPLA SFG laser spectrometer.[65]

The SFG system can be conceptually divided into two sections. The first section, shown in the right in Figure 1.3, is the fundamental portion of the system which actually generates the laser beams used in the course of SFG experimentation. The three main components of this first section are the Nd:YAG laser, the harmonics unit, and the optical parametric oscillator/amplifier and difference frequency generator, referred to in Figure

1.3 as the OPG/OPA/DFG. The second section, shown on the left in Figure 1.3, is the section where the sample itself is exposed to the beams and SFG signal is generated and collected, and the geometry of this section can be changed depending on what experiments are being run. What follows is a brief description of how the three fundamental components of the first section are and how they are used.

1.3.3.1 Nd:YAG Laser

Neodymium-doped yttrium aluminum garnet ($Nd:Y_3Al_5O_{12}$) is a crystal widely used as the active laser medium for solid-state lasers. The laser is optically pumped using flashlamps and emits light with a wavelength of 1064 nm. As a Nd:YAG laser, it is operated using passive mode-locking. The light generated in the laser cavity is passed through a laser dye, which acts as a saturable absorber. The dye exhibits an intensity-dependent transmission, meaning it behaves differently depending on the intensity of the light passing through it. For passive mode-locking, ideally a saturable absorber will selectively transmit high intensity light while absorbing low intensity light. However, when the laser is initially triggered, it is not initially mode-locked. Any un-modelocked laser will experience random, intense spikes in radiation, and those spikes will be preferentially transmitted by the dye. As the light in the laser cavity oscillates, this process repeats, which leads to the selective amplification of the high intensity spikes and the suppression by absorption of the low intensity light. After many round trips in the cavity, this leads to a train of pulses and the mode-locking of the laser. In addition, Pockel cells are also used in the laser cavity to assist in the generation a fundamental laser beam at a sufficiently high intensity.[62]

1.3.3.2 Harmonics Unit

The harmonics unit is important to the SFG laser setup because it generates the visible beam for SFG experiments. It also produces a 355 nm beam for the OPG/OPA/DFG system to generate the frequency tunable mid-IR beam. To do this, the fundamental wavelength emitted from the Nd:YAG laser is frequency doubled and tripled by having the beam pass through the nonlinear crystals generating a corresponding harmonic. The wavelengths are summarized below in Table 1.1.

Table 1.1 Summary of wavelengths generated and used in SFG laser setup.

Wavelength (nm)	Harmonic	Spectral Region
1064	Fundamental	Infrared
532	2^{nd}	Visible (green)
355	3^{rd}	Ultraviolet

The harmonic radiation propagates collinearly with the fundamental beam. To maximize the efficiency of the conversion to harmonics, it is necessary for the path of the input fundamental beam to lie along a unique axis of fixed orientation relative to the axis of the crystal. This condition is referred to as phase matching. The harmonics generation is done in K*DP (potassium dideuterium phosphate) nonlinear crystals, and the second and third harmonics are obtained in the harmonics unit. The purity of the third harmonic is enhanced using a system of two reflections from two mirrors, a step which is necessary because the process of converting to the third harmonic is not 100% efficient.[63]

1.3.3.3 OPG/OPA/DFG

The OPG/OPA/DFG system is the device used to generate a tunable IR beam. As previously stated, a tunable IR beam is necessary for SFG experimentation to determine the vibrational resonances of the molecule under study. It functions by combining a lithium borate (LBO) crystal-based optical parametric generator/amplifier and a difference frequency generator on an $AgGaS_2$ (silver gallium sulfate) crystal, and uses the fundamental and third harmonic beams to generate the tunable IR signal. The 355 nm beam passes through the nonlinear LBO crystal and is separated into two beams, a signal beam and an idler beam. The wavelengths of the two generated beams are determined by the phase matching condition, which can be changed simply by rotating the axis of the crystal. This allows for the tuning of the eventual final beam to a desired wavelength. Once the signal beam is separated from the parametric generator outputs, the desired wavelength is then passed through the $AgGaS_2$ crystal collinearly with the fundamental beam, resulting in a beam at the difference of the two frequencies. This is also controlled by tilting the axis of the crystal to ensure the beams are collinear. The resulting beam is the tunable IR beam used in the SFG experiment, which ranges from 4300-1000 cm^{-1}.[64]

1.3.4 Experimental Setup

The visible and tunable IR beams are overlapped both temporally and spatially on the sample with incident beams of 60 ° and 54 °, respectively, versus the surface normal. The pulse energy of the visible beam is approximately 200 μJ, and the pulse energy of the IR beam is approximately 100 μJ. Both beams have a diameter of roughly 0.5 mm. The SFG signal from the sample surface or interface is then collected by a photomultiplier tube and processed with a gated integrator. Two photodiodes are used to monitor the input visible beam and IR beam powers by collecting the back reflections of those two

beams from focus lenses. This is extremely important for data collection because the SFG spectra can be normalized by the powers of the input lasers. This allows for comparison between spectra taken at different times and days. The SFG intensity is measured as a function of the input IR frequency, generating a vibrational spectrum of the sample surface or interface. The polarization of the input and output beams can be altered, and by changing the polarizations of those beams, SFG spectra with different polarization combinations can be collected.[40] The combinations ssp (s-polarized SFG output, s-polarized visible input, and p-polarized IR input), sps, and ppp are most commonly collected in this lab.

Different geometries have been employed to collect SFG spectra, and the geometry of the sample can have a significant effect on the signal detected. For example, a common method of sample preparation in this lab is spin-coating a thin polymer film onto an appropriate IR transparent window. In the face-down geometry which is shown in Figure 1.4, the two input beams travel through the window and then overlap on the polymer film. This geometry not only allows SFG spectra to be obtained from sample in air, but it also allows contact between the sample and a liquid, thus enabling the collection of spectra from sample/liquid interfaces *in situ*. Another example also has samples facing-down but on a prism surface (shown in Figure 1.4 right). This geometry is called near total internal reflection geometry where the angles of the incident beams and the sum frequency beam are close to the critical angles. It has been proved that using this geometry, the signals from the interface are greatly enhanced. As a result, it facilitates detection of signals that would, in any other experimental setup, be too weak to detect such as those from peptides or proteins.

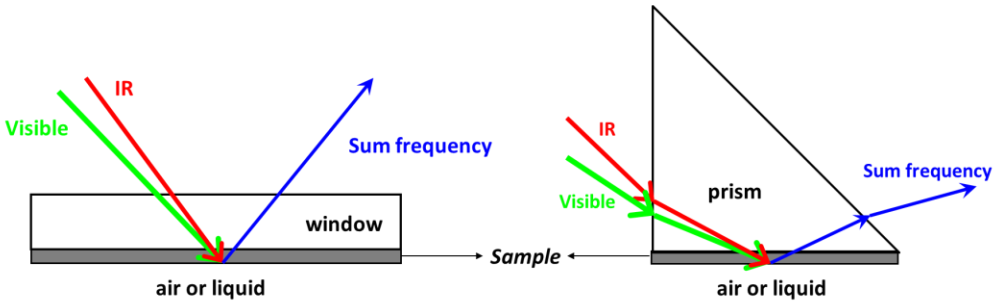

Figure 1.4 The SFG sample experimental geometry. Left: window face-down geometry; Right: prism geometry (can be used for the near total reflection geometry).

1.4 OBJECTIVES AND PRESENTED RESEARCH

The objectives of this presented research are to correlate surface structures of bioactive materials with their bioactivity and thus to propose optimization strategies for the development of improved bioactive materials. The inherent surface sensitive SFG technique will be used primarily to understand how the bioactive materials under study restructure themselves upon contacting biologically relevant environments or biomolecules from the perspectives of molecular conformation and orientation.

In Chapter 2, several kinds of antibiofouling materials incorporating both antifouling quaternary ammonium salt (QAS) components and a fouling-releasing poly dimethylsiloxane (PDMS) matrix will be evaluated. By measuring a series of PDMS coatings containing either a QAS with a single ammonium salt group per molecule or quaternary ammonium-functionalized polyhedral oligomeric silsesquioxane (Q-POSS) with SFG in air, water, and artificial sea water (ASW), it will be shown that slight variations of the QAS structure can lead to substantial differences in the interfacial surface structures of these materials and thus in their antifouling properties. Indeed, the

SFG results presented in this chapter will indicate that the surface structures of these materials depend on several factors, such as the extent of quaternization, the molecular weight of the PDMS component, and the functional groups of the QAS used for incorporation into the PDMS matrix.

Chapter 3 will focus on peptide-immobilized materials including model self-assembled monolayers (SAMs), spin-coated pre-functionalized polymers and functionalized chemical vapor deposited (CVD) polymers. Antimicrobial peptides (AMPs) are chosen for immobilization because their functions are easy to characterize and to compare to the structural study using SFG. The AMPs are immobilized to the surface via the cysteine residue added to the sequence intentionally and the surface maleimide functionality. The effect of peptide concentration, solvent hydrophobicity, tethering site, and the properties of surfaces on the structure and orientation of immobilized AMPs will be investigated using SFG and correlated to their antimicrobial activity. It will be presented that both the tethering terminus and the interaction between AMPs and surfaces greatly alter the activity of the immobilized AMPs. Moreover, molecular dynamics (MD) simulations will be employed to identify AMP sequence/structures that are inherently rigid and will not be altered by immobilization. The interfacial behavior predicted by MD simulation on surface immobilized molecules will be confirmed by SFG studies.

Finally, Chapter 4 will expand the observations from Chapter 3 to larger proteins and investigate enzyme-immobilized materials. In this chapter, specific immobilization of a model enzyme 6-phospho-β-galactosidase (β-Gal) through intentionally mutated unique cysteine residue will be achieved to surfaces containing maleimide functionality. A

systematic means to characterize interfacial orientation of immobilized enzymes has been developed using combined studies with SFG and ATR–FTIR. The possible orientations of the immobilized β-Gal will be determined, which are well correlated to its tested activity. In addition, we will examine how attaching the enzyme to the surface changes its activity by comparing it with randomly adsorbed enzyme molecules on a hydrophobic surface. Furthermore, the effect of the variation of the enzyme attaching cysteine site on enzyme orientation will be evaluated by engineering the cysteine residue at desired positions. It will be shown that activity and stability of enzyme-immobilized materials highly depends on the structure and orientation of the enzyme molecules after immobilization.

The presented work explores the working mechanisms of several bioactive materials in biological-relevant environments. By unveiling the details regarding the interfacial structures *in situ* at a molecular level, we have expanded the knowledge on the structure/activity relationships of these materials, aiding in the design and development of bioactive materials with improved performance.

1.5 REFERENCES

(1) Magin, C. M.; Cooper, S. P.; Brennan, A. B., Non-Toxic Antifouling Strategies. *Mater. Today* **2010,** *13*, 36-44.

(2) Hellio, C.; Yebra, D., *Advances in Marine Antifouling Coatings and Technologies*. Woodhead ; CRC: Oxford : Boca Raton, FL, 2009.

(3) Pelton, R., Bioactive Paper Provides a Low-Cost Platform for Diagnostics. *Trac-Trend Anal Chem* **2009,** *28*, 925-942.

(4) Gill, I., Bio-Doped Nanocomposite Polymers: Sol-Gel Bioencapsulates. *Chem. Mater.* **2001,** *13*, 3404-3421.

(5) Wilson, C. J.; Clegg, R. E.; Leavesley, D. I.; Pearcy, M. J., Mediation of Biomaterial-Cell Interactions by Adsorbed Proteins: A Review. *Tissue Eng.* **2005,** *11*, 1-18.

(6) Cui, H. G.; Webber, M. J.; Stupp, S. I., Self-Assembly of Peptide Amphiphiles: From Molecules to Nanostructures to Biomaterials. *Biopolymers* **2010,** *94*, 1-18.

(7) Gomes, S.; Leonor, I. B.; Mano, J. F.; Reis, R. L.; Kaplan, D. L., Natural and Genetically Engineered Proteins for Tissue Engineering. *Prog. Polym. Sci.* **2012,** *37*, 1-17.

(8) Arcos, D.; Vallet-Regi, M., Sol-Gel Silica-Based Biomaterials and Bone Tissue Regeneration. *Acta Biomater.* **2010,** *6*, 2874-2888.

(9) Jung, J. P.; Gasiorowski, J. Z.; Collier, J. H., Fibrillar Peptide Gels in Biotechnology and Biomedicine. *Biopolymers* **2010,** *94*, 49-59.

(10) Ansari, S. A.; Husain, Q., Potential Applications of Enzymes Immobilized on/in Nano Materials: A Review. *Biotechnol. Adv.* **2012,** *30*, 512-523.

(11) Coelho, P. G.; Granjeiro, J. M.; Romanos, G. E.; Suzuki, M.; Silva, N. R. F.; Cardaropoli, G.; Thompson, V. P.; Lemons, J. E., Basic Research Methods and Current Trends of Dental Implant Surfaces. *J Biomed Mater Res B* **2009,** *88B*, 579-596.

(12) Garcia-Galan, C.; Berenguer-Murcia, A.; Fernandez-Lafuente, R.; Rodrigues, R. C., Potential of Different Enzyme Immobilization Strategies to Improve Enzyme Performance. *Adv. Synth. Catal.* **2011,** *353*, 2885-2904.

(13) Zhou, M.; Smith, A. M.; Das, A. K.; Hodson, N. W.; Collins, R. F.; Ulijn, R. V.; Gough, J. E., Self-Assembled Peptide-Based Hydrogels as Scaffolds for Anchorage-Dependent Cells. *Biomaterials* **2009,** *30*, 2523-2530.

(14) Horbett, T. A.; Brash, J. L., *Proteins at Interfaces II: Fundamentals and Applications*. American Chemical Society: Washington, DC: 1995; Vol. 602.

(15) Giangaspero, A.; Sandri, L.; Tossi, A., Amphipathic Alpha Helical Antimicrobial Peptides - a Systematic Study of the Effects of Structural and Physical Properties on Biological Activity. *Eur. J. Biochem.* **2001,** *268*, 5589-5600.

(16) Tweedle, M. F., Peptide-Targeted Diagnostics and Radiotherapeutics. *Acc. Chem. Res.* **2009,** *42*, 958-968.

(17) Heitz, F.; Morris, M. C.; Divita, G., Twenty Years of Cell-Penetrating Peptides: From Molecular Mechanisms to Therapeutics. *Br. J. Pharmacol.* **2009,** *157*, 195-206.

(18) Chen, H. Q.; Xu, Z. N.; Peng, L.; Fang, X. M.; Yin, X. F.; Xu, N. Z.; Cen, P. L., Recent Advances in the Research and Development of Human Defensins. *Peptides* **2006,** *27*, 931-940.

(19) Jin, W.; Brennan, J. D., Properties and Applications of Proteins Encapsulated within Sol-Gel Derived Materials. *Anal. Chim. Acta* **2002,** *461*, 1-36.

(20) Benkovic, S. J.; Hammes-Schiffer, S., A Perspective on Enzyme Catalysis. *Science* **2003,** *301*, 1196-1202.
(21) Schuck, P., Use of Surface Plasmon Resonance to Probe the Equilibrium and Dynamic Aspects of Interactions between Biological Macromolecules. *Annu. Rev. Biophys. Biomol. Struct.* **1997,** *26*, 541-566.
(22) Marx, K. A., Quartz Crystal Microbalance: A Useful Tool for Studying Thin Polymer Films and Complex Biomolecular Systems at the Solution−Surface Interface. *Biomacromolecules* **2003,** *4*, 1099-1120.
(23) Roach, P.; Parker, T.; Gadegaard, N.; Alexander, M. R., Surface Strategies for Control of Neuronal Cell Adhesion: A Review. *Surf. Sci. Rep.* **2010,** *65*, 145-173.
(24) Santos, O.; Kosoric, J.; Hector, M. P.; Anderson, P.; Lindh, L., Adsorption Behavior of Statherin and a Statherin Peptide onto Hydroxyapatite and Silica Surfaces by in situ Ellipsometry. *J. Colloid Interface Sci.* **2008,** *318*, 175-182.
(25) Campbell, C. T.; Kim, G., Spr Microscopy and Its Applications to High-Throughput Analyses of Biomolecular Binding Events and Their Kinetics. *Biomaterials* **2007,** *28*, 2380-2392.
(26) Mozsolits, H.; Aguilar, M. I., Surface Plasmon Resonance Spectroscopy: An Emerging Tool for the Study of Peptide-Membrane Interactions. *Biopolymers* **2002,** *66*, 3-18.
(27) Vanea, E.; Simon, V., XPS Study of Protein Adsorption onto Nanocrystalline Aluminosilicate Microparticles. *Appl. Surf. Sci.* **2011,** *257*, 2346-2352.
(28) Baugh, L.; Weidner, T.; Baio, J. E.; Nguyen, P. C. T.; Gamble, L. J.; Slayton, P. S.; Castner, D. G., Probing the Orientation of Surface-Immobilized Protein G B1 Using Tof-Sims, Sum Frequency Generation, and NEXAFS Spectroscopy. *Langmuir* **2010,** *26*, 16434-16441.
(29) Henry, M.; Dupont-Gillain, C.; Bertrand, P., Conformation Change of Albumin Adsorbed on Polycarbonate Membranes as Revealed by Tof-Sims. *Langmuir* **2003,** *19*, 6271-6276.
(30) Wagner, M. S.; McArthur, S. L.; Shen, M. C.; Horbett, T. A.; Castner, D. G., Limits of Detection for Time of Flight Secondary Ion Mass Spectrometry (Tof-Sims) and X-Ray Photoelectron Spectroscopy (XPS): Detection of Low Amounts of Adsorbed Protein. *J Biomat Sci-Polym E* **2002,** *13*, 407-428.
(31) Wark, A. W.; Lee, J.; Kim, S.; Faisal, S. N.; Lee, H. J., Bioaffinity Detection of Pathogens on Surfaces. *Journal of Industrial and Engineering Chemistry* **2010,** *16*, 169-177.
(32) Woodcock, S. E.; Johnson, W. C.; Chen, Z., Collagen Adsorption and Structure on Polymer Surfaces Observed by Atomic Force Microscopy. *J. Colloid Interface Sci.* **2005,** *292*, 99-107.
(33) Gross, P. C.; Zeppezauer, M., Infrared Spectroscopy for Biopharmaceutical Protein Analysis. *J. Pharm. Biomed. Anal.* **2010,** *53*, 29-36.
(34) Sharon, M.; Oren, Z.; Shai, Y.; Anglister, J., 2D-NMR and ATR-FTIR Study of the Structure of a Cell-Selective Diastereomer of Melittin and Its Orientation in Phospholipids. *Biochemistry* **1999,** *38*, 15305-15316.
(35) Chittur, K. K., FTIR/ATR for Protein Adsorption to Biomaterial Surfaces. *Biomaterials* **1998,** *19*, 357-369.
(36) Tatulian, S. A.; Jones, L. R.; Reddy, L. G.; Stokes, D. L.; Tamm, L. K., Secondary Structure and Orientation of Phospholamban Reconstituted in Supported Bilayers from Polarized Attenuated Total-Reflection FTIR Spectroscopy. *Biochemistry* **1995,** *34*, 4448-4456.
(37) Wen, Z. Q.; Li, G. Y.; Ren, D., Detection of Trace Melamine in Raw Materials Used for Protein Pharmaceutical Manufacturing Using Surface-Enhanced Raman Spectroscopy (Sers) with Gold Nanoparticles. *Appl. Spectrosc.* **2011,** *65*, 514-521.
(38) Opdahl, A.; Somorjai, G. A., *Langmuir* **2002,** *18*, 9409-9412.

(39) Wang, J.; Chen, C.; Buck, S. M.; Chen, Z., Molecular Chemical Structure on Poly (Methyl Methacrylate)(PMMA) Surface Studied by Sum Frequency Generation (SFG) Vibrational Spectroscopy. *J. Phys. Chem. B* **2001,** *105*, 12118-12125.
(40) Chen, Z.; Shen, Y. R.; Somorjai, G. A., Studies of Polymer Surfaces by Sum Frequency Generation Vibrational Spectroscopy. *Annu. Rev. Phys. Chem.* **2002,** *53*, 437-465.
(41) Yang, P.; Boughton, A.; Homan, K.; Tesmer, J.; Chen, Z., Membrane Orientation of Gαiβ1γ2 and Gβ1γ2 Determined Via Combined Vibrational Spectroscopic Studies. *J. Am. Chem. Soc.* **2013,** *135*, 5044-5051.
(42) Han, X.; Uzarski, J. R.; Mello, C. M.; Chen, Z., Different Interfacial Behaviors of N- and C-Terminus Cysteine-Modified Cecropin P1 Chemically Immobilized onto Polymer Surface. *Langmuir* **2013,** *29*, 11705-11712.
(43) Liu, Y.; Jasensky, J.; Chen, Z., Molecular Interactions of Proteins and Peptides at Interfaces Studied by Sum Frequency Generation Vibrational Spectroscopy. *Langmuir* **2012,** *28*, 2113-2121.
(44) Ding, B.; Chen, Z., Molecular Interactions between Cell Penetrating Peptide Pep-1 and Model Cell Membranes. *J. Phys. Chem. B* **2012,** *116*, 2545-2552.
(45) Yang, P.; Ramamoorthy, A.; Chen, Z., Membrane Orientation of MSI-78 Measured by Sum Frequency Generation Vibrational Spectroscopy. *Langmuir* **2011,** *27*, 7760-7767.
(46) Ye, S. J.; Nguyen, K. T.; Boughton, A. P.; Mello, C. M.; Chen, Z., Orientation Difference of Chemically Immobilized and Physically Adsorbed Biological Molecules on Polymers Detected at the Solid/Liquid Interfaces in Situ. *Langmuir* **2010,** *26*, 6471-6477.
(47) Ye, S. J.; Majumdar, P.; Chisholm, B.; Stafslien, S.; Chen, Z., Antifouling and Antimicrobial Mechanism of Tethered Quaternary Ammonium Salts in a Cross-Linked Poly(Dimethylsiloxane) Matrix Studied Using Sum Frequency Generation Vibrational Spectroscopy. *Langmuir* **2010,** *26*, 16455-16462.
(48) Boughton, A. P.; Andricioaei, I.; Chen, Z., Surface Orientation of Magainin 2: Molecular Dynamics Simulation and Sum Frequency Generation Vibrational Spectroscopic Studies. *Langmuir* **2010,** *26*, 16031-16036.
(49) Nguyen, K. T.; Le Clair, S. V.; Ye, S. J.; Chen, Z., Molecular Interactions between Magainin 2 and Model Membranes in Situ. *J. Phys. Chem. B* **2009,** *113*, 12358-12363.
(50) Ye, S. J.; McClelland, A.; Majumdar, P.; Stafslien, S. J.; Daniels, J.; Chisholm, B.; Chen, Z., Detection of Tethered Biocide Moiety Segregation to Silicone Surface Using Sum Frequency Generation Vibrational Spectroscopy. *Langmuir* **2008,** *24*, 9686-9694.
(51) Chen, X.; Tang, H. Z.; Even, M. A.; Wang, J.; Tew, G. N.; Chen, Z., Observing a Molecular Knife at Work. *J. Am. Chem. Soc.* **2006,** *128*, 2711-2714.
(52) Chen, X.; Chen, Z., SFG Studies on Interactions between Antimicrobial Peptides and Supported Lipid Bilayers. *BBA-Biomembranes* **2006,** *1758*, 1257-1273.
(53) Shen, Y. R., *The Principles of Nonlinear Optics*. J. Wiley: New York, 1984.
(54) Bain, C. D., Sum-Frequency Vibrational Spectroscopy of the Solid/Liquid Interface. *Journal of the Chemical Society, Dalton Transactions* **1995,** *91*, 1281-1296.
(55) Buck, M.; Himmelhaus, M., Vibrational Spectroscopy of Interfaces by Infrared-Visible Sum Frequency Generation. *Journal of Vacuum Science and Technology A* **2001,** *19*, 2717-2736.
(56) Zhuang, X.; Miranda, P. B.; Kim, D.; Shen, Y. R., Mapping Molecular Orientation and Conformation at Interfaces by Surface Nonlinear Optics. *Phys Rev B* **1999,** *59*, 12632-12640.
(57) Lee, S. H.; Wang, J.; Krimm, S.; Chen, Z., Irreducible Representation and Projection Operator Application to Understanding Nonlinear Optical Phenomena: Hyper-Raman, Sum Frequency Generation, and Four-Wave Mixing Spectroscopy. *J. Phys. Chem. A* **2006,** *110*, 7035-7044.

(58) Nguyen, K. T.; Le Clair, S. V.; Ye, S. J.; Chen, Z., Orientation Determination of Protein Helical Secondary Structures Using Linear and Nonlinear Vibrational Spectroscopy. *J. Phys. Chem. B* **2009,** *113*, 12169-12180.
(59) Chen, X.; Wang, J.; Boughton, A. P.; Kristalyn, C. B.; Chen, Z., Multiple Orientation of Melittin inside a Single Lipid Bilayer Determined by Combined Vibrational Spectroscopic Studies. *J. Am. Chem. Soc.* **2007,** *129*, 1420-1427.
(60) Wang, J.; Lee, S. H.; Chen, Z., Quantifying the Ordering of Adsorbed Proteins in Situ. *J. Phys. Chem. B* **2008,** *112*, 2281-2290.
(61) Boughton, A. P.; Yang, P.; Tesmer, V. M.; Ding, B.; Tesmer, J. J. G.; Chen, Z., Heterotrimeric G Protein Beta(1)Gamma(2) Subunits Change Orientation Upon Complex Formation with G Protein-Coupled Receptor Kinase 2 (Grk2) on a Model Membrane. *Proc. Natl. Acad. Sci. USA* **2011,** *108*, E667-E673.
(62) EKSPLA, Pl2143 Series Laser. In *Technical description and user's manual*, Vilnius: 2003.
(63) EKSPLA, Harmonics Unit. In *Technicial description and user's manual*, Vilnius: 2000.
(64) EKSPLA, Optical Parametric Oscillator Pg401vir/Dfg. In *Technical description and user's manual*, Vilnius: 2000.
(65) Woodcock, S. E. Interfacial Studies of Polymers and Proteins with Atomic Force Microscopy. University of Michigan, Ann Arbor, MI, 2005.

CHAPTER 2

ANTIBIOFOULING MECHANISM STUDIES ON PDMS INCORPORATED WITH QAS MOLECULES

2.1 INTRODUCTION

Marine biofouling is generally defined as the undesirable attachment and growth of macro- and micro-organisms on surfaces immersed in seawater. Once established, it can cause a multitude of problems for ships in operation and in the harbor. Extensive research has been performed in recent years to develop new antifouling coating technologies that possess superior antifouling efficiency, longer performance lifetimes, and non-toxic mechanisms of activity.[1-6]

Polydimethysiloxane (PDMS) materials have demonstrated good fouling-release (FR) performance due to their low surface energy,[1, 2] low glass transition temperature,[3] and low elastic modulus.[4, 5] In addition, biocides have been incorporated into PDMS matrices to form successful antibacterial materials.[6-8] Thus, researchers have applied this idea to generate FR and antifouling coatings using PDMS with chemically bound (i.e., tethered) biocide moieties[9-11] and quaternary ammonium salts (QAS) are one of the most widely used biocides to inhibit microbial growth.[12-14] They are very effective in killing a broad spectrum of microorganisms such as Gram-positive and Gram-negative bacteria, yeast, and mold.[13, 15-17]

Extensive research has demonstrated that QAS-incorporated PDMS materials are good candidates for antifouling coatings that possess both FR and antifouling capabilities.[9, 18-22] To optimize the performance of various coating materials, it is crucial to characterize their surface chemical structures at a molecular level because such surface structures determine the antifouling properties of the coating materials. More importantly, because these materials are used underwater, it is crucial to monitor their surface structures *in situ* in water.[22] However, most of the currently available surface sensitive analytical techniques cannot meet the above requirements simultaneously.

Sum frequency generation vibrational spectroscopy (SFG) has been shown to be a powerful tool to study polymer surface structures at the molecular level in different chemical environments. SFG can provide information such as functional group composition and orientation at a surface or interface with a submonolayer sensitivity.[23-34] In addition, SFG can be used to study *in situ* surface restructuring behavior of polymer materials in water.[35-41] Details of the SFG theory and experimental setup have been discussed in chapter one and will not be repeated here.

Recently, we applied SFG to study a QAS-tethered PDMS system, focusing on the QAS surface chemical composition in air, water and nutrient growth medium.[22] The results of these studies indicated that the surface structure of the coating largely depended on the length of the alkyl chain attached to the nitrogen atom of the QAS moiety as well as the length of alkyl chain spanning between the nitrogen atom in the QAS moiety and the silicon atom of PDMS. The surface structures detected using SFG correlated well with their antimicrobial/antifouling activity.

In this chapter, SFG was used to monitor the surface structures of the two different types of QAS-incorporated PDMS coatings. Emphasis was placed on the effects of the functional groups of the QAS used for incorporating, the extent of quaternization, and the length of the alkyl chain attached to the nitrogen atom on the structures of the coating surfaces when exposed to each environment. The antifouling activities of these QAS-incorporated PDMS materials were tested in tandem with the above described SFG studies. The results from these studies indicated that: (1) PDMS materials with QAS tethered using the ethoxysilane functional group exhibited better antifouling activity than those prepared with methoxysilane; (2) PDMS materials with lower quaternization of Q-POSS exhibited better antifouling performance than those possessing a higher extent of Q-POSS quaternization. These results contradict the intuition that higher quaternization should lead to better antifouling performance due to the higher number of QAS moieties. Also because the ethoxy and methoxy functional groups were lost in the reaction tethering QAS to PDMS, they should not lead to differed antifouling activities. The results obtained from our SFG studies correlated well to these experimental observations in antifouling properties, providing an in-depth understanding on surface structure-function relationships of PDMS materials incorporated with QAS-incorporated biocides.

The SFG studies on PDMS materials with QAS tethered using different silane functional group were carried in collaboration with a group member Chuan Leng. All the antimicrobial/antifouling activity testing experiments were performed by our collaborators at North Dakota State University.

2.2 EXPERIMENTAL

2.2.1 Materials

2.2.1.1 QAS-tethered PDMS system

Silanol-terminated PDMS with a molecular weight of 49,000 g/mol (49K-PDMS) was purchased from Gelest, Inc. (Tullytown, PA) and was diluted in toluene to 80 wt%. Quaternary ammonium salts octadecyldimethyl(3-trimethoxysilylpropyl) ammonium chloride (C18-TMS) and octadecyldimethyl(3-triethoxysilylpropyl) ammonium chloride (C18-TES) were synthesized using a published protocol by our collaborators at North Dakota State University.[42] Tetrahydrofuran, tetrabutylammonium fluoride (TBAF) in tetrahydrofuran (1.0 M), and 4-methyl-2-pentanone (MIBK) were purchased from Aldrich (Milwaukee, WI). For coating solutions, a TBAF catalyst solution (50 mM) was prepared by dispensing 1.25 mL of 1.0 M TBAF solution in a 25 mL volumetric flask and adding MIBK volumetrically to 25 mL. Coating samples were prepared by blending 18K-PDMS or 49K-PDMS, methyltriacetoxysilane, TBAF catalyst solution, and different amounts of 50% (w/w) solution of a QAS in methanol (Table 2.1, Samples A-D). The coating solutions were stirred overnight and then spin-coated on fused silica windows (1 inch in diameter, 1/8 inch thick, obtained from ESCO Products Inc.). The spin coated films were stored at ambient conditions for 24 h to cure the films. To ensure full cure, the samples were then heated overnight at 50 ℃. Molecular formulas for PDMS, cross-linker, catalyst and QAS are shown in Figure 2.1A.

Table 2.1 Compositions of the PDMS coatings incorporated with QAS (all values are in grams)

Sample	PDMS	QAS type	QAS Amount	MeAc	50 mM Catalyst
A	49K: 6.25	C18-TMS	1.24	0.75	0.75
B	49K: 6.25	C18-TES	1.61	0.75	0.75
C	18K: 5.00	C18-TMS	1.24	0.75	0.75
D	18K: 5.00	C18-TES	1.61	0.75	0.75
E	18K: 3.50	Q-POSS 1	1.32	0.525	0.525
F	18K: 3.50	Q-POSS 2	2.06	0.525	0.525
G	18K: 3.50	Q-POSS 3	1.39	0.525	0.525
H	18K: 3.50	Q-POSS 4	2.10	0.525	0.525

Table 2.2 Q-POSS molecules studied (30 wt% in THF)

Sample	Q-POSS structure	
	R	Extent of quaternization
Q-POSS 1	$C_{16}H_{33}$-	82.9%
Q-POSS 2	$C_{16}H_{33}$-	38.2%
Q-POSS 3	$C_{18}H_{37}$-	81.7%
Q-POSS 4	$C_{18}H_{37}$-	38.9%

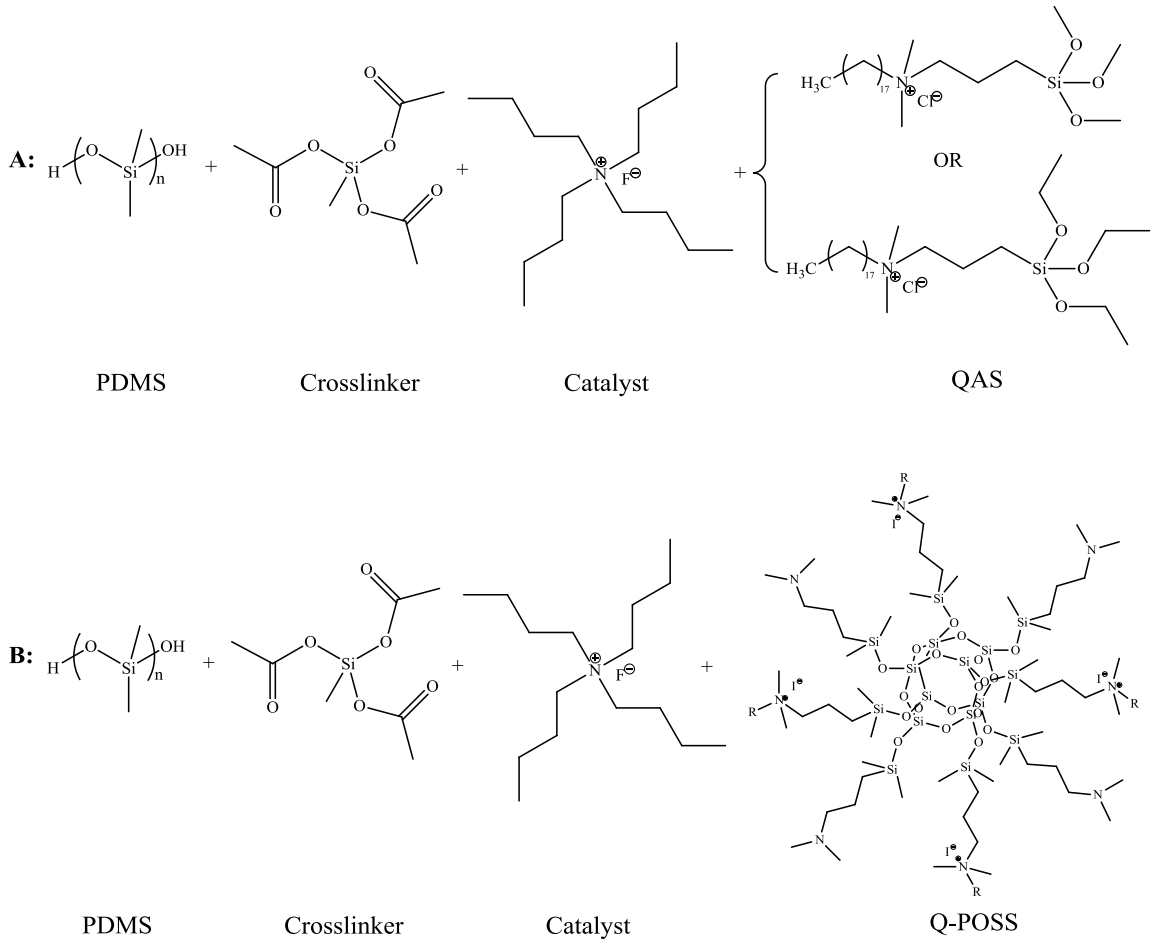

Figure 2.1 Chemical structures of the QAS incorporated PDMS systems (A: QAS-tethered system; B: Q-POSS-incorporated PDMS system)

2.2.1.2 Q-POSS incorporated PDMS system

Silanol-terminated PDMS with a molecular weight of 18,000 g/mol (18K-PDMS) and methyltriacetoxysilane were ordered from Gelest, Inc. (Tullytown, PA). Various quaternary ammonium functionalized-POSS (Q-POSS) (Table 2.2) were synthesized by our collaborators at North Dakota State University.[19] For coating solutions, a TBAF catalyst solution (50 mM) was prepared by dispensing 1.25 mL of 1.0 M TBAF solution in a 25 mL volumetric flask and adding MIBK volumetrically up to 25 mL. Coating samples were prepared by blending 18K-PDMS, methyltriacetoxysilane, TBAF catalyst

solution, and different amounts of 30 wt% solution of a Q-POSS in tetrahydrofuran (Table 2.1, Samples E-H). These coating solutions were stirred overnight and then spin-coated on fused silica windows. The films were cured at ambient conditions for 24 h. To ensure full cure, the samples were then heat overnight at 50 ℃. Molecular formulas for PDMS, cross-linker, catalyst and Q-POSS are shown in Figure 2.1B.

2.2.2 Instrumentation

Details about SFG theories and instrumentation have been described in sections **1.3.2**, **1.3.3** and **1.3.4** in Chapter 1. SFG is a second order nonlinear process which selectively probes systems with no inversion symmetry. Since most bulk materials have inversion symmetry, SFG is an intrinsic surface sensitive technique and has been proven to provide submonolayer surface sensitivity.[23-34] In this study, face-down sample geometry was used in which two input laser beams travel through the fused silica windows and overlap on the polymer/air or polymer/liquid (Millipore water or artificial sea water) interface (Figure 2.2). SFG spectra with a polarization combination of ssp (s-polarized sum frequency output, s-polarized visible input, and p-polarized infrared input) were collected. All SFG spectra were normalized according to the intensities of the input IR and visible beams. Previous studies have demonstrated that SFG signals are dominated by the polymer/air or polymer/liquid interface, with almost no polymer/substrate or polymer bulk contributions to the spectra collected using this experimental geometry. [11, 22, 33-36]

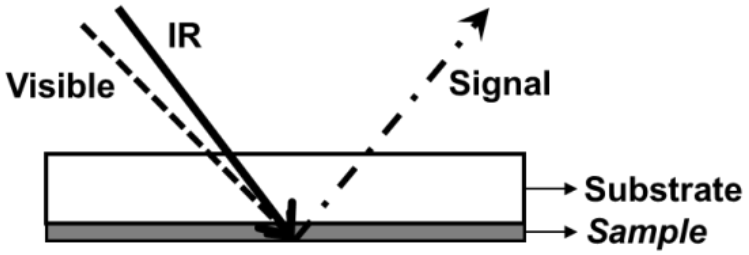

Figure 2.2 SFG experimental face-down sample geometry

2.3 RESULTS AND DISCUSSION

2.3.1 QAS-tethered PDMS coatings

Surface Structures in Air. The ssp SFG spectra collected from the surfaces of the four samples are dominated by peaks centered at 2850, 2875, 2915, 2940 and 2965 cm^{-1}, which are assigned to the CH_2 symmetric stretching, CH_3 symmetric stretching, Si-CH_3 C-H symmetric stretching, CH_3 Fermi resonance modes, C-H asymmetric stretching of regular methyl and/or Si-CH_3 groups, respectively (Figure 2.3a). [11, 22, 43] The 2850, 2875, 2940 and 2965 cm^{-1}peaks are believed to be contributed from QAS while the peaks at 2915 cm^{-1} and 2965 cm^{-1} are from the Si-CH_3 C-H symmetric and asymmetric stretching modes in PDMS. This is because SFG spectra detected from the pure PDMS surface reported before have only two peaks in the C-H stretching frequency region from the Si-CH_3 C-H symmetric (~2915 cm^{-1}) and asymmetric (~2965 cm^{-1}) stretching modes.[11, 22, 38] The four materials did not display discernible differences in their surface structures; both PDMS and the QAS molecules are present on the surface and the PDMS generates the dominating signal from these surfaces. Therefore their different antifouling activities cannot be interpreted by their surface structures in air.

Surface Structures in Water. The antifouling materials evaluated in this study were designed to be used in aqueous environments such as seawater or biological fluids. As a result, SFG spectra were also acquired from the interfaces between QAS-tethered PDMS materials and water (Millipore, 18.2 MΩ·cm resistivity) (Figure 2.3b). The four ssp spectra collected from samples which were cured either using different functional groups on QAS or using different MWs of PDMS all differed in their C-H frequency stretching region, however were similar in the water O-H stretching frequency region (Figure 2.3b). Overall, the C-H stretching signals are very weak and the spectra are dominated by the O-H stretching signals of water molecules at the interface.

SFG spectra collected from the interface between water and PDMS incorporated with QAS of higher MW of PDMS (49K-PDMS) have no discernible signal in the C-H stretching frequency region but have strong water signal with peaks at 3200 and 3450 cm^{-1}, assigned as "ice-like" water, and "liquid-like" water, respectively.[29, 31, 32, 44, 45] The ssp spectra collected from the 18K-PDMS with QAS/water interfaces, however, have distinguishable signals in the C-H stretching frequency region. For two 18K-PDMS materials, the SFG spectrum collected from the interface between water and the material made of C18-TMS has a stronger CH_2 contribution (at 2850 cm^{-1}) while the material containing C18-TES has a stronger CH_3 contribution. This indicates that the QAS chains are protruding out more on the surface in water for the later sample. All four SFG spectra exhibit strong water signals especially at 3200 cm^{-1}, indicating that the majority surface QAS alkyl chains fold back and the charged nitrogen atoms are exposed to water, inducing ordered water molecules at these interfaces.

Surface Structures in Artificial Sea Water (ASW). SFG spectra were also collected from the material/ASW (Aldrich, Milwaukee, WI) interface. Salt ions in sea water may induce surface reorientation of the coating materials which might provide a better understanding of their antifouling performance (Figure 2.3c). The ions in ASW randomize the orientation of the interfacial water molecules resulting in no detected water O-H stretching signal (not shown). As a result, only C-H stretching frequency region of the SFG spectra are displayed (Figure 2.3c). The spectral signatures and relative intensities are different for each of the four samples, indicating that both the functional group on QAS and the MW of PDMS play a role in determining the interfacial structures of these materials in ASW. These differences show that QAS molecules on surfaces, especially alkyl chains which are attached to quaternized nitrogen atoms, organized differently in ASW. Therefore both the functional group of QAS and MW of PDMS affect the surface structures of the QAS molecules.

Two observations can be made from the four SFG spectra displayed in Figure 2.3c. First, the materials made of C18-TES have notably stronger CH_3 signals at 2880 and 2940 cm^{-1} than the analogues made of C18-TMS. This suggests that on the surface in ASW, the alkyl chains on the QAS prepared with TES-QAS have a longer extension and protrude out farther from the surface while the alkyl chains on the QAS prepared with TMS-QAS fold back and are more disordered. The second observation is that the materials made of 18K-PDMS have relatively stronger SFG signals than those from the analogues made of 49K-PDMS. As a result, the alky chains on the surface of 49K-PDMS are more disordered than those on 18K-PDMS surface in ASW.

Antifouling Activity. According to antifouling experiments performed previously, using various marine microorganism-based laboratory assays, the QAS-tethered PDMS materials prepared with TES-QAS were more effective in preventing microbial biofilm growth than those prepared with TMS-QAS.[42] Furthermore, the biofilms attached to the surfaces of the QAS-tethered PDMS materials prepared with TES-QAS were much easier to remove. Previous atomic force microscopic (AFM) results indicated that QAS-tethered PDMS prepared with TES-QAS leads to greater segregation of QAS groups to the coating surface than that prepared with TMS-QAS.[42] This may be attributed to the lower reactivity of the ethoxysilane groups,[46, 47] which resulted in additional time for the diffusion of TES-QAS to the surface.

The above AFM results are consistent with our SFG data, as QAS-tethered PDMS prepared with TES-QAS exhibited stronger methyl signals in aqueous environment, especially in ASW. As discussed above, it is necessary to have the alkyl groups of the QAS protruding out from the surface of the QAS-tethered PDMS to kill the bacteria. It can be deduced from the SFG results that the alkyl chains on surfaces prepared from TES-QAS were ordered and extended out in ASW whereas coatings from TMS-QAS do not have extended alkyl chains on the surfaces (Figure 2.4). The results on QAS incorporated to PDMS discussed here correlated well to those of the PDMS materials incorporated with Q-POSS, which is presented below.

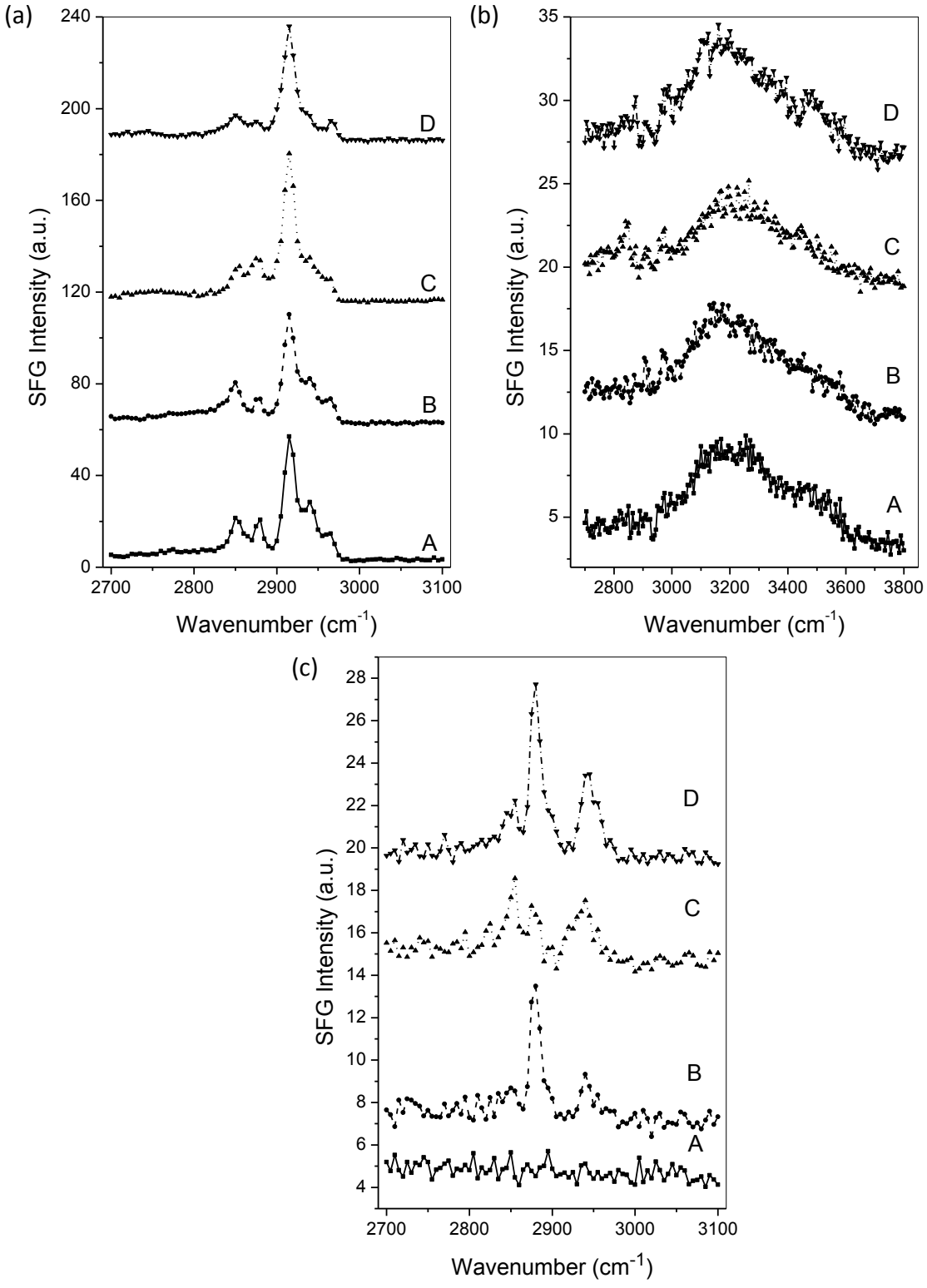

Figure 2.3 SFG ssp spectra collected from QAS-tethered PDMS systems in (a) air, (b) water, and (c) ASW. The four samples studied are: (A) 49K-PDMS, C18-TMS; (B) 49K-PDMS, C18-TES; (C) 18K-PDMS, C18-TMS; (D) 18K-PDMS, C18-TES.

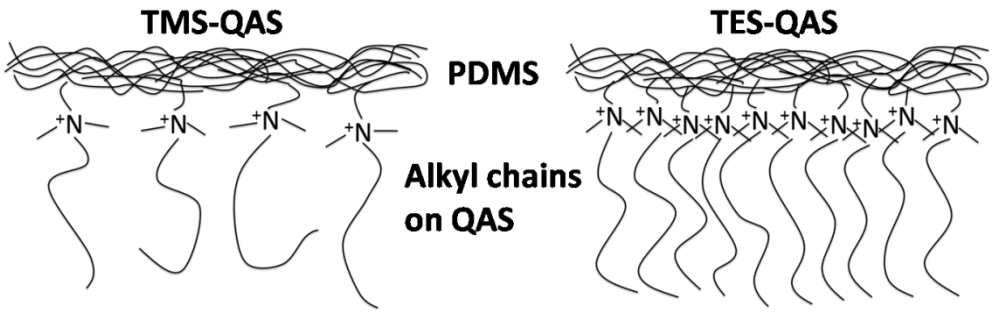

Figure 2.4 Illustration showing the surface structures of QAS-tethered PDMS system in aqueous environment. Different head groups of QAS lead to different alkyl chain ordering of the system.

2.3.2 Q-POSS incorporated PDMS coatings

Surface Structures in Air. The ssp SFG spectra collected from the surfaces of the four Q-POSS incorporate PDMS samples in air are dominated by peaks at 2850, 2875, 2915, 2940 and 2965 cm^{-1}, which are assigned to the CH_2 symmetric stretching, CH_3 symmetric stretching, Si-CH_3 C-H symmetric stretching, CH_3 Fermi resonance modes, and C-H asymmetric stretching modes of regular CH_3 or Si-CH_3, respectively (Figure 2.5a).[11, 22, 43] Similar to the previous tethered QAS case, the 2850, 2875 and 2940 cm^{-1} peaks are contribute from the Q-POSS alkyl chains of QAS. Here, the ~2915 cm^{-1} signal comes from the symmetric C-H stretching mode of the Si-CH_3 groups, but the ~2965 cm^{-1} peak may contain contributions from the C-H asymmetric stretching modes of both QAS CH_3 and Si-CH_3. The four materials did not display discernible differences in their surface structures detected from their SFG spectra—both PDMS and the Q-POSS molecules are present on these surfaces and the PDMS dominates the surfaces due to its large 2915 cm^{-1}peak. Therefore, the SFG results detected in air cannot determine the difference in antifouling performance of these four samples.

Surface Structures in Water. SFG spectra were acquired when the materials were contacting with water (Figure 2.5b). The ssp spectra collected from the samples with high extent of quaternized Q-POSS are different from those with low extent of quaternized Q-POSS in the C-H stretching frequency region (2800-3000 cm^{-1}) but they have similar water O-H stretching spectra (3000-3700 cm^{-1}). The SFG spectra collected in air (as mentioned in the previous section) are dominated by signals contributing from the PDMS Si-CH_3 groups. In water, we see that SFG spectra are dominated by the Q-POSS methylene C-H stretching signals at 2850 cm^{-1}, due to the hydrophilic nature of these Q-POSS molecules. This, in contrast with the hydrophobic PDMS Si-CH_3matrix allows for Q-POSS to segregate to the surface in water.

The ssp SFG spectra collected from the interface between PDMS incorporated with high extent of quaternized Q-POSS and water have dominating peaks at 2850, 2910, 2970, 3200 and 3500 cm^{-1}. They have been assigned to CH_2 symmetric stretching, CH_2 asymmetric stretching, CH_3 asymmetric stretching of the Q-POSS, O-H stretching signals in "ice-like" water, and in "liquid-like" water, respectively.[29, 31, 32, 44, 45] The ssp spectra collected from the interfaces between PDMS incorporated with low extent of quaternized Q-POSS and water have dominating peaks at 2850, 2970, 3200 and 3500 cm^{-1}, respectively. They were assigned to CH_2 symmetric stretching, CH_2 asymmetric stretching, CH_3 asymmetric stretching of the Q-POSS, O-H stretching signals in "ice-like" water, and in "liquid-like" water, respectively.

It has been shown that positively charged surfaces can order the interfacial water molecules at a neutral pH, indicated by SFG water O-H stretching signals at around 3200 and 3400 cm^{-1}, with a stronger peak at 3200 cm^{-1}.[48, 49] In this system, the quaternized

nitrogen atoms are surrounded by alkyl groups. These alkyl groups can either surround the nitrogen, shielding the charges leading to a weak water signal, or fold back which exposes the charged nitrogen atoms to water to generate a strong water signal. SFG spectra collected here at the polymer/water interfaces all show very strong SFG water signal, suggesting that the charged quaternized nitrogen atoms are exposed.

PDMS samples with high extent of quaternized Q-POSS generated stronger CH_2 signals than that of PDMS samples with low extent of quaternized Q-POSS. It is speculated that this is due to the higher surface concentration of the R groups attached to nitrogen or more gauche defects in the QAS chains in the high extent of quaternized Q-POSS versus lower quaternized Q-POSS. All four SFG spectra have weaker CH_3 signals than CH_2 signals indicating a lack of ordered CH_3 groups present on the surface and a larger contribution of gauche defects. These results confirm that the alkyl chains fold back and the resulting surfaces are positively charged nitrogen atoms.

Surface Structures in Artificial Sea Water (ASW). SFG spectra were also collected from the material/ASW interfaces (Figure 2.5c). The spectral signatures and the relative intensities of different peaks are slightly different between PDMS with high extent of quaternized Q-POSS and that with low extent. These differences indicate that the Q-POSS molecules, especially the alkyl chains that are attached to quaternized nitrogen atoms, behave differently on the polymer surfaces in ASW between PDMS with high extent of quaternized Q-POSS and that with low extent. The alkyl chain length, on the other hand, does not play a noticeable role in determining the interfacial structure.

The SFG ssp spectra collected from the interface between PDMS incorporated with high extent of quaternized Q-POSS and ASW have dominating peaks at 2850, 2880,

2915, and 2940 cm^{-1}, which can be attributed to CH_2 symmetric stretching, CH_3 symmetric stretching, CH_2 asymmetric stretching, and CH_3 Fermi resonance of the Q-POSS, respectively. The ssp spectra collected from PDMS incorporated with low extent of quaternized Q-POSS/water interface have dominating peaks at 2850, 2880, 2900, 2940, and 2965 cm^{-1}, which were assigned to CH_2 symmetric stretching, CH_3 symmetric stretching, PDMS Si-CH_3 symmetric stretching, CH_3 Fermi resonance, and CH_3 asymmetric stretching of the Q-POSS, respectively.

Previous publications have shown that when alkyl chains are well-ordered on surfaces, the methylene groups generate minimal SFG signals while the methyl end groups generate large SFG signals.[22, 50] Comparing the SFG ssp spectra collected from the ASW interface with PDMS incorporated with high extent of quaternized Q-POSS and with low extent of quaternized Q-POSS, CH_3 contributions are slightly larger in materials with low extent of quaternization while the CH_2 contributions are slightly larger in materials with high extent of quaternization. This shows that the alkyl chains attached to lower quaternized Q-POSS extend out more while the alkyl chains in the highly quaternized Q-POSS are folded back. We believe that the ions in the ASW minimize the positive charge on quaternized Q-POSS surface and provide more freedom to the alkyl chains. Results here differ from the scenario observed on polymer surfaces in pure water.

Antimicrobial Activity. It has been shown that for the Q-POSS-incorporated PDMS materials, the coatings incorporating Q-POSS with lowest extent of quaternization displayed antimicrobial activity while analogous coatings produced using Q-POSS possessing the highest extent of quaternization showed no antimicrobial activity.[19]

Combining the SFG results shown above, it is believed that the extended alkyl chains on the lower quaternized Q-POSS surfaces are actively used in killing bacteria. This proposed method of action has been illustrated in Figure 2.6. The alkyl chains in the highly quaternized Q-POSS consequently have less freedom of movement and lower bacteria accessibility while those in the lower quaternized Q-POSS can extend readily.

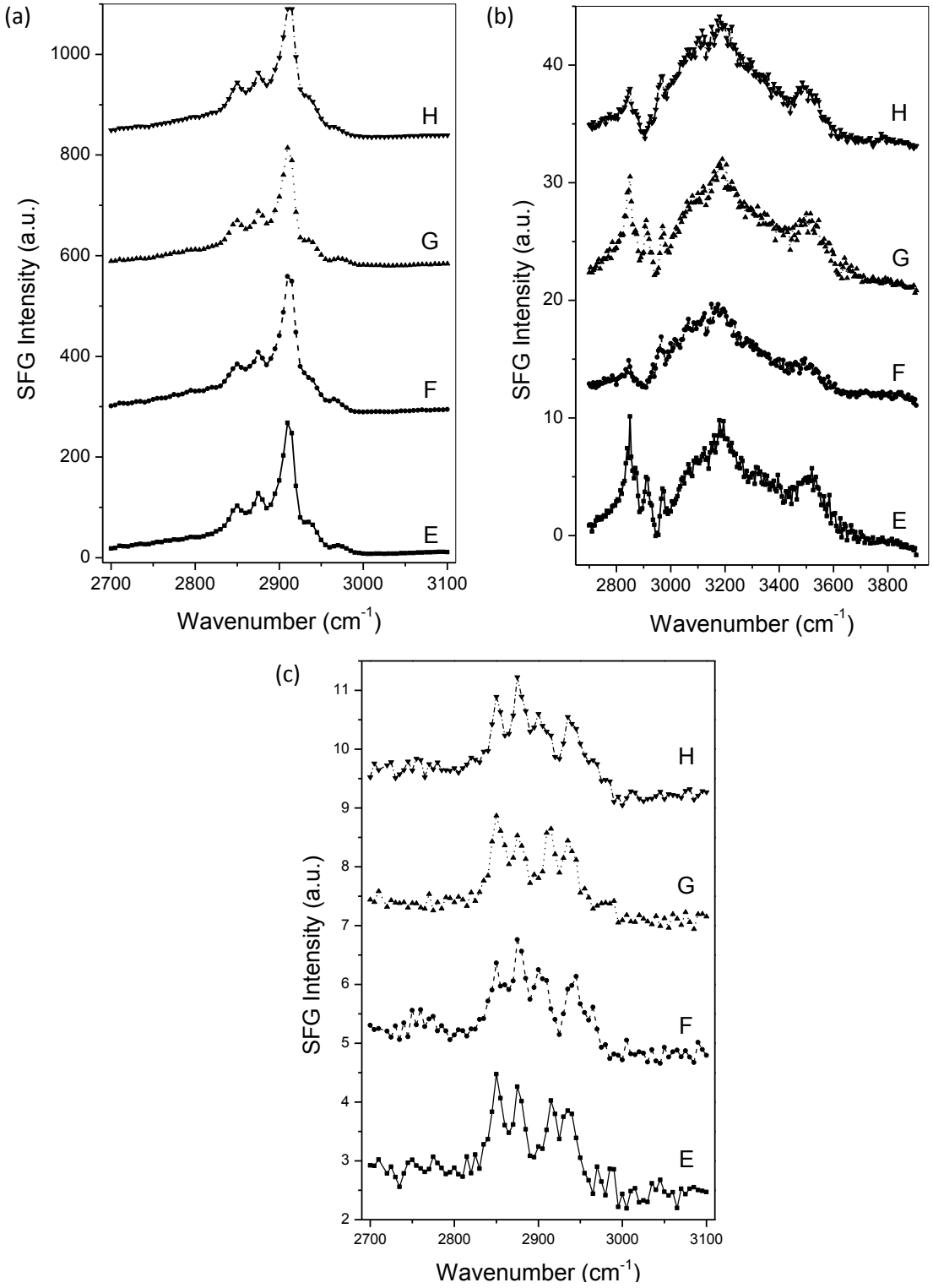

Figure 2.5 SFG ssp spectra collected from Q-POSS-incorporated PDMS materials in (a) air, (b) water, and (c) ASW. The four samples are (E) R=$C_{16}H_{33}$-, high extent of quaternization; (F) R=$C_{16}H_{33}$-, low extent of quaternization; (G) R=$C_{18}H_{37}$-, high extent of quaternization; (H) R=$C_{18}H_{37}$-, low extent of quaternization.

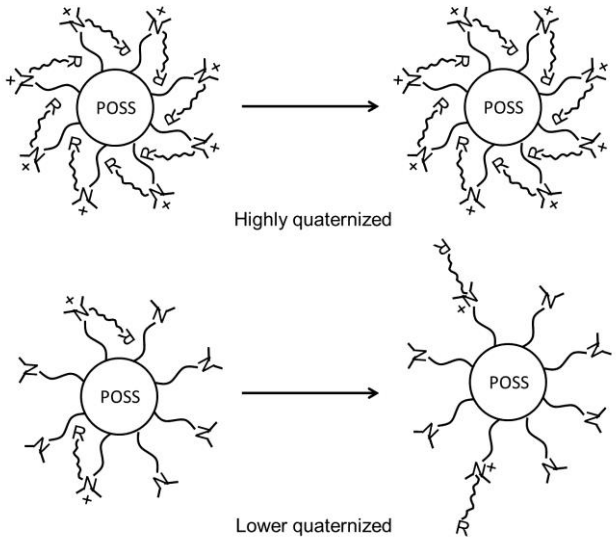

Figure 2.6 Schematic showing the surface structures of Q-POSS-incorporated PDMS systems in aqueous environment. Different extents of quaternization result in different mobility of the alkyl chains.

2.4 CONCLUSION

In this chapter, SFG has been applied to investigate surface structures of PDMS materials incorporated with QAS-based biocides *in situ* for FR and antifouling coatings. Two different PDMS systems, one tethered with QAS and one incorporated with Q-POSS, were studied in air, water and artificial sea water. Interestingly, in the QAS tethered PDMS system, polymers prepared from TES-QAS resulted in better antifouling coatings. SFG studies showed that they generated stronger signals from alkyl groups in aqueous environments, especially in ASW. This shows that the different reaction dynamics of methoxysilane and ethoxysilane can lead to different surface structures of QAS-tethered PDMS, resulting in different antifouling activities. In addition, coatings prepared from QAS-tethered 18K-PDMS generated stronger SFG signals from the QAS alkyl chains than those prepared from the QAS-tethered 49K-PDMS because 18K-PDMS

could provide more end groups for QAS tethering. In the Q-POSS-PDMS system, materials with a lower extent of quaterniztion exhibited better anti-biofouling properties. Our SFG studies indicated that PDMS with low quaternization generated stronger signals from methyl end groups of the alkyl chains attached to Q-POSS. This shows that a lower degree of quaternization offers more freedom for the alkyl groups to extend and penetrate into microbial membranes, thereby neutralizing the microorganisms upon contact.

In summary, the degree of extension of the alkyl chains in QAS plays an important role in preventing bacterial biofilm growth. The correlations made between the SFG studies and antifouling properties in this study also agreed well with our previous studies on PDMS materials incorporated with QAS possessing different alkyl chain lengths.[28] These studies provide a general set of guidelines to follow when designing PDMS materials incorporated with QAS to generate antifouling coatings: The QAS groups need to segregate to the surface and the QAS alkyl chains need to extend fully into the aqueous environment. As a result, the long alkyl chains can penetrate into the cell membrane and kill microorganisms.

2.5 REFERENCES

(1) Acker, R. F., *Proceedings of the Third International Congress on Marine Corrosion and Fouling, October 2-6, 1972, Gaithersburg, Maryland*. Northwestern University Press: Evanston, Ill., 1973.

(2) Dexter, S. C.; Sullivan, J. D.; Williams, J.; Watson, S. W., Influence of Substrate Wettability on the Attachment of Marine Bacteria to Various Surfaces. *Appl. Microbiol.* **1975,** *30*, 298-308.

(3) Dickie, R. A.; Meeting, A. S.; Society, A., *Proceedings of the 21st Annual Meeting of the Adhesion Society: Savannah, Georgia, February 22 - 25, 1998*. Adhesion Society: 1998.

(4) Brady, R. F.; Singer, I. L., Mechanical Factors Favoring Release from Fouling Release Coatings. *Biofouling* **2000,** *15*, 73-81.

(5) Sun, Y. J.; Guo, S. L.; Walker, G. C.; Kavanagh, C. J.; Swain, G. W., Surface Elastic Modulus of Barnacle Adhesive and Release Characteristics from Silicone Surfaces. *Biofouling* **2004,** *20*, 279-289.

(6) Lambropoulou, D. A.; Sakkas, V. A.; Albanis, T. A., Analysis of Antifouling Biocides Irgarol 1051 and Sea Nine 211 in Environmental Water Samples Using Solid-Phase Microextraction and Gas Chromatography. *J. Chromatogr. A* **2002,** *952*, 215-227.

(7) Pant, R. R.; Fulmer, P. A.; Harney, M. B.; Buckley, J. P.; Wynne, J. H., Synthesis and Biocidal Efficacy of Self-Spreading Polydimethylsiloxane Oligomers Possessing Oxyethylene-Functionalized Quaternary Ammoniums. *J. Appl. Polym. Sci.* **2009,** *113*, 2397-2403.

(8) Tiller, J. C.; Sprich, C.; Hartmann, L., Amphiphilic Conetworks as Regenerative Controlled Releasing Antimicrobial Coatings. *J. Controlled Release* **2005,** *103*, 355-367.

(9) Majumdar, P.; Lee, E.; Ward, K.; Chisholm, B. J., Incorporation of Quaternary Ammonium Salts in Silanol Terminated Polydimethylsiloxane Using a High-Throughput Combinatorial Approach. *Abstr. Papers Am. Chem. Soc.* **2007,** *233*.

(10) Thomas, J.; Choi, S. B.; Fjeldheim, R.; Boudjouk, P., Silicones Containing Pendant Biocides for Antifouling Coatings. *Biofouling* **2004,** *20*, 227-236.

(11) Ye, S. J.; McClelland, A.; Majumdar, P.; Stafslien, S. J.; Daniels, J.; Chisholm, B.; Chen, Z., Detection of Tethered Biocide Moiety Segregation to Silicone Surface Using Sum Frequency Generation Vibrational Spectroscopy. *Langmuir* **2008,** *24*, 9686-9694.

(12) McBain, A. J.; Ledder, R. G.; Moore, L. E.; Catrenich, C. E.; Gilbert, P., Effects of Quaternary-Ammonium-Based Formulations on Bacterial Community Dynamics and Antimicrobial Susceptibility. *Appl. Environ. Microbiol.* **2004,** *70*, 3449-3456.

(13) Hazzizalaskar, J.; Helary, G.; Sauvet, G., Biocidal Polymers Active by Contact .4. Polyurethanes Based on Polysiloxanes with Pendant Primary Alcohols and Quaternary Ammonium Groups. *J. Appl. Polym. Sci.* **1995,** *58*, 77-84.

(14) Snow, S. A., Synthesis, Characterization, Stability, Aqueous Surface-Activity, and Aqueous-Solution Aggregation of the Novel, Cationic Siloxane Surfactants $(Me_3sio)_2si(Me)$-$(Ch_2)_3{}^{+}Nme_2(Ch_2)_2or\ x^{-}$ (R=H, C(O)Me, C(O)Nh(Ph) X=Cl, Br, I, No_3, $Meoso_3$). *Langmuir* **1993,** *9*, 424-430.

(15) Hugo, W. B., The Mode of Action of Antibacterial Agents. *J. Appl. Bacteriol.* **1967,** *30*, 17-50.

(16) Gottenbos, B.; van der Mei, H. C.; Klatter, F.; Nieuwenhuis, P.; Busscher, H. J., In Vitro and in Vivo Antimicrobial Activity of Covalently Coupled Quaternary Ammonium Silane Coatings on Silicone Rubber. *Biomaterials* **2002,** *23*, 1417-1423.
(17) Tashiro, T., Antibacterial and Bacterium Adsorbing Macromolecules. *Macromol. Mater. Eng.* **2001,** *286*, 63-87.
(18) Majumdar, P.; Lee, E.; Gubbins, N.; Christianson, D. A.; Stafslien, S. J.; Daniels, J.; VanderWal, L.; Bahr, J.; Chisholm, B. J., Combinatorial Materials Research Applied to the Development of New Surface Coatings Xiii: An Investigation of Polysiloxane Antimicrobial Coatings Containing Tethered Quaternary Ammonium Salt Groups. *J. Comb. Chem.* **2009,** *11*, 1115-1127.
(19) Majumdar, P.; Lee, E.; Gubbins, N.; Stafslien, S. J.; Daniels, J.; Thorson, C. J.; Chisholm, B. J., Synthesis and Antimicrobial Activity of Quaternary Ammonium-Functionalized Poss (Q-Poss) and Polysiloxane Coatings Containing Q-Poss. *Polymer* **2009,** *50*, 1124-1133.
(20) Stafslien, S.; Daniels, J.; Chisholm, B.; Christianson, D., Combinatorial Materials Research Applied to the Development of New Surface Coatings Iii. Utilisation of a High-Throughput Multiwell Plate Screening Method to Rapidly Assess Bacterial Biofilm Retention on Antifouling Surfaces. *Biofouling* **2007,** *23*, 37-44.
(21) Stafslien, S. J.; Daniels, J.; Bahr, J. A.; Mayo, B.; Chisholm, B. J.; Pieper, R. J.; Webster, D.; Ribeiro, E., Automated Software Tool for the Rapid Evaluation of Bacterial Biofilm Retraction on Rouling-Release Marine Coatings. *Abstr. Papers Am. Chem. Soc.* **2007,** *233*.
(22) Ye, S. J.; Majumdar, P.; Chisholm, B.; Stafslien, S.; Chen, Z., Antifouling and Antimicrobial Mechanism of Tethered Quaternary Ammonium Salts in a Cross-Linked Poly(Dimethylsiloxane) Matrix Studied Using Sum Frequency Generation Vibrational Spectroscopy. *Langmuir* **2010,** *26*, 16455-16462.
(23) Ye, S.; Noda, H.; Morita, S.; Uosaki, K.; Osawa, M., Surface Molecular Structures of Langmuir-Blodgett Films of Stearic Acid on Solid Substrates Studied by Sum Frequency Generation Spectroscopy. *Langmuir* **2003,** *19*, 2238-2242.
(24) Anglin, T. C.; Conboy, J. C., Lateral Pressure Dependence of the Phospholipid Transmembrane Diffusion Rate in Planar-Supported Lipid Bilayers. *Biophys J* **2008,** *95*, 186-193.
(25) Bain, C. D., Sum-Frequency Vibrational Spectroscopy of the Solid-Liquid Interface. *J. Chem. Soc., Faraday Trans.* **1995,** *91*, 1281-1296.
(26) Belkin, M. A.; Shen, Y. R., Non-Linear Optical Spectroscopy as a Novel Probe for Molecular Chirality. *Int. Rev. Phys. Chem.* **2005,** *24*, 257-299.
(27) Chen, Z., Understanding Surfaces and Buried Interfaces of Polymer Materials at the Molecular Level Using Sum Frequency Generation Vibrational Spectroscopy. *Polym. Int.* **2007,** *56*, 577-587.
(28) Dreesen, L.; Humbert, C.; Sartenaer, Y.; Caudano, Y.; Volcke, C.; Mani, A. A.; Peremans, A.; Thiry, P. A.; Hanique, S.; Frere, J. M., Electronic and Molecular Properties of an Adsorbed Protein Monolayer Probed by Two-Color Sum-Frequency Generation Spectroscopy. *Langmuir* **2004,** *20*, 7201-7207.
(29) Gopalakrishnan, S.; Liu, D. F.; Allen, H. C.; Kuo, M.; Shultz, M. J., Vibrational Spectroscopic Studies of Aqueous Interfaces: Salts, Acids, Bases, and Nanodrops. *Chem. Rev.* **2006,** *106*, 1155-1175.
(30) Kim, C.; Gurau, M. C.; Cremer, P. S.; Yu, H., Chain Conformation of Poly(Dimethyl Siloxane) at the Air/Water Interface by Sum Frequency Generation. *Langmuir* **2008,** *24*, 10155-10160.
(31) Moore, F. G.; Richmond, G. L., Integration or Segregation: How Do Molecules Behave at Oil/Water Interfaces? *Acc. Chem. Res.* **2008,** *41*, 739-748.

(32) Shen, Y. R.; Ostroverkhov, V., Sum-Frequency Vibrational Spectroscopy on Water Interfaces: Polar Orientation of Water Molecules at Interfaces. *Chem. Rev.* **2006,** *106*, 1140-1154.
(33) Wang, J.; Chen, C.; Buck, S. M.; Chen, Z., Molecular Chemical Structure on Poly (Methyl Methacrylate)(PMMA) Surface Studied by Sum Frequency Generation (SFG) Vibrational Spectroscopy. *J. Phys. Chem. B* **2001,** *105*, 12118-12125.
(34) Chen, C.; Even, M. A.; Wang, J.; Chen, Z., Sum Frequency Generation Vibrational Spectroscopy Studies on Molecular Conformation of Liquid Polymers Poly(Ethylene Glycol) and Poly(Propylene Glycol) at Different Interfaces. *Macromolecules* **2002,** *35*, 9130-9135.
(35) Wang, J.; Woodcock, S. E.; Buck, S. M.; Chen, C.; Chen, Z., Different Surface-Restructuring Behaviors of Poly(Methacrylate)S Detected by SFG in Water. *J. Am. Chem. Soc.* **2001,** *123*, 9470-9471.
(36) Wang, J.; Paszti, Z.; Even, M. A.; Chen, Z., Measuring Polymer Surface Ordering Differences in Air and Water by Sum Frequency Generation Vibrational Spectroscopy. *J. Am. Chem. Soc.* **2002,** *124*, 7016-7023.
(37) Chen, C.; Even, M. A.; Chen, Z., Detecting Molecular-Level Chemical Structure and Group Orientation of Amphiphilic Peo-Ppo-Peo Copolymers at Solution/Air and Solid/Solution Interfaces by SFG Vibrational Spectroscopy. *Macromolecules* **2003,** *36*, 4478-4484.
(38) Chen, C.; Wang, J.; Chen, Z., Surface Restructuring Behavior of Various Types of Poly(Dimethylsiloxane) in Water Detected by SFG. *Langmuir* **2004,** *20*, 10186-10193.
(39) Chen, C.; Clarke, M. L.; Wang, J.; Chen, Z., Comparison of Surface Structures of Poly(Ethyl Methacrylate) and Poly(Ethyl Acrylate) in Different Chemical Environments. *Phys. Chem. Chem. Phys.* **2005,** *7*, 2357-2363.
(40) Chen, Q.; Zhang, D.; Somorjai, G.; Bertozzi, C. R., Probing the Surface Structural Rearrangement of Hydrogels by Sum-Frequency Generation Spectroscopy. *J. Am. Chem. Soc.* **1999,** *121*, 446-447.
(41) Dreesen, L.; Humbert, C.; Hollander, P.; Mani, A. A.; Ataka, K.; Thiry, P. A.; Peremans, A., Study of the Water/Poly(Ethylene Glycol) Interface by IR-Visible Sum-Frequency Generation Spectroscopy. *Chem. Phys. Lett.* **2001,** *333*, 327-331.
(42) Majumdar, P.; Crowley, E.; Htet, M.; Stafslien, S. J.; Daniels, J.; VanderWal, L.; Chisholm, B. J., Combinatorial Materials Research Applied to the Development of New Surface Coatings Xv: An Investigation of Polysiloxane Anti-Fouling/Fouling-Release Coatings Containing Tethered Quaternary Ammonium Salt Groups. *ACS Comb. Sci.* **2011,** *13*, 298-309.
(43) Gragson, D. E.; McCarty, B. M.; Richmond, G. L., Ordering of Interfacial Water Molecules at the Charged Air/Water Interface Observed by Vibrational Sum Frequency Generation. *J. Am. Chem. Soc.* **1997,** *119*, 6144-6152.
(44) Vidal, F.; Tadjeddine, A., Sum-Frequency Generation Spectroscopy of Interfaces. *Rep. Prog. Phys.* **2005,** *68*, 1095-1127.
(45) Richmond, G. L., Molecular Bonding and Interactions at Aqueous Surfaces as Probed by Vibrational Sum Frequency Spectroscopy. *Chem. Rev.* **2002,** *102*, 2693-2724.
(46) Altmann, S.; Pfeiffer, J., The Hydrolysis/Condensation Behaviour of Methacryloyloxyalkylfunctional Alkoxysilanes: Structure-Reactivity Relations. *Monatsh. Chem.* **2003,** *134*, 1081-1092.
(47) Osterholtz, F. D.; Pohl, E. R., Kinetics of the Hydrolysis and Condensation of Organofunctional Alkoxysilanes: A Review. *J. Adhes. Sci. Technol.* **1992,** *6*, 127-149.
(48) Ye, S.; Nihonyanagi, S.; Uosaki, K., pH-Dependent Water Structure at a Quartz Surface Modified with an Amino-Terminated Monolayer Studied by Sum Frequency Generation (SFG). *Chem. Lett.* **2000**, 734-735.

(49) Nihonyanagi, S.; Ye, S.; Uosaki, K., Sum Frequency Generation Study on the Molecular Structures at the Interfaces between Quartz Modified with Amino-Terminated Self-Assembled Monolayer and Electrolyte Solutions of Various pH and Ionic Strengths. *Electrochim. Acta* **2001,** *46*, 3057-3061.
(50) Chen, X.; Tang, H. Z.; Even, M. A.; Wang, J.; Tew, G. N.; Chen, Z., Observing a Molecular Knife at Work. *J. Am. Chem. Soc.* **2006,** *128*, 2711-2714.

CHAPTER 3

ANTIMICROBIAL SURFACE STUDIES— ANTIMICROBIAL PEPTIDE (AMP) IMMOBILIZATION TO DIFFERENT SURFACES

3.1 INTRODUCTION

Surface immobilization of antimicrobial peptide (AMP) molecules is important in many applications such as biosensors, implant devices and nanofabrication.[1-8] AMPs are known to be the new generation antibiotics that combat bacterial pathogens with broad-spectrum activity.[9-13] Unlike the currently available antibiotics, which are facing antibiotic resistance developed by various bacteria thus leading to a large amount of medical expenses as well as patients' deaths, AMPs have wide spectrum of activity, target specificity and low propensity for developing resistance.[14-17] The immobilization of AMPs onto a biomaterial surface not only generates biofunctional surfaces but also helps to circumvent AMPs' potential limitations such as short half-life and cytotoxicity associated with higher concentrations of soluble peptides.[1, 3, 18, 19]

The immobilization of AMPs has been realized mainly through two routes—physical adsorption, or tethering via chemical bonding.[1, 3, 20, 21] Shukla et al. incorporated AMP ponericin G1 into a layer-by-layer polyelectrolyte degradable multilayer film and reported that the film-released AMP remained active and inhibited bacteria attachment while all the AMP contained films were found to be biocompatible.[4] Soliman et al. investigated the behavior of AMP carnobacteriocin B2 on different model self-assembled

monolayers (SAMs) using molecular dynamics simulations. They indicated that hydrophobic interactions between SAM and AMPs resulted in the strongest adsorption and maintained the integrity of the peptide; electrostatic interactions, on the other hand, increased the solubility of the peptide and caused substantial changes in the conformation of the peptide.[22] To overcome the leaching and short-lifetime problems of the physical immobilized AMPs, covalently-based immobilization methods have been applied.[1, 23-27] Mixed thiolated SAM was built to covalently couple AMP Magainin I to the surface by Humblot et al. and it was shown that the bacterial adhesion was reduced, the release of peptide was minimized and the life time was prolonged.[28] In 2011, AMP Tet213 was chemically conjugated to polymer brushes by Gao et al. They found that the immobilized peptide density depended on the grafting density and the composition of the polymer brushes and they also related the peptide density with activity.[29]

To control the functions and activities of surface immobilized peptides, it is crucial to investigate the structures of these surface-immobilized peptides.[23, 27, 30-32] However, the characterization of interfacial peptides in situ at solid/liquid interface is challenging due to the lack of appropriate analytical tools.[3, 33-35] Sum Frequency Generation (SFG) vibrational spectroscopy, which is again primarily utilized in this chapter, [36] is an intrinsically powerful technique to study molecular structures and orientations at surfaces and interfaces.[33, 37-46] The observed vibrational spectra contain IR vibrational signatures of the sample medium.

It has been shown in a previous publication from our lab that the orientation of physically adsorbed AMP cecropin P1 (CP1) on a polystyrene surface and chemically bound CP1 on functionalized polystyrene was different.[31] Chemical immobilization

conditions such as CP1 concentration and solvent hydrophobicity were also examined and it was found that the higher the peptide concentration, the faster the immobilization reaction could reach equilibrium. In addition, hydrophobic environment helped α-helical formation of AMP in solution so the immobilized CP1 had a more uniform conformation.[47]

In this chapter, the surface/interface specific technique SFG, has been applied to investigate peptide immobilization process on three different surface platforms. Firstly, a polymer (maleimide functionalized polystyrene PS-MA) surface is spin coated on the substrate, and the peptide amide I signal is monitored as a function of time after the polymer surface contacting with the peptide solution. Cecropin A (1-8)-melittin (1-18) hybrid (CEME)[26, 48, 49] peptide and sheep myeloid antimicrobial peptide (SMAP)[50-53] are used as model AMPs to understand the time dependent immobilization behavior *in situ* and in real time. Secondly, a self-assembled monolayer with maleimide end groups and ethylene glycol segments was constructed on substrate surface to prevent nonspecific binding and also to increase the surface maleimide density for surface binding. CP1 was immobilized to the maleimide-terminated SAM via two different attachment points and the final orientation and conformation of the immobilized CP1 were determined. Thirdly, to improve the stability of the platform, a maleimide-functionalized polymer was deposited on the substrate by a chemical vapor deposition (CVD) method. The immobilization of CP1 to this platform was investigated.

3.2 EXPERIMENTAL

3.2.1 Materials and Sample Preparation

Potassium phosphate (monobasic and dibasic) solutions (1 M), tris(2-carboxyethyl)phosphine hydrochloride solution (TCEP, 0.5 M, pH 7.0), dichloromethane, anhydrous toluene and 2,2,2-trifluoroethanol (TFE) were all purchased from Sigma-Aldrich (Milwaukee, WI, USA) and used without further treatment. Sheep Myeloid Antimicrobial Peptide (SMAP, sequence: RGLRRLGRKIAHGVKKYGPTVLRIIRIAG, MW=3359 g/mol, ≥98%) with a cysteine residue at the C-terminus, Cecropin A (1-8)-Melittin (1-18) hybrid (CEME, sequence: KWKLFKKIGIGAVLKVLTTGLPALIS, MW=2898 g/mol, ≥98%) with a cysteine residue at the C-terminus, cecropin P1 (CP1, sequence: SWLSKTAKKLENSAKKRISEGIAIAIQGGPR, MW=3442 g/mol, ≥98%) with a cysteine residue either at the C-terminus (CP1c) or at the N-terminus (cCP1) were all synthesized by New England Peptide (Gardner, MA, USA) and used without further purification.

Right-angle CaF_2 prisms were purchased from Altos Photonics (Bozeman, MT). These CaF_2 prisms were soaked in toluene for 24 h and then sonicated in 1% Contrex^{TM} AP solution from Decon Labs (King of Prussia, PA, USA) for 1 h. The prisms were thoroughly rinsed with Millipore water (18.2 MΩ·cm) and dried under N_2. They were placed into an oxygen bench-top plasma cleaner (PE-25-JW) purchased from Plasma Etch (Carson City, NV, USA) for 4 min immediately before using.

3.2.1.1 PS-MA film preparation

(4-Maleimidobutyramidomethyl)-polystyrene (PS-MA, molecular formula shown in Figure 3.1) films were spin-coated onto clean CaF_2 prisms using a spin coater (Specialty Coating Systems, Indianapolis, Indiana, USA) from a 0.01% PS-MA/dichloromethane

solution at 1500 rpm. The polymer films were kept at room temperature for 24 h prior to SFG experiments.

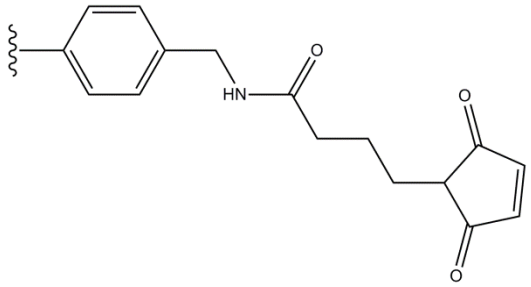

Figure 3.1 Molecular formula of PS-MA.

3.2.1.2 SAM preparation and antimicrobial activity test

A layer of 100 nm of SiO_2 was deposited onto clean CaF_2 prisms by an electron-beam deposition process using a SJ-26 Evaporator system at a pressure below 10^{-5} Torr. The deposition rate is 5 Å/s. The SiO_2 coated CaF_2 prisms were treated with the O_2 plasma cleaner for 4 min. These clean prisms were placed in freshly made 1 mM maleimide-EG4-silane (Mal-EG4, Creative PEGWorks, Winston Salem, NC, USA) in anhydrous toluene for 24 h at room temperature. The molecular structure for Mal-EG4 is shown in Figure 3.2. The functionalized prisms were rinsed with copious amounts of toluene followed by methanol and were dried under vacuum for 1 h.

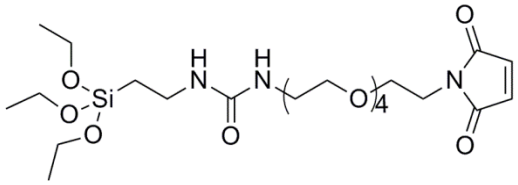

Figure 3.2 Molecular formula of maleimide-EG4-silane.

To test the antimicrobial activity of the immobilized peptide, glass slides were presoaked in Mal-EG4 solutions to prepare maleimide-functionalized SAMs for peptide immobilization. These slides were then incubated in a 1.87 μM CP1 PB solution (pH 7.2, containing 30 μM TCEP) for 2 h to immobilize the cysteine-modified CP1 onto the maleimide SAMs. After washed by DI water, these slides were then placed into a Corning 15 mL tube with 2 mL of Luria−Bertani (LB) media. Overnight-grown E. coli was inoculated at a concentration of $\sim 1 \times 10^5$ CFU/mL to each Corning tube, and tubes were placed in a 37.5 ℃ incubater with shaking at 150 rpm for 18 h.[54] After incubation, the slides were removed and rinsed with sterile 1× PBS buffer three times and then stained with appropriate concentration of fluorescent dyes, SYTO-9, and propidium iodide for 20 min in the dark according to the instructions for the LIVE/DEADBacLight bacterial viability kit (L7012, Invitrogen, Carlsbad, CA). Stained slides were observed under a fluorescence microscope (Olympus 1 × 71, Center Valley, PA) equipped with a fluorescence illumination system (X-Cite 120, EXFO) and appropriate filter sets. Images were acquired using a 60x objective lens at five random spots on slides.

3.2.1.3 CVD polymer preparation

The clean CaF_2 prisms were sent to our collaborator Professor Jeorg Lahann's group and PPX-dibromomaleimide (dibromomaleimide functionalized poly-p-xylene, structure shown in Figure 3.3) films were deposited on the prisms using chemical vapor deposition polymerization method.[55, 56] The films were controlled to be 10nm thick for optimal SFG signal generation.

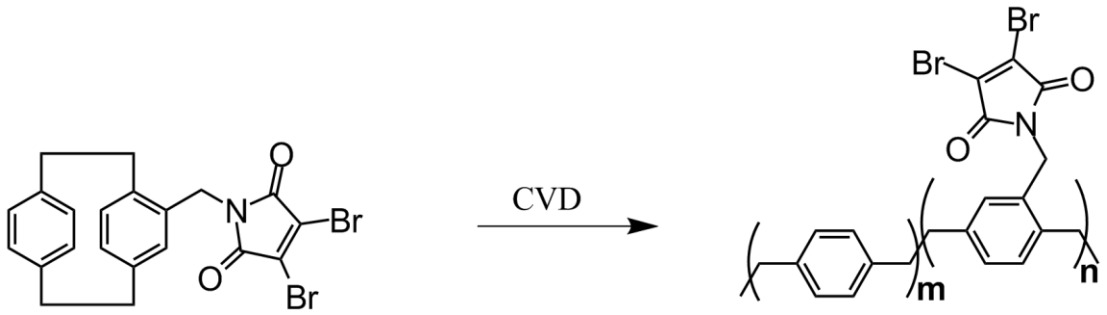

Figure 3.3 Molecular formula of PPX-dibromomaleimide.

3.2.2 Instrumentation and Experimental Setup

In this chapter a near-total-reflection SFG sample geometry with right-angle CaF_2 prism was used in which two input laser beams travel through one face of the prism and overlap on the other face with samples (shown in Figure 3.4). This surface was in contact with a reservoir of 2 mL TCEP and a mixture of pH 6.5 phosphate buffer (PB) and TFE. EDTA was added to chelate the possible Ca^{2+} ions released from CaF_2 prism in the solution. TCEP was added to reduce the disulfide bonds formation between peptide cysteine residues. Certain volume of an AMP stock solution (1 mg AMP/4 mL water, incubated with TCEP for 1 h) was injected to the reservoir to reach a desired peptide concentration. A magnetic micro-stirbar was used at a rate of 125 rpm to ensure a homogeneous concentration distribution of enzyme molecules in the subphase below the prism. After the system was equilibrated, SFG spectra with a polarization combination of ssp (s-polarized sum frequency output, s-polarized visible input, and p-polarized infrared input) and ppp were collected and used for orientation analysis. All SFG spectra were normalized according to the intensities of the input IR and visible beams.

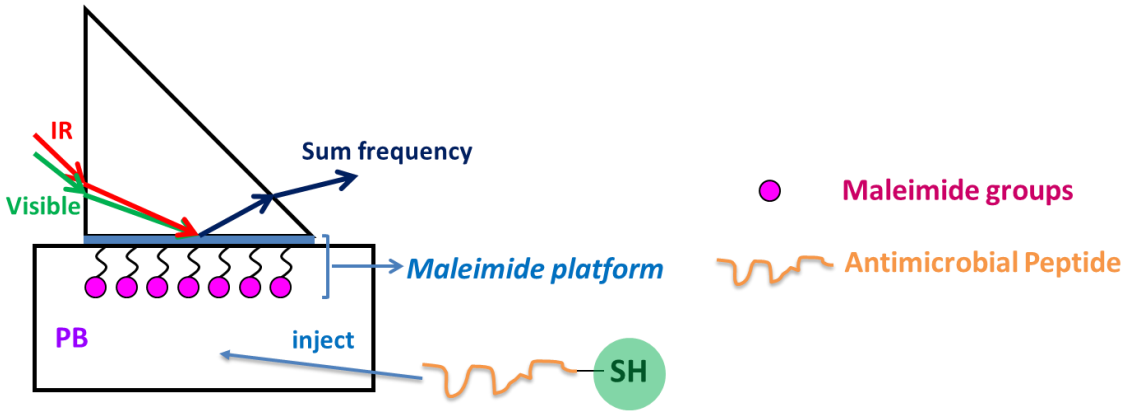

Figure 3.4 Schematics showing SFG experimental setup for immobilized peptides on surfaces.

3.3 RESULTS AND DISCUSSION

3.3.1 Immobilization Of AMP to Maleimide Functionalized Polystyrene (PS-MA) Surface

3.3.1.1 Solvent dependent behavior

Time dependent. The time-dependent SFG signal intensity at 1650 cm^{-1} under ppp polarization combination was monitored after the addition of CA-ME hybrid and SMAP (at time zero) to the subphase containing different percentages of TFE in PB (i.e. 0%, 25%, 50% and 75%), respectively (shown in Figure 3.5. A. CA-ME; B. SMAP. Time dependent signals were normalized to 1 according to the highest data point) to monitor the peptide immobilization process. It is clear in the figure that the more TFE content was present (more hydrophobic) in the subphase solution, the faster the SFG signal increased to a certain point. This was true for both CA-ME hybrid and SMAP immobilization. SFG signal detected at ~1650 cm^{-1} is contributed from the α-helical structure. In the solution with enough TFE, the peptides formed α-helical structure in the solution. Therefore when they were adsorbed/immobilized onto the surface, they were already α-helices, generating SFG signals at 1650 cm^{-1}.[47] Differently, in the solution with no or lower TFE content,

peptides adopted random coil structures in solution. Only when they were adsorbed/immobilized onto the PS-MA surface, they started to change to α-helical structure. This may take longer time compared to the high TFE content case above.[47] This explains the fast signal increase for high TFE content solution shown in Figure 3.5. The later SFG signal decrease in the high TFE case was due to the orientational change of the immobilized α-helices.[47] For the high TFE cases, the initially immobilized α-helical peptide may not have adopted optimized orientation; they would reorientate gradually due to the interactions between immobilized peptides. Differently, for the low TFE cases, the peptides formed helical structure gradually so they could adopt optimal orientation during the immobilization process. As a result, no signal decrease process was observed. These TFE-induced differences were observed in a previous publication from our group[47] which focused on the immobilization of AMP cecropin P1 to PS-MA surfaces. It is believed that the varied kinetics for AMPs immobilizing in solutions with different hydrophobicity might be a general observation.

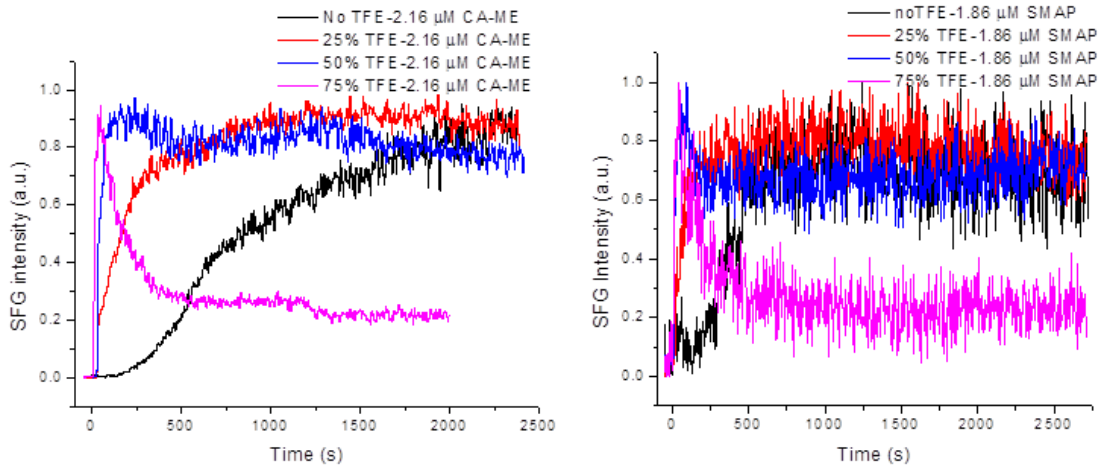

Figure 3.5 SFG time-dependent signal collected at 1650 cm^{-1} for CA-ME (left) and SMAP (right) when contacting PS-MA surfaces in different solvent composition (Black: 100% PB; Red: 25% TFE in PB; Blue: 50% TFE in PB; Pink: 75% TFE in PB)

Orientation of the immobilized peptide. SFG spectra were collected from the interface between PS-MA and AMP in solutions with different percentages of TFE in PB (i.e. 0%, 25%, 50% and 75%) using both ssp and ppp polarization combinations after the immobilization/reorientation reached an equilibrium state (as shown by a plateau on SFG time dependent signal for each case). A medium concentration of peptide was used in solution. The resulting spectra are shown in Figures 3.6 and 3.7. A Lorentzian function (Equation. 1.17) was used to fit these SFG spectra. The spectra are dominated by a peak at ~1650 cm^{-1}, indicating that the interfacial peptides are predominantly α-helical. Their signal strength ratio (χ_{ppp}/χ_{ssp}) can be calculated from the fitting parameters of the α-helical peak. For the four solvents used in this experiment, the ratios of CA-ME were measured to be 1.31, 1.55, 1.69 and 1.85 in 0%, 25%, 50% and 75% of TFE in PB, respectively. Using the measured ratios, the interfacial orientation of the immobilized peptide can be deduced (shown in Figure 3.8) if we assume a delta orientation distribution.[47] For CA-ME immobilized in solution without TFE, the ratio was found to not fall in the range for α-helical molecules with a delta orientation distribution. As previously discussed, the immobilized peptide molecules may have multiple orientations due to the fact that they needed to restructure themselves from predominantly random structures in PB to α-helices and during this process both chemical immobilization and physical adsorption occured.[46, 47] For CA-ME immobilized in the other three solvents with TFE, it was found that the more hydrophobic the solvent was, the more the peptides were lying down. TFE here promoted the fast formation of α-helical structures of the peptide which simplified the immobilization process so the immobilized peptide adopted a more uniform orientation than those in PB. The more lying down orientation for the

higher TFE content case also agrees with the SFG signal decrease as a function of time, which was discussed in the previous section. The same trend was found for the other AMP SMAP which had measured ratios in these four solvents to be 1.18, 1.54, 1.52 and 1.75, respectively. Based on these results and the similar observations for CP1 immobilization we published, it implies that higher hydrophobicity induces a more lying down orientation of immobilized AMPs might hold true for all AMPs.

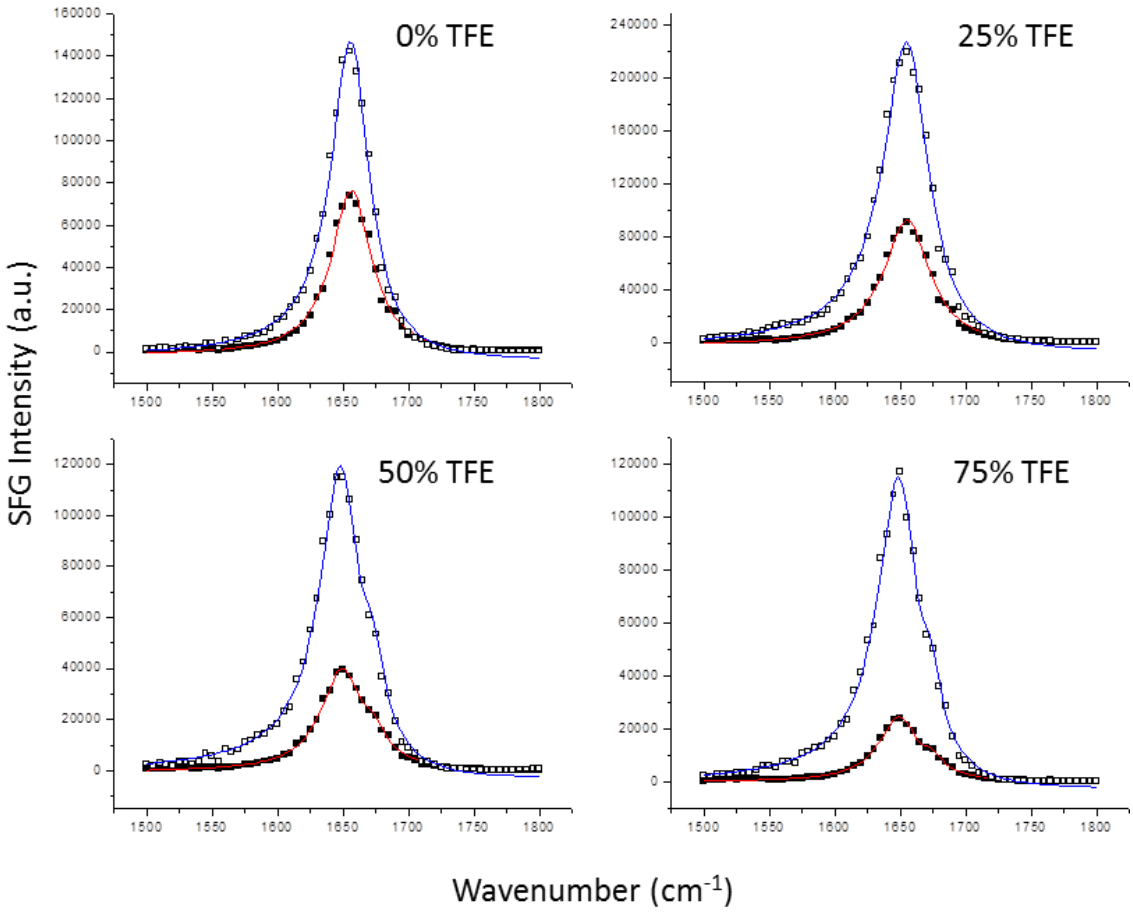

Figure 3.6 SFG ssp (red, filled squares) and ppp (blue, open squares) spectra collected from the immobilized CA-ME at the PS-MA/solution interface with different solvent compositions. Squares: experimental data; lines: fitting results.

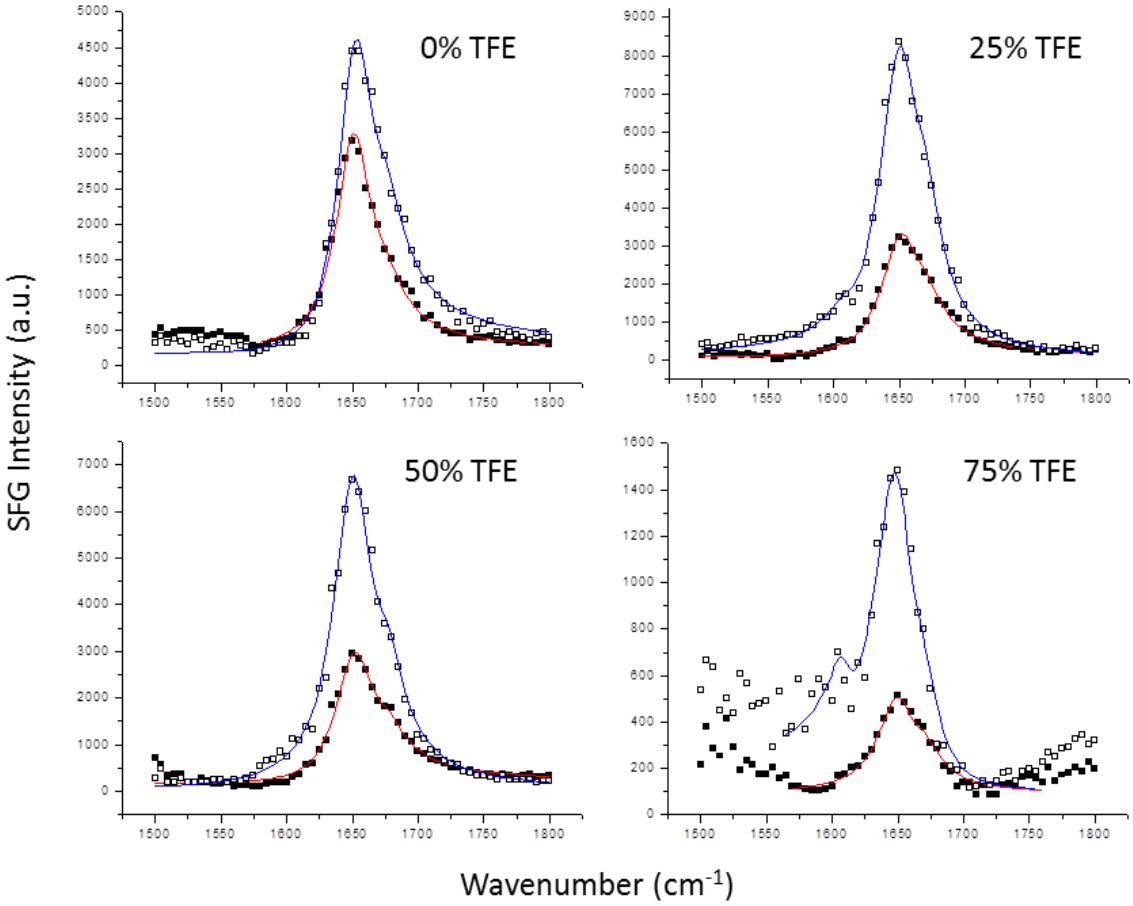

Figure 3.7 SFG ssp (red, filled squares) and ppp (blue, open squares) spectra collected from the immobilized SMAP at the PS-MA/solution interface with different solvent compositions. Squares: experimental data; lines: fitting results.

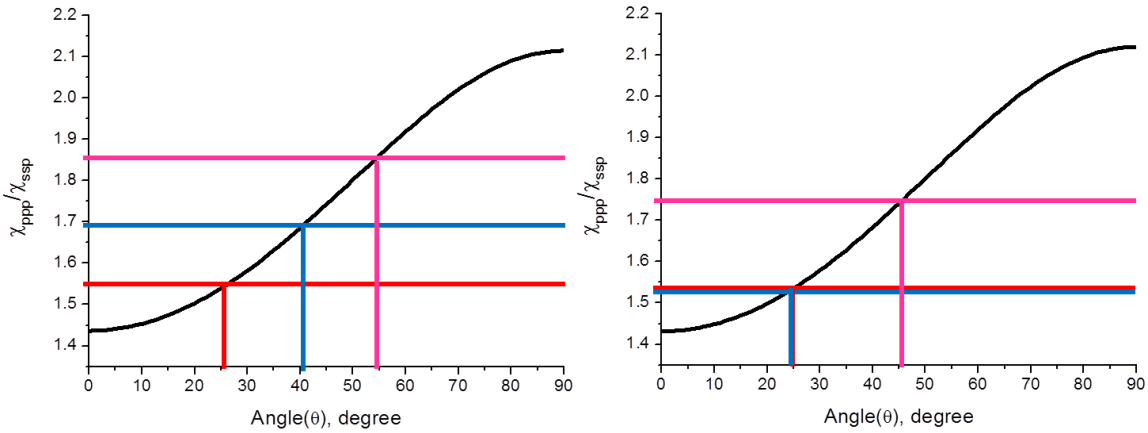

Figure 3.8 Relations between the SFG susceptibility tensor component ratio χ_{ppp}/χ_{ssp} and the orientation angle for CA-ME (left) and SMAP (right) assuming a delta orientation distribution. The colored plots showed the deduced orientations for AMPs immobilized in different solvent compositions (Black: 100% PB; Red: 25% TFE in PB; Blue: 50% TFE in PB; Pink: 75% TFE in PB)

3.3.1.2 Peptide concentration dependent behavior

Time dependent. The SFG signal intensity at 1650 cm^{-1} under ppp polarization combination was monitored after the addition of different amounts of CA-ME hybrid (0.72, 2.16 or 6.48 μM final concentrations) or SMAP (0.62, 1.86 or 5.58 μM final concentrations) at time zero to PB with or without TFE to reach different final peptide concentrations (shown in Figure 3.9. A. without TFE; B. with 50% TFE. Signal intensities were normalized to 1 according to the highest data point for comparison purposes). For peptides immobilized in a pure PB environment, the higher the peptide concentration, the faster the reaction reached equilibrium. This can be attributed to the stronger interaction between peptide molecules that accelerated the immobilization, α-helix formation, and reorientation.[47] We believe that, in general, for AMP immobilization in pure PB, higher peptide concentration leads to a faster immobilization process. For peptides immobilized in 50% TFE in PB, the reaction rate did not seem to be affected

significantly by the concentration of the peptides. It is believed that during the AMP immobilization, the role TFE plays as a helix inducer is more critical in the immobilization dynamics than the concentration of the peptide. Especially, in this case the immobilized peptides did not need to form helices at the interface, which may take the longest time during the whole immobilization process.

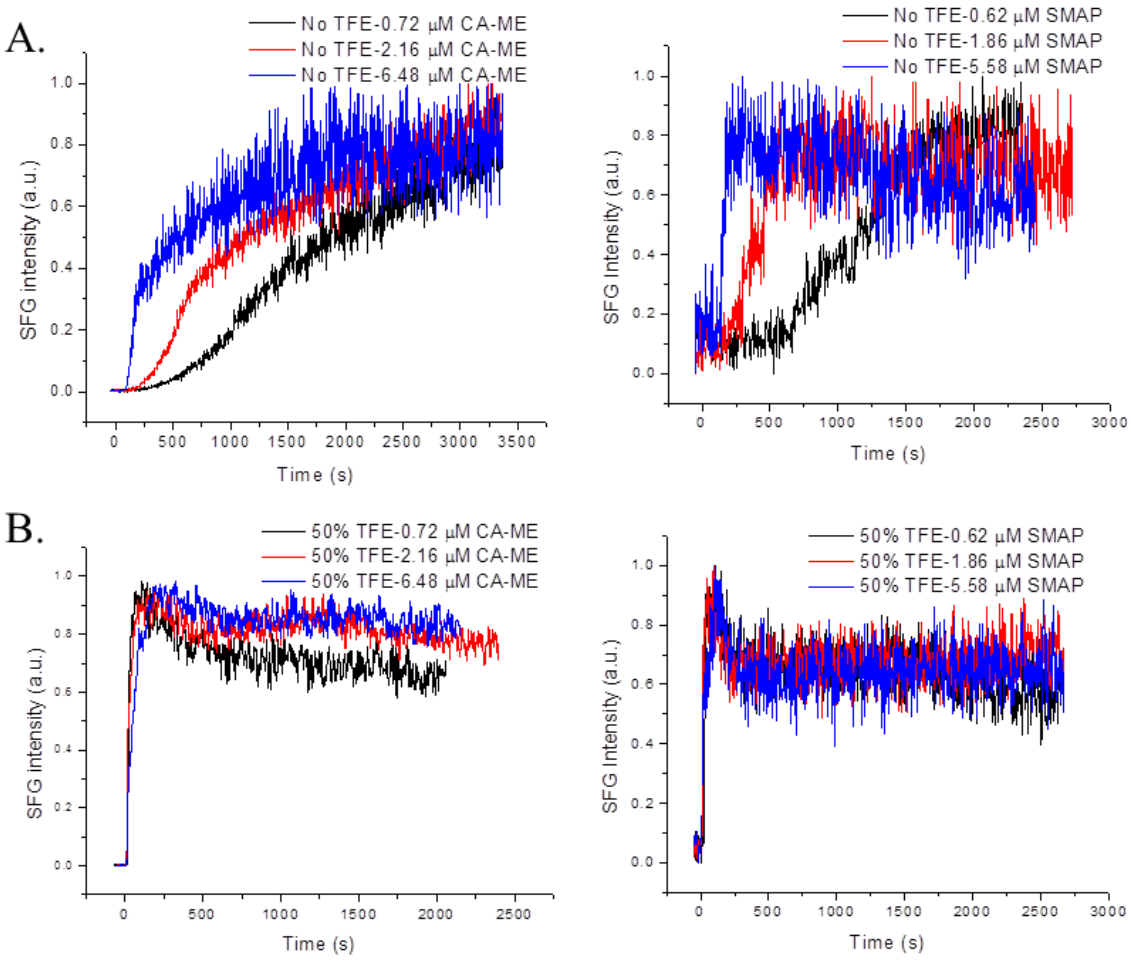

Figure 3.9 Time-dependent SFG signal at 1650 cm^{-1} collected from CA-ME (left) and SMAP (right) at the PS-MA/solution (with different peptide concentrations) interface. A: in PB without TFE; B: in PB with 50% TFE.

Orientation of the immobilized peptide. SFG spectra were collected from the PS-MA/AMP solution interface with different concentrations of CA-ME hybrid (0.72, 2.16 or 6.48 μM final concentrations) or SMAP (0.62, 1.86 or 5.58 μM final concentrations) in PB containing no or 50% TFE. The resulting spectra were all dominated by a 1650 cm^{-1} peak which was attributed to the α-helical structure. After fitting the spectra and using the parameters for the dominating 1650 cm^{-1} peak as describe above, the signal strength ratio (χ_{ppp}/χ_{ssp}) for CA-ME hybrid were calculated. For the immobilizations conducted in pure PB, both CA-ME and SMAP with varied concentrations had ratios between 1.1-1.3 which fall out of the orientation curves shown in Figure 3.8. This is indicative that the peptides immobilized in pure PB all adopted multiple orientations at the PS-MA/solution interface.[46, 47] As discussed above, this can be explained by the fact that they needed to restructure themselves from predominantly random structures in PB to α-helices during which both chemical immobilization and physical adsorption occured.[46, 47] For CA-ME immobilized in 50% TFE, the ratios were calculated to be 1,58, 1.69 and 1.61 for 0.72, 2.16 or 6.48 μM peptide solutions, respectively. χ_{ppp}/χ_{ssp} ratios for SMAP immobilized in 50% TFE were calculated to be 1.55, 1.52 and 1.54 for 0.62, 1.86 or 5.58 μM solutions, respectively. It is clear that the orientation of the peptides on the PS-MA surface were not affected by the peptide concentration used during immobilization. This again illustrates that the role of TFE to induce helical formation overwhelms peptide-peptide interactions and this also leads to a more uniform orientation of immobilized AMPs

3.3.1.3 Effect of physically adsorbed peptide

We replaced the subphase of AMP solution with Millipore water and washed the PS-MA/AMP surface thoroughly (at least 3 times) until the monitor of time dependent

spectra at 1650 cm^{-1} had no further decrease in the signal intensity. It was found that signal first decreased and then stabilized. This was believed to be the result of washing off free physically adsorbed peptide and the stabilized 1650 cm^{-1} signal indicated that there was chemically immobilized peptide present on the surface.[31] The washed surfaces were then contacted with their original solvent (without any AMPs) to investigate on the effect of free peptide on the orientation of the chemically immobilized peptide. SFG ssp and ppp spectra were collected from the interface between AMP and the solvent. They were further processed for orientation analysis as described above and the results are shown in the first two rows of Table 3.1 and Table 3.2. It was found that the orientation did not depend on the physically adsorbed peptide shown by similar χ_{ppp}/χ_{ssp} ratios before and after the washing process. This is suggesting that the orientation of the physically adsorbed peptide was the same as those that were chemically attached to PS-MA surfaces. It is believed that the orientation of the physically adsorbed peptides also rely on the solvent composition in the subphase it is contacting with. In other words, the hydrophobicity is the dominating factor in determining the orientation of the immobilized AMPs.

The impact of solvent hydrophobicity on the chemically immobilized peptide was also studied on each sample by substituting all the subphase to PB containing 50% TFE. The orientation results are shown in the last row of Table 3.1 and Table 3.2. It was concluded that the immobilized peptides were still flexible and mobile except for the 75% TFE cases. This is shown by the similar χ_{ppp}/χ_{ssp} ratios when they were brought into contact with PB containing 50% TFE. For the 75% TFE cases, on the other hand, the ratios did not change when the surfaces contacted 75% TFE compared to 50% TFE. It is

clear that the hydrophobicity of the contacting solution affects the orientation of the immobilized AMPs by interacting with the peptide residues. But if a preferred orientation (lying down) is reached by contacting a more hydrophobic solvent, the peptides may start interacting with the solid surfaces and thus the orientation cannot be restored to be more upright.

Table 3.1 χ_{ppp}/χ_{ssp} comparisons for immobilized CA-ME in different solvent compositions

Immobilization and washing conditions TFE:PB (v/v)	0:100	25:75	50:50	75:25
Before washing	*1.31 ±0.06*	*1.55 ±0.03*	*1.69 ±0.05*	*1.85 ±0.15*
After washing	*1.29 ±0.10*	*1.56 ±0.05*	*1.72 ±0.07*	*1.84 ±0.01*
Contact with 50:50 (After washing)	*1.71 ±0.07*	*1.68 ±0.03*	*1.72 ±0.07*	*1.85 ±0.07*

Table 3.2 χ_{ppp}/χ_{ssp} comparisons for immobilized SMAP in different solvent compositions

Immobilization and washing conditions TFE:PB (v/v)	0:100	25:75	50:50	75:25
Before washing	*1.20 ±0.06*	*1.54 ±0.05*	*1.52 ±0.08*	*1.75 ±0.13*
After washing	*1.29 ±0.01*	*1.55 ±0.04*	*1.53 ±0.07*	*1.77 ±0.15*
Contact with 50:50 (After washing)	*1.47 ±0.05*	*1.57 ±0.03*	*1.53 ±0.07*	*1.73 ±0.03*

3.3.2 Immobilization of CP1 to SAM Surfaces

3.3.2.1 Immobilization of CP1 via Different Attachment Points

A number of studies have been performed to test antimicrobial activity[19, 23] and lipopolysaccharides (LPS) binding ability of AMPs.[57] Uzarski and Mello found that the immobilized CP1 through the C-terminus tethered to SAM had much better LPS binding ability than peptides bound through the N-terminus. The CP1peptide has hydrophobic C-terminus and amphiphilic N-terminus. Immobilization through CP1 C-terminus or N-terminus on surface may substantially affect the peptide structure. On the basis of this assumption, we decided to determine the conformation and orientation of surface immobilized CP1 via C- and N-termini. Parameters such as conformation and orientation may have a significant impact on both LPS binding and antimicrobial activity; therefore, it is crucial to understand and characterize their interfacial behavior.

This research was carried out along with Dr. Xiaofeng Han in our group. CP1c was chemically immobilized onto Mal-EG4 SAM surface. SFG ssp and ppp spectra were collected from immobilized CP1c at the SAM/peptide PB solution interface and are shown in Figure 3.10a. In contrast with the interactions between CP1c and the PS-MA surface, which lead to both chemical immobilization and physical adsorption,[31] here SAMs with four EG segments were able to prevent physical adsorption from peptide to the surface. Figure 3.10b presents the SFG ssp and ppp spectra collected from interfacial CP1c at the SAM/PB interface after the SAM surface (with CP1c) washed several times using PB solution. Both spectral features and the signal intensities are similar to those detected from CP1c at the SAM/CP1c solution without washing. This shows that the CP1c molecules at the interface are chemically immobilized. If physically adsorbed molecules exist at the interface, they would be washed off by PB solution, leading to

reduced SFG signal intensity, which was not observed. Also, the measured signal strength ratio χ_{ppp}/χ_{ssp} from CP1c molecules at the SAM/CP1c PB solution interface leads to a delta orientation distribution, which is different from the CP1c at the PS-MA/CP1c PB solution interface. At the latter interface, the measured signal strength ratio χ_{ppp}/χ_{ssp} cannot satisfy a delta or Gaussian orientation distribution due to the presence of both chemically immobilized and physically adsorbed peptides. Here the delta orientation distribution again shows that all peptides are chemically immobilized. These results demonstrate that the EG segments in SAMs effectively prevent the physical adsorption of peptide.

The dominant peak in both ssp and ppp spectra shown in Figure 3.10 is centered at 1650 cm^{-1},which is mainly contributed from an α-helical conformation of CP1c. The SFG spectra can be fitted with two peaks: a weak peak at ~1610 cm^{-1} and a strong signal at 1650 cm^{-1}. The weak 1610 cm^{-1} peak is attributed to the CO signal of the maleimide group on the SAM surface. The signal strength ratio χ_{ppp}/χ_{ssp} can be calculated from the spectra fitting parameters of the amide I band in the ppp- and ssp-polarized SFG spectra. The deduced ratio from the chemically immobilized CP1c on Mal-EG4 SAM is 1.54, which corresponds to an orientation angle of ~35° versus the surface normal for the α-helical peptide assuming that the peptides exhibit a delta orientation distribution.

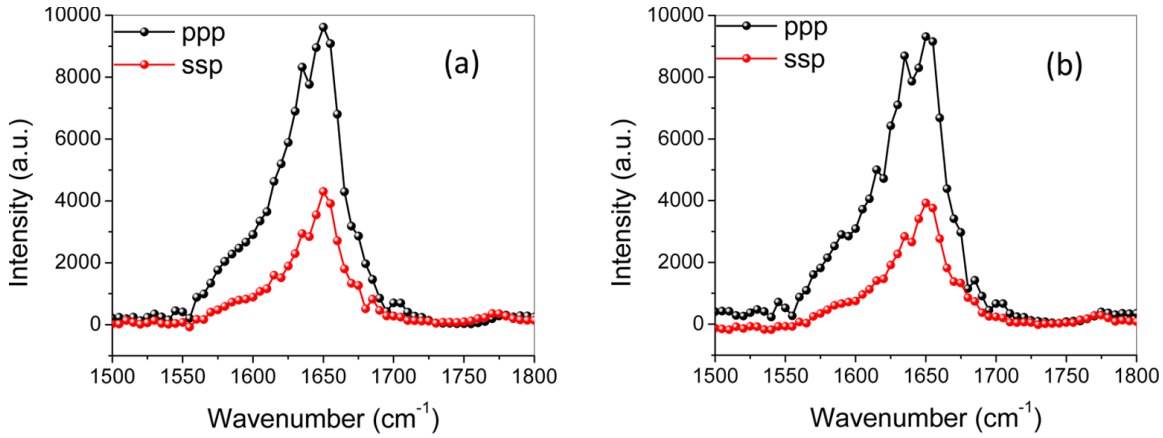

Figure 3.10 (a) SFG spectra of the Mal-EG4/CP1c PB interface. (b) SFG spectra of the Mal-EG4 SAM immobilized with CP1c in contact with a PB solution after PB wash.

Under the same conditions, cCP1 was immobilized onto Mal-EG4 SAMs. In contrast to the observation from the C-terminus binding, the cCP1 at the Mal-EG4 SAM/cCP1 PB solution interface showed a very weak SFG peak in amide I range. Figure 3.11a displays the SFG spectra of cCP1 at the Mal-EG4/cCP1 PB solution interface (open dot). The solid dots show the SFG spectra of pure Mal-EG4 SAM contacting with PB solution before adding cCP1. Again, the peak with a center at 1625 cm^{-1} is due to the maleimide group. Therefore, there is minimal difference in the observed SFG spectra upon cCP1 immobilization. No detected SFG signals from the peptide at the SAM/cCP1 solution interface may be due to no peptide binding to the maleimide-terminated SAM surface, a random coil structure of the peptide bound, or an α-helical structure lying down. The SAM surface was thrice washed then contacted with TFE-PB 50%−50% mixture solution. The amide I signal increased dramatically with its peak center at 1650 cm^{-1}, as shown in Figure 3.11b. This result indicates that cCP1 did immobilize on Mal-EG4 SAMs, but was in a random-coil structure or a lying-down helical structure and required TFE to induce

α-helical formation or orientational change. Figure 3.11c shows the ppp and ssp spectra detected from immobilized cCP1 at the Mal-EG4 SAM/TFE-PB 50%−50% solution interface. According to the spectral fitting results, the SFG signal strength ratio χ_{ppp}/χ_{ssp} is 1.94. Under this condition, the immobilized peptides have a single orientational distribution with the orientation angle of 67°. A schematic representing the cCP1 conformation change under different interface conditions (contacting with PB or TFE-PB mixture solution) is shown in Figure 3.11d. The N-terminus, having six charged residues, may have a strong interaction with the ethylene glycol groups, preventing the peptide from forming an α-helical structure. After cCP1 immobilization, the C-terminus, having hydrophobic residues, cannot favorably interact with water molecules and may induce the peptide to lie down on the surface. The different conformations/orientations of immobilized cCP1 and CP1c have been elucidated in more details using MD simulations.

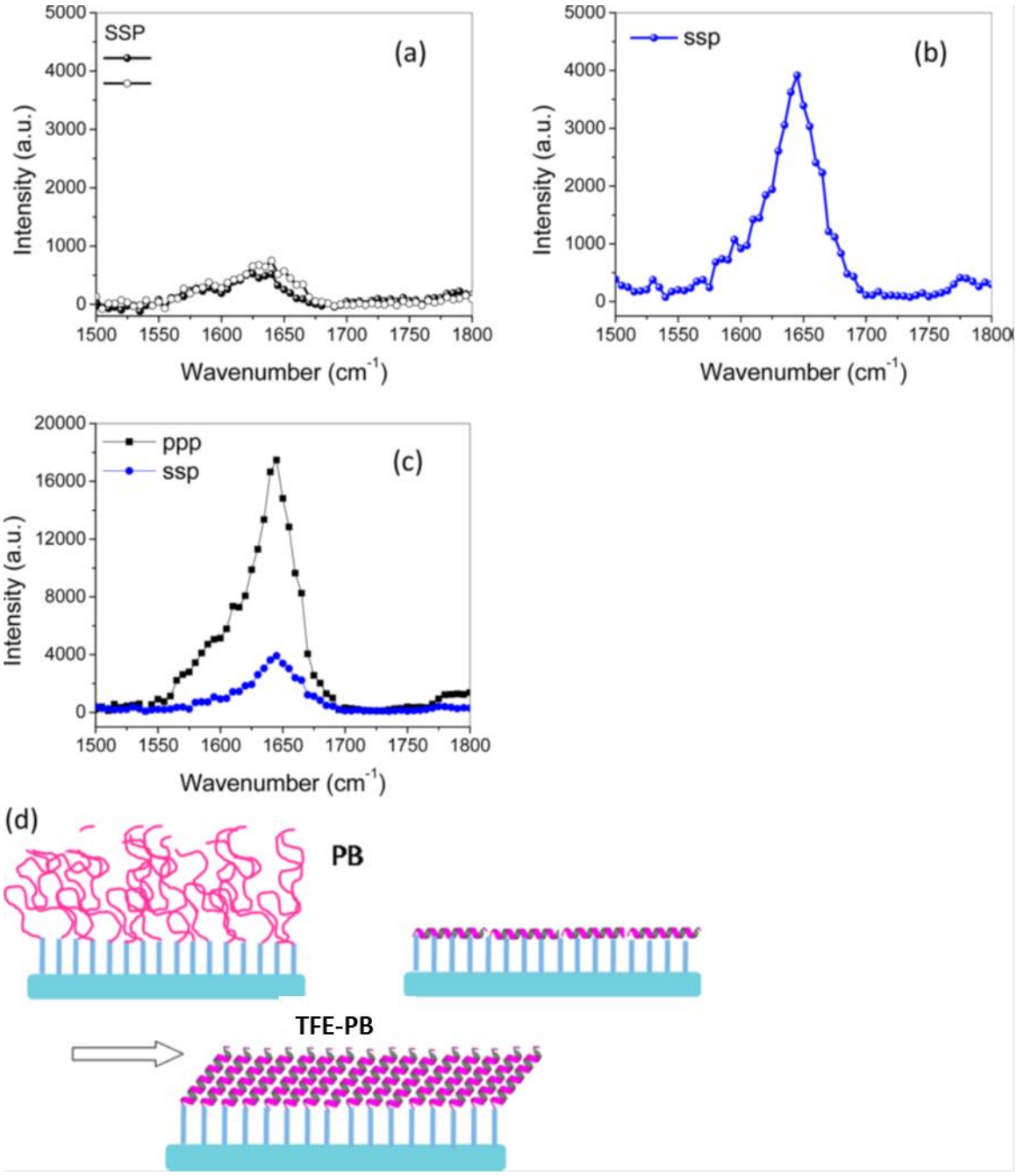

Figure 3.11 (a) SFG spectra of the Mal-EG4/PB solution interface (solid circle) and the Mal-EG4 SAM/cCP1 PB solution interface (open circle) (b) SFG spectrum of Mal-EG4 SAM immobilized with cCP1 in contact with a PB solution after PB wash. (c) SFG spectra of Mal-EG4 SAM immobilized with cCP1 in contact with a TFE-PB 50%−50% mixture solution (ppp and ssp). (d) Schematic of cCP1 conformation change at different interface conditions: contacting with PB or TFE-PB solution.

3.3.2.2 Antimicrobial properties of immobilized CP1 on SAMs

The SFG results demonstrate that different binding sites greatly affect the surface immobilized CP1 secondary structure and orientation. Solution-based antimicrobial tests were used here to investigate the relationship between immobilized peptide structure and the antimicrobial activity. Two kinds of CP1-immobilized surfaces (which were previously studied by SFG) were tested: Mal-EG4 SAM immobilized with CP1c, and Mal-EG4 SAM immobilized with cCP1. The glass slides with SAMs immobilized with CP1 were soaked in 10^5 CFU/mL E.coli containing culturing solution for 18 h at 37.5 ℃. Because the peptides were chemically immobilized on the surface of the test slides, no leaching of peptides into the solution is expected. No obvious inhibition on E. coli growth in the bacterial culture solution was observed.

We observed that the slide surfaces were attached with bacteria cells stained with the Bacterial LIVE/DEAD dyes by fluorescence microscopy. We observed the surface-attached bacteria on slides by fluorescence microscopy after bacterial cells were stained with Bacterial LIVE/DEAD staining dyes. Figure 3.12 displays fluorescence images showing bacteria on different surfaces of Mal-EG4 SAM immobilized with CP1c (a), and Mal-EG4 SAM immobilized with cCP1 (b). In these graphs, viable cells generate green, while dead or membrane-damaged cells generate red fluorescence signals. Composite figures of both alive and dead cells are shown in the left panels, whereas the right panels show only the dead cells from the corresponding image on the left. From these images, there was not a substantial difference in the numbers of attached or killed bacteria for either of the cecropin attachment sites on Mal-EG4; CP1c immobilization with an α-helical structure shows slightly better bacterial capturing/killing capability. If we assume that the CP1 peptides need to form (a standing-up) α-helical structure in the bacterial cell

membrane to capture and kill bacteria, the observation demonstrates that the immobilized peptides originally with a random-coil structure or lying-down helical structure will change into α-helical structure or change its orientation in the bacterial cell membrane to capture and kill the bacteria. The TFE contacting SFG experiments of cCP1 (shown in Figure 3.11c) demonstrated this possibility: immobilized cCP1 adopts a tilted α-helical structure.

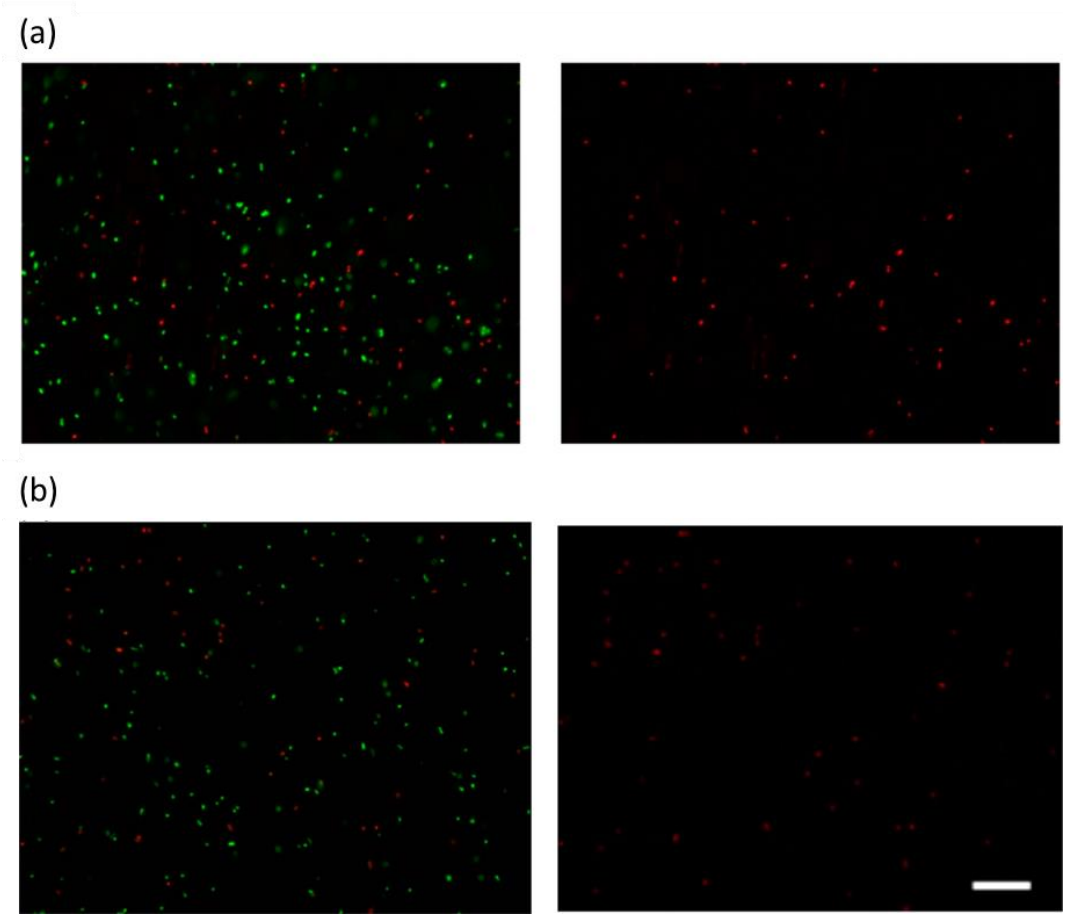

Figure 3.12 Representative fluorescence micrographs showing comparison of Mal-EG4 immobilized with (a) CP1c and (b) cCP1 after soaking in 10^5 CFU/mL *E. coli* containing 50 mM GSH for 18 h at 37.5 ℃. Bacterial cells were stained with Bacterial LIVE/DEAD staining dyes, and viable cells show green while dead or membrane damaged cells show red fluorescence in the images. Images shown in the left column contain a composite image of both alive and dead cells, whereas the right images contain only the dead cells from the corresponding images on the left. Scale bar represents 20 μm in length and applies to all images.

3.3.3 Immobilization of CP1 to Polymer Prepared by Chemical Vapor Deposition (CVD) Polymer

Professor Joerg Lahann's research group has developed a novel vapor-based surface modification technique using chemical vapor deposition (CVD) polymerization which creates a thin reactive polymeric film onto substrate surfaces. These coatings are made of poly-p-xyxlene (PPX) where different functional anchor moieties can be introduced in order to generate reactive functionalities for further surface modification.[55, 56] These films bear several advantages such as biocompatibility and excellent mechanical properties. Their compositons can be precisely controlled and they are uniform and byproducts-free. The uniformity, durability and versatile functionality make the CVD polymer coatings desired platforms for us to move on to investigate peptide immobilization after our model studies on SAMs. The functional moiety selected in this work is dibromomaleimide (structure shown in Figure 3.3). This moiety not only possesses the specific reactivity towards the thiol group in the cysteine residue, but it is also compatible with the CVD process while the regular maleimide moiety is not.

3.3.3.1 Reversible reaction between dibromomaleimide and CP1

It has been reported in previous publications that the dibromomaleimide functional group binds with protein via maleimide-thiol coupling chemistry. However, the resultant protein-maleimide products can be cleaved to regenerate the unmodified protein by the addition of a phosphine or a large excess of a disulfide bond breaker.[58, 59] As a result, before exploring the details of peptide immobilization on a dibromomaleimide CVD surface, we first investigated the reversible reaction between the peptide and dibromomaleimide.

The synthesis and characterization of the polymerization precursor was done by collaborators in Professor Lahann's group to confirm the presence of dibromomaleimide functionality by NMR, FTIR and XPS. The reactivity of the dibromomaleimide moiety towards cysteine thiols was also supported by imaging ellipsometry. My collaborators also performed an *ex situ* study on the reversibility of the reaction using XPS. In this section, SFG was employed to further examine the reaction and the reversibility *in situ* and in real time.

In the SFG experiment, the signal intensity at 1650 cm^{-1} in the amide I region was monitored which corresponds to the α-helical secondary structure in CP1c immobilized at the interface. CP1c buffer solutions (with 1:1 TCEP:CP1c to reduce possible disulfide bonds formed between CP1c molecules) was used in this study. After the PPX-dibromomaleimide surface was brought into contact with the CP1c solution, the SFG signal intensity from the CP1 α-helical structure was detected as a function of time Figure 3.13, panel A. This signal intensity increased as a function of time which indicates that the CP1c molecules were immobilized to the CVD polymer surface and formed aligned α-helical structure. In order to prove that chemical linkage did occur during the contact, the subphase was replaced at least three times by fresh buffer solution to wash off any physically adsorbed peptide.[31] The result SFG signal intensity decreased shown in Figure 3.13 panel B and according to this time dependent signal change, it is believed that certain CP1c molecules were physically adsorbed and were washed off. The rest of the CP1c molecules were chemically bound to the dibromomaleimide moieties thus could not be washed off. In panel C, an excessive amount of TCEP was added to the subphase in order to reverse the dibromomaleimide-thiol reaction. From this result, it is clear that

the chemically bound CP1c molecules were completely cleaved from the dibromomaleimide surface because the signal of the α-helical secondary structure in the amide I region decreased to zero. This was further confirmed by another washing cycle displayed in panel D which shows that not further signal decrease of the 1650 cm^{-1} signal was observed.

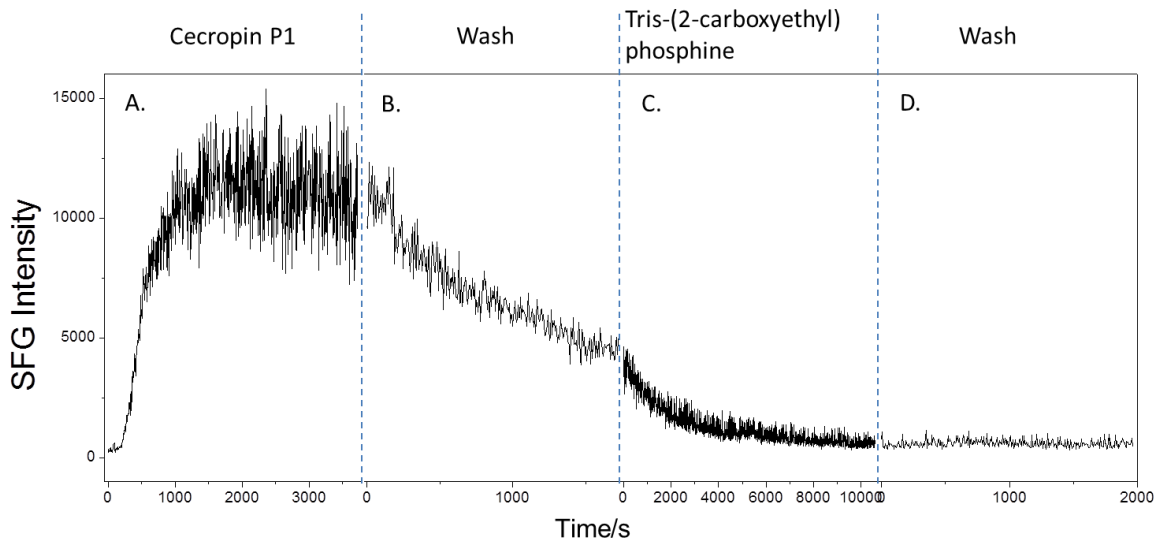

Figure 3.13 SFG time-dependent signal collected from CP1c immobilized at the PPX-dibromomaleimide/CP1c PB solution interface. A. after the addition of CP1c to the PB buffer; B. after washing the CP1c-immobilized surface with PB; C. after the addition of excessive amount of TCEP to PB; D: after final washing of the surface.

3.3.3.2 Immobilization of CP1 via different attachment points

To investigate peptide immobilization on the PPX-dibromomaleimide CVD polymer surface, CP1 was chosen as a model AMP to start with and the immobilization via either C-terminus or N-terminus was both conducted and analyzed. To avoid the effect from physically adsorbed peptide molecules, the surface was washed with fresh PB for at least three times after it was equilibrated with CP1. Data analysis was performed on these chemically bound CP1 molecules using SFG spectra taken at the amide I stretching

region. Both ssp and ppp polarization combinations were used for orientation determination.

According to the results shown in Figure 3.14 A and B, α-helical signal at 1650 cm^{-1} can be observed in ssp as well as ppp polarization combinations at both immobilized cCP1 and CP1c/PB interface after copiously washing off the physically adsorbed peptide. However, the intensities of SFG signals detected from CP1c were much higher than those from cCP1. For example, for ppp spectra, the signal intensity is more than ten times higher for CP1c than for cCP1. This difference was similar to what was observed on the Mal-EG4 SAM surface where cCP1 had a significantly lower α-helical signal compared to CP1c. This is again attributed to the stronger interaction between the peptide residues and the solid surface. The PPX-dibromomaleimide surface, compared to Mal-EG4, has no ethylene glycol segment and is more hydrophobic to favorably interact with the hydrophobic residues closer to the C-terminus. As a result, the "free" hydrophobic C-terminus of the immobilized cCP1 may tilt more towards the surface, leading to weaker signal.

After fitting the ssp and ppp spectra, it was concluded that the immobilized CP1c adopted multiple orientations and the immobilized cCP1 adopted a single orientation of about 47 °. Due to the strong 1650 cm^{-1} signal observed on CP1c/PB interface, it is likely that although they had multiple orientation but the orientations were close to the surface normal in upright positions. The cCP1, on the other hand, interacted more with the surface so the peptide molecules lied closer to the surface.

Based on the discussion about the effect of different attachment points on immobilization of peptide to both SAM and CVD polymer surfaces, it was concluded that the interaction between peptide amino acid residues (especially the amino acids near the "free terminus") and the solid surface plays an important role in determining the conformation and orientation of the immobilized peptide. This was confirmed by the molecular dynamics (MD) simulation on the immobilized CP1c and cCP1 performed by Professor Charles Brooks' research group. MD simulation results indicated that the peptide-surface interaction strongly depends on the hydrophobicity and charge properties of residues of the peptides, especially those near the two termini. Using MD simulation they also proposed a new sequence of modified cCP1 by mutating several residues (CSWLSKTAKKLENSAKKRISEG**A**A**Q**A**A**QGGPR, MW=3373 g/mol). This sequence was proven in MD simulation to help stabilize the structure and orientation of immobilized cCP1 on maleimide surfaces because it minimizes the peptide/solid surface interactions.

An SFG experiment was performed on this proposed stable cCP1 in comparison with regular cCP1. As shown in Figure 3.14C, the SFG signal contributed from α-helical structures formed at the interface increased about 4 times for stable cCP1 in comparison to regular cCP1. Fitting the ssp and ppp spectra gave us a χ_{ppp}/χ_{ssp} ratio of 1.41 which indicates that the immobilized stable cCP1 stand upright on the interface with a tilt angle of about 20°. This immobilized stable cCP1 had orientation standing more upright at the interface than the 48° deduced for regular cCP1. This is evidence to show that the proposed stable cCP1 did actually minimize the interaction between the peptide molecules with the solid maleimide surface. In theory, we believe the stable cCP1 can

yeild a better antimicrobial surface by making the peptide more readily exposable to cell membranes.

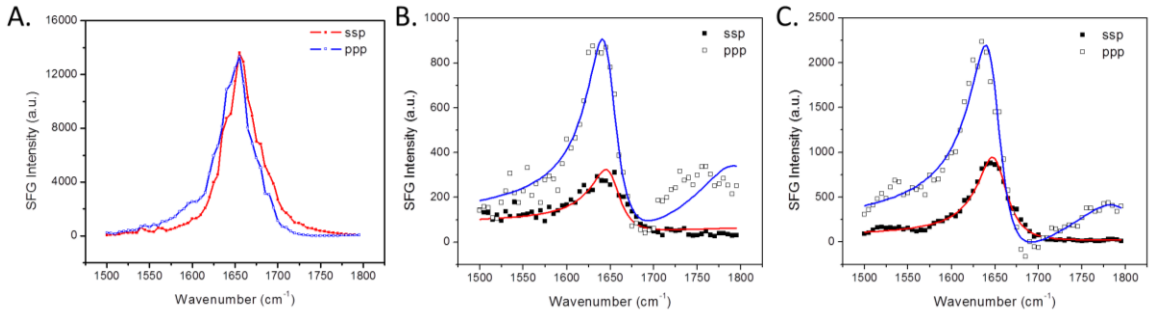

Figure 3.14 SFG ssp and ppp spectra collected from PPX-dibromomaleimide/PB interfaces with immobilization of A. CP1c; B. cCP1 and C. Stable cCP1.

3.4 SUMMARY

In this chapter, various factors associated with peptide immobilization were studied in order to understand their effects especially on the conformation and orientation of the immobilized peptide by using *in situ* surface sensitive SFG spectroscopy. Different surface platforms were constructed to improve the packing density of functional groups, controllability, and durability. On a PS-MA surface, it was found that the peptide solution concentration and solvent composition both influenced the immobilization process and the final orientation of the immobilized peptides while the physically adsorbed peptide did not affect the orientation very much. To increase the surface density of maleimide functionality and to minimize physical adsorption, a maleimide terminated SAM with an ethylene glycol segment was constructed on substrates. The immobilization of peptide through the C-terminus to Mal-EG4 showed a single orientation distribution with an orientation angle of 35 °versus surface normal while the N-terminus immobilized peptide either adopted a random-coil structure or a lying-down helical structure. To expand the

application of immobilized peptides to any substrates, a polymeric film with good mechanical properties was formed by CVD polymerization, which can be deposited on any substrates. The immobilization condition of peptides on such a CVD polymer surface was first evaluated and model peptide was immobilized on this surface through either C- or N-terminus. Again, compared to C-terminus immobilization, N-terminus immobilization resulted in a more random structured or lying-down peptide layer. MD simulations were then employed to unveil the mechanism that led to the differences of immobilization via different attachment points. It was demonstrated that the hydrophobicity of peptide residues (especially those near the free terminus) plays important roles in determining the interaction with the surface and thus the conformation and orientation of the peptide. A stable N-terminus CP1 was proposed with three of its residue mutated. Both MD simulations and SFG experiments showed that this stable cCP1 resulted in less interaction with the surface, leading to a better folded and oriented CP1 immobilized on the surface.

From these results, we have identified factors that affect peptide immobilization in general including solvent composition and peptide concentration. We further demonstrated that the same peptide immobilized using different sites can adopt varied the conformations and/or orientations, due to the different interactions between the surface and the immobilized peptide. Such interactions can be elucidated in detail using MD simulations. MD simulations can also be used to designed peptides to minimize the surface interaction to adopt desired structures, which can be tested using SFG experiments. It is believed that the study in this chapter will help to design peptides with optimized sequences to maximize the activity after the surface immobilization.

3.5 REFERENCES

(1) Costa, F.; Carvalho, I. F.; Montelaro, R. C.; Gomes, P.; Martins, M. C. L., Covalent Immobilization of Antimicrobial Peptides (AMPs) onto Biomaterial Surfaces. *Acta Biomater.* **2011,** *7*, 1431-1440.

(2) Glinel, K.; Thebault, P.; Humblot, V.; Pradier, C. M.; Jouenne, T., Antibacterial Surfaces Developed from Bio-Inspired Approaches. *Acta Biomater.* **2012,** *8*, 1670-1684.

(3) Onaizi, S. A.; Leong, S. S. J., Tethering Antimicrobial Peptides: Current Status and Potential Challenges. *Biotechnol. Adv.* **2011,** *29*, 67-74.

(4) Shukla, A.; Fleming, K. E.; Chuang, H. F.; Chau, T. M.; Loose, C. R.; Stephanopoulos, G. N.; Hammond, P. T., Controlling the Release of Peptide Antimicrobial Agents from Surfaces. *Biomaterials* **2010,** *31*, 2348-2357.

(5) Seker, U. O. S.; Demir, H. V., Material Binding Peptides for Nanotechnology. *Molecules* **2011,** *16*, 1426-1451.

(6) de La Rica, R.; Pejoux, C.; Matsui, H., Assemblies of Functional Peptides and Their Applications in Building Blocks for Biosensors. *Adv. Funct. Mater.* **2011,** *21*, 1018-1026.

(7) Cretich, M.; Damin, F.; Pirri, G.; Chiari, M., Protein and Peptide Arrays: Recent Trends and New Directions. *Biomol. Eng* **2006,** *23*, 77-88.

(8) Mannoor, M. S.; Zhang, S. Y.; Link, A. J.; McAlpine, M. C., Electrical Detection of Pathogenic Bacteria Via Immobilized Antimicrobial Peptides. *Proc. Natl. Acad. Sci. USA* **2010,** *107*, 19207-19212.

(9) Boman, H. G., Antibacterial Peptides: Basic Facts and Emerging Concepts. *J. Intern. Med.* **2003,** *254*, 197-215.

(10) Giuliani, A.; Pirri, G.; Bozzi, A.; Di Giulio, A.; Aschi, M.; Rinaldi, A. C., Antimicrobial Peptides: Natural Templates for Synthetic Membrane-Active Compounds. *Cell. Mol. Life Sci.* **2008,** *65*, 2450-2460.

(11) Giuliani, A.; Pirri, G.; Nicoletto, S. F., Antimicrobial Peptides: An Overview of a Promising Class of Therapeutics. *Cent. Eur. J. Biol.* **2007,** *2*, 1-33.

(12) Tossi, A.; Sandri, L.; Giangaspero, A., Amphipathic, Alpha-Helical Antimicrobial Peptides. *Biopolymers* **2000,** *55*, 4-30.

(13) Yeaman, M. R.; Yount, N. Y., Mechanisms of Antimicrobial Peptide Action and Resistance. *Pharmacol. Rev.* **2003,** *55*, 27-55.

(14) Guani-Guerra, E.; Santos-Mendoza, T.; Lugo-Reyes, S. O.; Teran, L. M., Antimicrobial Peptides: General Overview and Clinical Implications in Human Health and Disease. *Clin. Immunol.* **2010,** *135*, 1-11.

(15) Kulagina, N. V.; Shaffer, K. M.; Ligler, F. S.; Taitt, C. R., Antimicrobial Peptides as New Recognition Molecules for Screening Challenging Species. *Sensor Actuat B-Chem* **2007,** *121*, 150-157.

(16) Melo, M. N.; Ferre, R.; Castanho, M. A. R. B., Opinion Antimicrobial Peptides: Linking Partition, Activity and High Membrane-Bound Concentrations. *Nat. Rev. Microbiol.* **2009,** *7*, 245-250.

(17) Wimley, W. C., Describing the Mechanism of Antimicrobial Peptide Action with the Interfacial Activity Model. *ACS Chem. Biol.* **2010,** *5*, 905-917.

(18) de Azeredo, H. M. C., Nanocomposites for Food Packaging Applications. *Food Res. Int.* **2009,** *42*, 1240-1253.

(19) Bagheri, M.; Beyermann, M.; Dathe, M., Immobilization Reduces the Activity of Surface-Bound Cationic Antimicrobial Peptides with No Influence Upon the Activity Spectrum. *Antimicrob. Agents Chemother.* **2009,** *53*, 1132-1141.
(20) Kohn, M., Immobilization Strategies for Small Molecule, Peptide and Protein Microarrays. *J. Pept. Sci.* **2009,** *15*, 393-397.
(21) Statz, A. R.; Park, J. P.; Chongsiriwatana, N. P.; Barron, A. E.; Messersmith, P. B., Surface-Immobilised Antimicrobial Peptoids. *Biofouling* **2008,** *24*, 439-448.
(22) Soliman, W.; Bhattacharjee, S.; Kaur, K., Adsorption of an Antimicrobial Peptide on Self-Assembled Monolayers by Molecular Dynamics Simulation. *J. Phys. Chem. B* **2010,** *114*, 11292-11302.
(23) Bagheri, M.; Beyermann, M.; Dathe, M., Mode of Action of Cationic Antimicrobial Peptides Defines the Tethering Position and the Efficacy of Biocidal Surfaces. *Bioconjugate Chem.* **2012,** *23*, 66-74.
(24) Li, Y.; Santos, C. M.; Kumar, A.; Zhao, M. R.; Lopez, A. I.; Qin, G. T.; McDermott, A. M.; Cai, C. Z., "Click" Immobilization on Alkylated Silicon Substrates: Model for the Study of Surface Bound Antimicrobial Peptides. *Chem. Eur. J.* **2011,** *17*, 2656-2665.
(25) Shamsi, F.; Coster, H.; Jolliffe, K. A.; Chilcott, T., Characterization of the Substructure and Properties of Immobilized Peptides on Silicon Surface. *Mater. Chem. Phys.* **2011,** *126*, 955-961.
(26) North, S. H.; Wojciechowski, J.; Chu, V.; Taitt, C. R., Surface Immobilization Chemistry Influences Peptide-Based Detection of Lipopolysaccharide and Lipoteichoic Acid. *J. Pept. Sci.* **2012,** *18*, 366-372.
(27) Gregory, K.; Mello, C. M., Immobilization of Escherichia Coli Cells by Use of the Antimicrobial Peptide Cecropin P1. *Appl. Environ. Microbiol.* **2005,** *71*, 1130-1134.
(28) Humblot, V.; Yala, J. F.; Thebault, P.; Boukerma, K.; Hequet, A.; Berjeaud, J. M.; Pradier, C. M., The Antibacterial Activity of Magainin I Immobilized onto Mixed Thiols Self-Assembled Monolayers. *Biomaterials* **2009,** *30*, 3503-3512.
(29) Gao, G. Z.; Lange, D.; Hilpert, K.; Kindrachuk, J.; Zou, Y. Q.; Cheng, J. T. J.; Kazemzadeh-Narbat, M.; Yu, K.; Wang, R. Z.; Straus, S. K.; Brooks, D. E.; Chew, B. H.; Hancock, R. E. W.; Kizhakkedathu, J. N., The Biocompatibility and Biofilm Resistance of Implant Coatings Based on Hydrophilic Polymer Brushes Conjugated with Antimicrobial Peptides. *Biomaterials* **2011,** *32*, 3899-3909.
(30) Uzarski, J. R.; Tannous, A.; Morris, J. R.; Mello, C. M., The Effects of Solution Structure on the Surface Conformation and Orientation of a Cysteine-Terminated Antimicrobial Peptide Cecropin P1. *Colloids Surf., B* **2008,** *67*, 157-165.
(31) Ye, S. J.; Nguyen, K. T.; Boughton, A. P.; Mello, C. M.; Chen, Z., Orientation Difference of Chemically Immobilized and Physically Adsorbed Biological Molecules on Polymers Detected at the Solid/Liquid Interfaces in Situ. *Langmuir* **2010,** *26*, 6471-6477.
(32) Hilpert, K.; Elliott, M.; Jenssen, H.; Kindrachuk, J.; Fjell, C. D.; Korner, J.; Winkler, D. F. H.; Weaver, L. L.; Henklein, P.; Ulrich, A. S.; Chiang, S. H. Y.; Farmer, S. W.; Pante, N.; Volkmer, R.; Hancock, R. E. W., Screening and Characterization of Surface-Tethered Cationic Peptides for Antimicrobial Activity. *Chem. Biol.* **2009,** *16*, 58-69.
(33) Liu, Y. W.; Jasensky, J.; Chen, Z., Molecular Interactions of Proteins and Peptides at Interfaces Studied by Sum Frequency Generation Vibrational Spectroscopy. *Langmuir* **2012,** *28*, 2113-2121.
(34) Blondelle, S. E.; Lohner, K.; Aguilar, M. I., Lipid-Induced Conformation and Lipid-Binding Properties of Cytolytic and Antimicrobial Peptides: Determination and Biological Specificity. *BBA-Biomembranes* **1999,** *1462*, 89-108.

(35) Rigler, P.; Ulrich, W. P.; Hoffmann, P.; Mayer, M.; Vogel, H., Reversible Immobilization of Peptides: Surface Modification and in situ Detection by Attenuated Total Reflection FTIR Spectroscopy. *ChemPhysChem* **2003,** *4*, 268-275.
(36) Shen, Y. R., Surface-Properties Probed by 2nd-Harmonic and Sum-Frequency Generation. *Nature* **1989,** *337*, 519-525.
(37) Chen, X.; Clarke, M. L.; Wang, J.; Chen, Z., Sum Frequency Generation Vibrational Spectroscopy Studies on Molecular Conformation and Orientation of Biological Molecules at Interfaces. *Int. J. Mod. Phys. B* **2005,** *19*, 691-713.
(38) Boughton, A. P.; Andricioaei, I.; Chen, Z., Surface Orientation of Magainin 2: Molecular Dynamics Simulation and Sum Frequency Generation Vibrational Spectroscopic Studies. *Langmuir* **2010,** *26*, 16031-16036.
(39) Chen, X.; Chen, Z., SFG Studies on Interactions between Antimicrobial Peptides and Supported Lipid Bilayers. *BBA-Biomembranes* **2006,** *1758*, 1257-1273.
(40) Chen, X.; Tang, H. Z.; Even, M. A.; Wang, J.; Tew, G. N.; Chen, Z., Observing a Molecular Knife at Work. *J. Am. Chem. Soc.* **2006,** *128*, 2711-2714.
(41) Chen, X.; Wang, J.; Boughton, A. P.; Kristalyn, C. B.; Chen, Z., Multiple Orientation of Melittin inside a Single Lipid Bilayer Determined by Combined Vibrational Spectroscopic Studies. *J. Am. Chem. Soc.* **2007,** *129*, 1420-1427.
(42) Chen, X.; Wang, J.; Sniadecki, J. J.; Even, M. A.; Chen, Z., Probing Alpha-Helical and Beta-Sheet Structures of Peptides at Solid/Liquid Interfaces with SFG. *Langmuir* **2005,** *21*, 2662-2664.
(43) Nguyen, K. T.; King, J. T.; Chen, Z., Orientation Determination of Interfacial Beta-Sheet Structures in Situ. *J. Phys. Chem. B* **2010,** *114*, 8291-8300.
(44) Nguyen, K. T.; Le Clair, S. V.; Ye, S. J.; Chen, Z., Molecular Interactions between Magainin 2 and Model Membranes in Situ. *J. Phys. Chem. B* **2009,** *113*, 12358-12363.
(45) Nguyen, K. T.; Le Clair, S. V.; Ye, S. J.; Chen, Z., Orientation Determination of Protein Helical Secondary Structures Using Linear and Nonlinear Vibrational Spectroscopy. *J. Phys. Chem. B* **2009,** *113*, 12169-12180.
(46) Yang, P.; Ramamoorthy, A.; Chen, Z., Membrane Orientation of MSI-78 Measured by Sum Frequency Generation Vibrational Spectroscopy. *Langmuir* **2011,** *27*, 7760-7767.
(47) Han, X.; Soblosky, L.; Slutsky, M.; Mello, C. M.; Chen, Z., Solvent Effect and Time-Dependent Behavior of C-Terminus-Cysteine-Modified Cecropin P1 Chemically Immobilized on a Polymer Surface. *Langmuir* **2011,** *27*, 7042-7051.
(48) Diaz-Achirica, P.; Ubach, J.; Guinea, A.; Andreu, D.; Rivas, L., The Plasma Membrane of Leishmania Donovani Promastigotes Is the Main Target for Ca(1-8)M(1-18), a Synthetic Cecropin a-Melittin Hybrid Peptide. *Biochem. J* **1998,** *330*, 453-460.
(49) Tauro, S.; Coutinho, E.; Srivastava, S., Conformation of the Cecropin-Melittin Hybrid, Cecropin a(1-8)-Melittin (1-18) Antibacterial Peptide. *Protein Peptide Lett.* **2004,** *11*, 115-124.
(50) Dawson, R. M.; Liu, C. Q., Cathelicidin Peptide SMAP-29: Comprehensive Review of Its Properties and Potential as a Novel Class of Antibiotics. *Drug Dev. Res.* **2009,** *70*, 481-498.
(51) Neville, F.; Ivankin, A.; Konovalov, O.; Gidalevitz, D., A Comparative Study on the Interactions of SMAP-29 with Lipid Monolayers. *BBA-Biomembranes* **2010,** *1798*, 851-860.
(52) Skerlavaj, B.; Benincasa, M.; Risso, A.; Zanetti, M.; Gennaro, R., SMAP-29: A Potent Antibacterial and Antifungal Peptide from Sheep Leukocytes. *FEBS Lett.* **1999,** *463*, 58-62.
(53) Tack, B. F.; Sawai, M. V.; Kearney, W. R.; Robertson, A. D.; Sherman, M. A.; Wang, W.; Hong, T.; Lee, M. B.; Wu, H.; Waring, A. J.; Lehrer, R. I., SMAP-29 Has Two LPS-Binding Sites and a Central Hinge. *Eur. J. Biochem.* **2002,** *269*, 1181-1189.

(54) Cai, W. Y.; Wu, J. F.; Xi, C. W.; Ashe, A. J.; Meyerhoff, M. E., Carboxyl-Ebselen-Based Layer-by-Layer Films as Potential Antithrombotic and Antimicrobial Coatings. *Biomaterials* **2011,** *32*, 7774-7784.
(55) Deng, X. P.; Eyster, T. W.; Elkasabi, Y.; Lahann, J., Bio-Orthogonal Polymer Coatings for Co-Presentation of Biomolecules. *Macromol. Rapid Commun.* **2012,** *33*, 640-645.
(56) Deng, X. P.; Friedmann, C.; Lahann, J., Bio-Orthogonal "Double-Click" Chemistry Based on Multifunctional Coatings. *Angew. Chem. Int. Ed.* **2011,** *50*, 6522-6526.
(57) Uzarski, J. R.; Mello, C. M., Detection and Classification of Related Lipopolysaccharides Via a Small Array of Immobilized Antimicrobial Peptides. *Anal. Chem.* **2012,** *84*, 7359-7366.
(58) Smith, M. E. B.; Schumacher, F. F.; Ryan, C. P.; Tedaldi, L. M.; Papaioannou, D.; Waksman, G.; Caddick, S.; Baker, J. R., Protein Modification, Bioconjugation, and Disulfide Bridging Using Bromomaleimides. *J. Am. Chem. Soc.* **2010,** *132*, 1960-1965.
(59) Tedaldi, L. M.; Smith, M. E. B.; Nathani, R. I.; Baker, J. R., Bromomaleimides: New Reagents for the Selective and Reversible Modification of Cysteine. *Chem. Commun.* **2009**, 6583-6585.

CHAPTER 4

ENZYME IMMOBILIZATION THROUGH DIFFERENT ATTACHMENT SITES

4.1 INTRODUCTION

The immobilization of enzymes on solid supports [1-4] has found many applications ranging from biosensors used in energy and medical fields to other biocatalyst carriers such as antifouling coatings, food packaging materials and biofuel cells.[5-16] The advantages of using immobilized enzymes, as opposed to using them in free solution, include improved stability, reusability and localization. These features allow better control of manufacturing processes and reduce production costs by efficiently recycling the enzymes.[4, 17] Additionally, the architecture, chemical and mechanical properties of solid supports can be manipulated to improve the loading capacity and modulate the selectivity and activity of the attached enzymes.[10, 18-20] Advances in molecular biology such as the availability of gene synthesis have made it possible to easily tailor enzymes to facilitate various immobilization strategies.

A number of techniques have been used for enzyme immobilization, including entrapment, encapsulation, surface immobilization through non-covalent bonds such as physical adsorption (hydrophobic-hydrophobic interaction) or ionic binding and, lastly, covalent attachment to the surface.[1, 13, 21] Physical adsorption is commonly used because of its simplicity. However, the non-covalent nature of physical adsorption often results in

leaching of enzyme from the surface over time. Leaching is prevented by covalently binding the enzyme to appropriately functionalized surfaces. A frequently used approach involves crosslinking the enzyme to the surface through lysine residues on the protein using reagents such as glutaraldehyde or carbodiimides.[4, 8] However, because proteins typically have multiple lysine residues, this leads to random surface orientation, multiple crosslinks and often unfolding, all of which reduce enzyme activity. A more specific approach involves tethering the enzyme through cysteine residues, which are infrequently found on the exterior of proteins, and that can be chemically linked to maleimide-functionalized surfaces. Unique cysteine residues can easily be introduced by mutagenesis into the enzyme at a well-defined position on the protein's surface. This, in principle, allows the orientation of the enzyme with respect to the surface to be controlled.

Enzymes tend to lose their activity when in contact with a support surface,[22-24] a phenomenon that has been attributed to unfavorable orientation and (partial) unfolding. However, detailed information about the structure and orientation of surface-immobilized enzymes remains lacking due to the technical difficulties associated with characterizing a single layer of enzyme molecules on a surface. To address this problem we have used surface sensitive vibrational spectroscopies such as sum frequency generation spectroscopy (SFG) which involves a second order nonlinear optical process and is intrinsically surface sensitive. [25-33] It has been shown to be an extremely powerful tool for studying the secondary structures and orientations of interfacial peptides and proteins. [34-50] Attenuated total reflectance-Fourier transform infrared spectroscopy (ATR-FTIR) provides another technique to study peptide/protein interfacial structure and orientation with penetration depth of a few microns.[51-54] A combination of SFG and ATR-FTIR has

been used to determine complicated orientations of peptides and orientation of complex proteins. [55-57]

In the chapter, we have used 6-phospho-β-galactosidases (β-Gal) from *Lactococcus lactis* as a model enzyme for which detailed structural and kinetic information is available. [58] We engineered this enzyme to contain a unique surface cysteine. This allowed the protein to be attached through unique, chemically defined linkage to a chemically well-defined surface, in this case a maleimide-terminated self-assembled monolayer (SAM) assembled on a silica surface. [43, 59-61] We have selectively picked the engineering site to be either on the side of the enzyme opposite to or close to its active site to investigate the orientation of the immobilized enzyme with respect to the surface normal using SFG and ATR-FTIR, and examined how attaching the enzyme to the surface changes its activity.

4.2 EXPERIMENTAL

4.2.1 Materials and Methods

All chemicals and reagents were purchased from Sigma-Aldrich (St. Louis, MO, USA) and used without further purification unless otherwise stated.

4.2.2 Synthesis of Model Enzymes with Cysteine at Selected Sites

This work was performed by collaborators from Professor Marsh group. β-Gal (PDB 2PBG)[58] from *Lactococcus lactis* was synthesized by gene expression in *E. coli*. The sequence was modified to replace all native cysteine residues with alanine. And constructs of β-Gal with cysteine residue at desired positions were made by using site-directed mutagenesis. The activity of different constructs was confirmed to be similar to the wild type in solution.

4.2.3 Functionalization of Substrates

Right-angle CaF_2 prisms were purchased from Altos Photonics (Bozeman, MT, USA). These CaF_2 prisms were soaked in toluene for 24 h and then sonicated in 1% Contrex^{TM} AP solution from Decon Labs (King of Prussia, PA, USA) for 10 min. The prisms were thoroughly rinsed with Millipore water (18.2 MΩ·cm) and dried under N_2. They were placed into an oxygen bench-top plasma cleaner (PE-25-JW) purchased from Plasma Etch (Carson City, NV, USA) for 4 min immediately before being coated with SiO_2. A layer of 100 nm of SiO_2 was deposited onto the CaF_2 prisms by an electron-beam deposition process using a SJ-26 Evaporator system at a pressure below 10^{-5} Torr. The deposition rate is 5 Å/s.

The SiO_2 coated CaF_2 prisms were treated with the O_2 plasma cleaner for 4 min. These clean prisms were placed in freshly made 1 mM maleimide-EG4-silane (Mal-EG4, Creative PEGWorks, Winston Salem, NC, USA) or octadecyl trichlorosilane (OTS) in anhydrous toluene for 24 h at room temperature. The molecular structures for Mal-EG4 and OTS are shown in Figure 4.1A. The functionalized prisms were rinsed with copious amounts of toluene followed by methanol and were dried under vacuum for 1 h. Both SAMs were characterized by using x-ray photoelectron spectroscopy (XPS) to demonstrate their chemical composition.

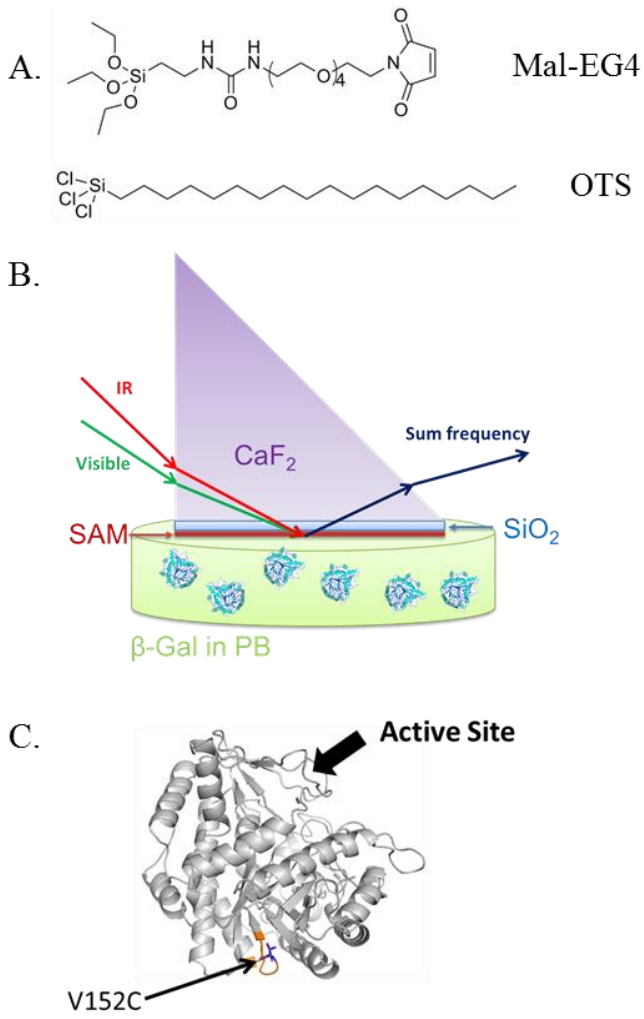

Figure 4.1 A: Molecular formulas for Mal-EG4 and OTS. B: SFG experimental geometry used in this study. This is a near-total-reflection geometry. The sample surface is in contact with a reservoir of buffer solution containing enzyme molecules. C: Crystal structure of β-Gal-V152C. The cysteine group can bind to the maleimide group on Mal-EG4 SAM to immobilize β-Gal to the surface. The binding site is opposite to the enzyme active site.

4.2.4 Instrumentation and Setup

4.2.4.1 SFG

The SFG details have been described in previous chapters. In this study, a near-total-reflection geometry (shown in Figure 4.1B) with right-angle CaF_2 prism was used, in which two input laser beams travel through one face of the prism and overlap on the other

face coated with a SAM grown on a deposited SiO_2 thin layer. This surface was in contact with a reservoir of 2 mL containing 5 mM pH 7.2 phosphate buffer (PB) and 0.1 mM TCEP. The appropriate volume of an enzyme stock solution (1 mM TCEP was added to the enzyme stock solution and incubated with gentle shaking at room temperature for 2h beforehand to reduce potential disulfide bonds) was injected to the reservoir to reach a concentration of 4 μM. A magnetic micro-stir bar was used at a rate of 125 rpm to ensure a homogeneous concentration distribution of enzyme molecules in the subphase below the prism. After the system was equilibrated, SFG spectra with a polarization combination of ssp (s-polarized sum frequency output, s-polarized visible input, and p-polarized infrared input) and ppp were collected and used for orientation analysis. All SFG spectra were normalized according to the intensities of the input IR and visible beams.

The primary experimentally measured quantity used for orientation analysis in SFG study for this research is the ratio of effective second-order nonlinear optical susceptibility tensor components detected in the ppp and ssp polarizations: $\chi_{zzz}^{(2)}/\chi_{xxz}^{(2)}$ (after deconvoluting the Fresnel coefficients). Methods of determining molecular orientation for single peptides and larger proteins have been reported before.[38, 40, 41, 62-65] We have previously developed a computer program that performs these calculations in a semi-automated fashion for proteins that contain many α-helices, and this program makes it possible to characterize the orientation of complex molecules in terms of the tilt (θ) and twist angles (ψ).[41, 56]

4.2.4.2 ATR-FTIR

ATR-FTIR experiments were carried out with a Nicolet Magna 550 FTIR spectrometer using a detachable ZnSe total internal reflection crystal (Specac Ltd. Slough, England). The ZnSe crystal surface was cleaned with methanol, 1% Contrex^{TM} AP solution, and Millipore water and then treated in the O_2 plasma chamber for 2 min immediately before SiO_2 (50 nm by electron-beam deposition as described above) deposition. The SiO_2 coated ZnSe crystal was treated with the O_2 plasma chamber for 2 min and the same preparation procedure for above discussed SFG study was followed to functionalize the surface of the ZnSe crystal with maleimide-EG4-silane. After the SAM was formed on the crystal surface, pH 7.2 phosphate buffer and TCEP solution in D_2O was added to the trough of 1.6 mL above the crystal to reach a final concentration of 5 mM and 0.1 mM, respectively. D_2O was used to avoid possible signal confusion between the O-H bending mode and the peptide amide I mode and to ensure a better S/N ratio in the peptide amide I band region. After taking the background spectra, the appropriate volume of an enzyme stock solution (1 mM TCEP was added to the enzyme stock solution and incubated with gentle shaking at room temperature for 2h beforehand to reduce potential disulfide bonds) was injected into the subphase to achieve the desired enzyme concentration of 4 μM. The s- and p-polarized ATR-FTIR spectra of the enzyme interacted with SAM were taken for orientation analysis after the system reached equilibrium.

We also developed a computer program similar to the SFG data analysis program to analyze ATR-FTIR data.[56] This program was used to analyze ATR-FTIR spectra to relate protein orientation to the dichroic ratio R^{ATR} which is related to the fitted peak intensities

(or integrated absorbance) of a peak in the parallel or perpendicular polarizations respectively.

To enable direct comparisons between ATR-FTIR and SFG orientation analysis methodologies for α-helices, we have derived the helical orientation relations for ATR-FTIR using a consistent set of rotation conventions.[56] Due to the large number of terms in the resulting equations, the algebraic details are not presented here, but these equations have been directly integrated into the computer software for SFG and ATR-FTIR data analysis.[56]

4.3 RESULTS AND DISCUSSION

4.3.1 Molecular Orientation of Enzymes Attached to Surfaces through Defined Chemical Linkages

6-phospho-β-galactosidase (β-Gal) from *Lactococcus lactis* was chosen as a model enzyme for this research because it is predicted to generate a large SFG signal due to its α-helical structure (based on calculations using the computer software discussed above). Previous reports had demonstrated that the enzyme maintains activity when immobilized on various solid supports via physical adsorption, covalent binding, chemical aggregation, encapsulation, and entrapment to increase their stability and reusability.[66-72] β-galactosidase activity can be assayed using commercially available chromogenic or fluorogenic substrates, providing simple and sensitive ways to investigate the effects of immobilization on enzyme activity. The enzyme adopts a β_8/α_8-barrel fold [58] (PDB 2PBG) with all the α-helixes pointing in approximately the same direction (Figure 4.1C). This is important, because it allows the orientation of the immobilized enzyme with respect to the surface to be experimentally determined by SFG spectroscopy.

4.3.2 SFG and ATR-FTIR experiments and data analysis for β-Gal on Mal-EG4 SAM

4.3.2.1 Evidence of elimination of non-specific binding with EG4 segments

To prevent or minimize the physical adsorption of β-Gal molecules on the surface, oligo-ethylene glycol (OEG) "spacer" groups were incorporated into SAM molecules. [60, 73, 74] Previous studies have shown that both tightly bound water associated with OEG chains and their high flexibility play important role in preventing non-specific protein adhesion.[73, 75-77] SFG ssp spectra were collected from the interface of Mal-EG4 SAM and buffer solution before and after the addition of "no cysteine" β-Gal. The similarity of spectra in the amide I region (Figure 4.2) shows that either no enzyme was adsorbed onto the SAM surface or the adsorbed enzymes are randomly oriented. However, the similarity of spectra in the C-H and O-H regions recorded before and after the introduction of β-Gal indicates that bound water molecules were not replaced by enzyme [77] showing that unlikely enzyme is adsorbed to the Mal-EG4 SAM by physical interactions.

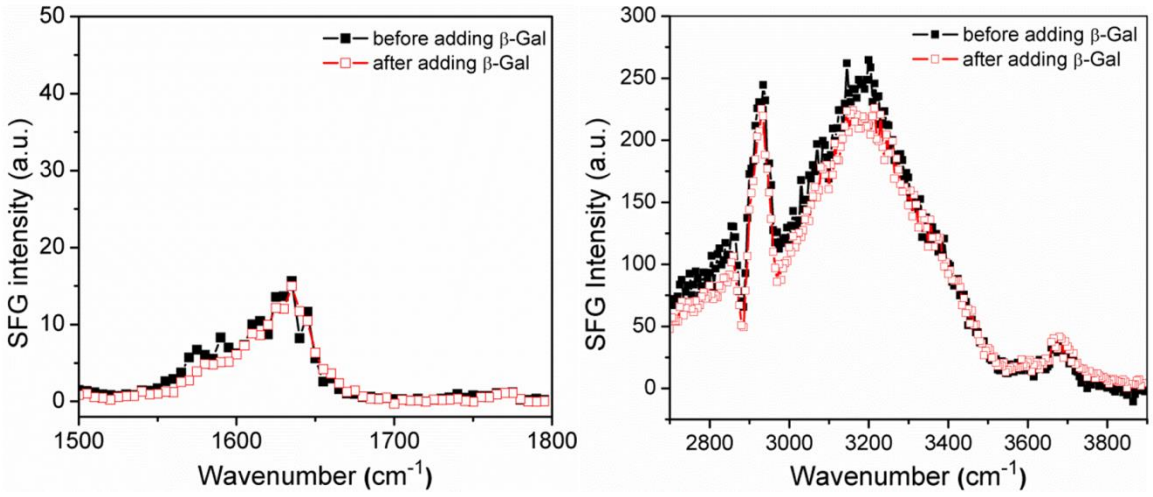

Figure 4.2 SFG ssp spectra collected from the Mal-EG4/PB solution interface before (black, filled squares) and after (red, open squares) introducing "no cysteine" β-Gal to the buffer solution in the amide I (left) and C-H/O-H stretching frequency regions.

4.3.2.2 Evidence of the direct single-point chemical attachment between Mal-EG4 SAM and cysteine-modified β-Gal

Figure 4.3 shows that SFG ssp spectra from the maleimide-terminated SAM/buffer solution interface, recorded in the absence of β-Gal-V152C (spectrum in black). A weak SFG signal was detected from the maleimide groups of the SAM with a peak centered around 1620 cm^{-1}. After incubating the maleimide-terminated surface with β-Gal-V152C, SFG amide I signal centered at ~1650 cm^{-1} was observed (Figure 4.3 in red). SFG spectra were again collected after extensively washing the interface with buffer to remove any non-covalently adsorbed protein. The SFG signal does not have a noticeable change after washing, consistent with the conclusion that β-Gal-V152C molecules are chemically immobilized on the Mal-EG4 surface (Figure 4.3, spectrum in blue). The spectrum is dominated by a peak at ~1650 cm^{-1} which is contributed by the α-helical components and a peak at ~1635 cm^{-1} which is contributed by the β-sheet components in β-Gal immobilized at the SAM/protein solution interface.

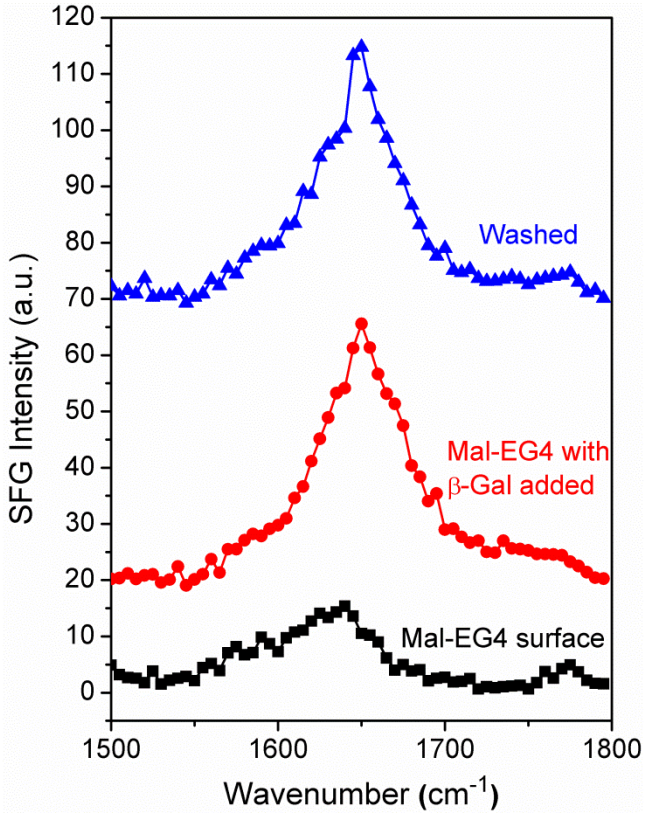

Figure 4.3 SFG ssp spectra collected from the Mal-EG4 SAM/buffer solution interface before (black, squares) and after (red, circles) the addition of β-Gal-V152C. Strong SFG signal was observed after the addition of β-Gal-V152C, indicating the surface immobilization. SFG signal remains the same (blue, triangles) after washing the interface with buffer, showing that the chemical immobilization occurred.

4.3.2.3 Orientation determination

a) SFG results

In addition to the ssp SFG spectrum, SFG ppp spectrum was also collected for β-Gal-V152C chemically immobilized on the maleimide-terminated SAM. Both spectra are shown in Figure 4.4A. After fitting, the ratio of χ_{ppp}/χ_{ssp} at 1650 cm^{-1} was determined to be 1.70. The fitting parameters are shown in Table 4.1. After correcting the effect of Fresnel coefficients on the two polarization combinations, it was deduced that the measured χ_{zzz}/χ_{xxz} value was 1.91 for the immobilized β-Gal. As we showed in ref. 56,

plotting this value on the theoretical contour map of χ_{zzz}/χ_{xxz} (calculated as a function of the tilt angle and twist angle for this enzyme using the computer software [56] based on the β-Gal crystal structure), we were able to deduce the possible orientation regions of the immobilized β-Gal at the Mal-EG4 SAM/enzyme solution interface (Figure 4.4C). In the orientation determination, the enzyme reference position (0,0 – tilt angle, twist angle) is defined using a β-Gal orientation in which the surface cysteine residue chemically binds to the surface maleimide group (Figure 4.4B).

Figure 4b indicates that many tilt and twist angle combinations can satisfy the deduced experimental results. To place more constraints and thus narrow down the possible orientations for β-Gal at the interface, we incorporated the polarized ATR-FTIR measurements below. SFG and ATR-FTIR measure different structural information and so these measurements provide independent information on protein orientation.[55, 62]

Table 4.1. SFG fitting parameters

SAM	Polarization combinations	Peak center (cm^{-1})	Peak width (cm^{-1})	Signal Strength	Assignment
Mal-EG4	ssp	1620	10.0	10.7	Maleimide C=O groups from SAM
		1635	10.0	10.7	β-sheets in β-Gal
		1650	15.0	91.0	α-helices in β-Gal
	ppp	1620	10.0	18.0	Maleimide C=O groups from SAM
		1635	10.0	15.45	β-sheets in β-Gal
		1650	15.0	154	α-helices in β-Gal
OTS	ssp	1600	15.0	11.3	Side chains in β-Gal
		1625	10.0	6.81	β-sheets in β-Gal
		1644	15.0	37.5	Random β-Gal structure
		1650	16.0	55.3	α-helices in β-Gal
		1680	10.0	14.2	β-sheets in β-Gal
		1710	10.0	15.4	Side chains in β-Gal
	ppp	1600	15.0	12.1	Side chains in β-Gal
		1625	10.0	19.9	β-sheets in β-Gal
		1644	15.0	43.4	Random β-Gal structure
		1650	16.0	106	α-helices in β-Gal
		1680	10.0	15.9	β-sheets in β-Gal
		1710	10.0	27.9	Side chains in β-Gal

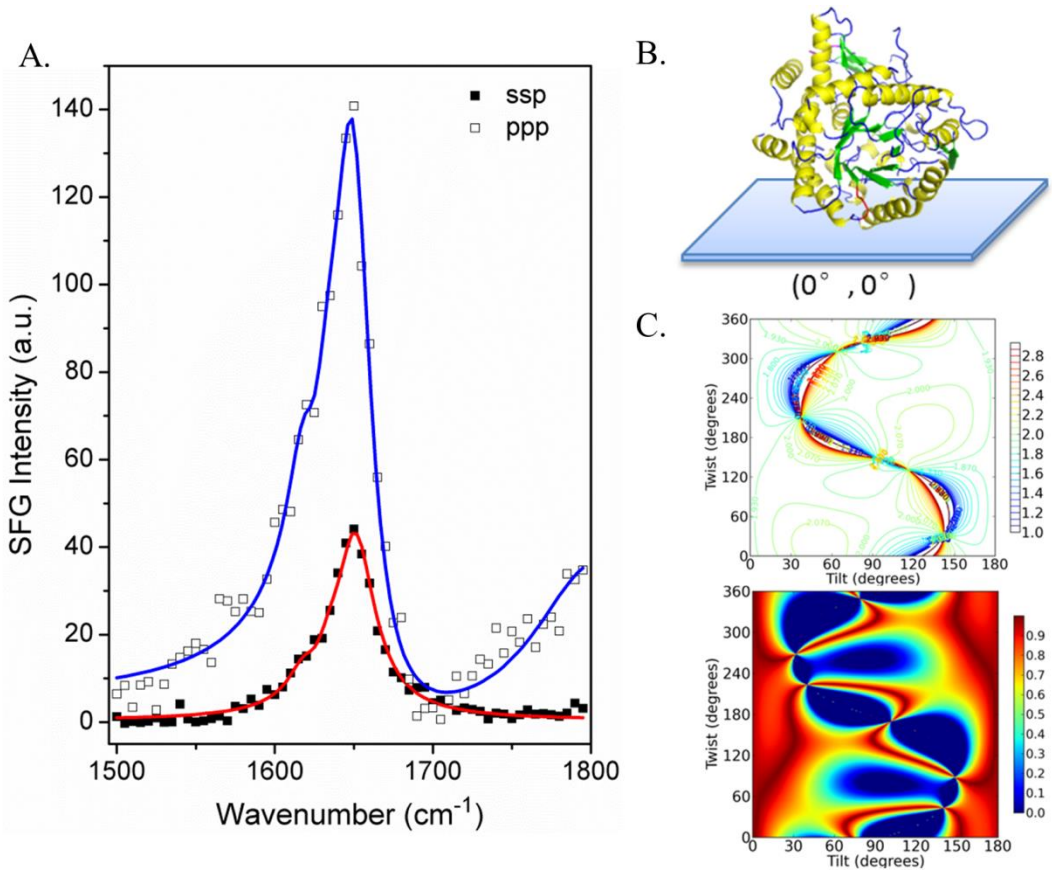

Figure 4.4. A: SFG ssp (red, filled squares) and ppp (blue, open squares) spectra collected from the immobilized β-Gal-V152C at the Mal-EG4 SAM/solution interface. Squares: experimental data; lines: fitting results. B: The orientation of β-Gal with tilt angle = 0, twist angle = 0. The cysteine functionalized site is shown in red. SAM is shown as a blue plane. C: Top: Dependence of the SFG χ_{zzz}/χ_{xxz} ratio on the tilt/twist angles of β-Gal calculated using the newly developed computer package.[56] Bottom: Possible orientation angle regions deduced based on the experimentally measured χ_{zzz}/χ_{xxz} ratio of β-Gal-V152C. Colors indicate the quality of the match (1=exact).

b) ATR-FTIR results

ATR-FTIR spectra were collected using the p-polarized and s-polarized IR beams (Figure 4.5A). Polarized ATR-FTIR spectra have been used to study peptide and protein

orientations.[51, 52] Especially, the amide I ATR-FTIR spectra (mainly contributed by the backbone C=O stretches) were chosen for analysis because the amide I signals have different peak centers for different protein secondary structures, which were discussed in detail in literature. [51, 52] By fitting the amide I ATR-FTIR spectra using Gaussian peaks, the peak centers are in direct correlation with the secondary structures contained in a protein. The ATR-FTIR spectra in Figure 4.5A were fitted and the dichroic ratio was deduced for the signal at ~1655 cm^{-1} which is attributed to α-helical components of β-Gal. The fitting results are shown in Table 4.2 and the dichroic ratio was calculated to be 1.67. Unlike SFG, ATR-FTIR is not inherently sensitive to ordered structures (e.g., α-helices), and consequently the ATR-FTIR spectra contained more vibrational peak centers corresponding to additional secondary structures (e.g., random coil at 1644 cm^{-1}). From the fitting results, we can see that the ATR-FTIR spectra contain contributions from the α-helix, β-sheet and random coil structures in this immobilized enzyme. Similar to the SFG data analysis, the theoretical ATR-FTIR signal response from β-Gal was also calculated as a function of the tilt and twist angles.[56] By combining the computed ATR-FTIR response and the experimentally deduced R^{ATR} of 1.67, the possible combinations of the tilt and twist angles of the immobilized β-Gal can be deduced at the Mal-EG4 SAM/enzyme solution interface (Figure 4.5B). Similar to the SFG result, many possible combinations of the tilt and twist angles can satisfy the experimental data so that a unique orientation of β-Gal with respect to the interface could not be determined by ATR-FTIR alone.

Table 4.2. ATR-FTIR fitting parameters

Polarization	Peak center (cm^{-1})	Peak width (cm^{-1})	Intensity	Assignment
S	1631	10.0	0.00171	β-sheets in β-Gal
	1640	10.0	0.00286	Random coils in β-Gal
	1655	12.0	0.0112	α-helices in β-Gal
p	1631	10.0	0.00211	β-sheets in β-Gal
	1640	10.0	0.00542	Random coils in β-Gal
	1655	12.0	0.0187	α-helices in β-Gal

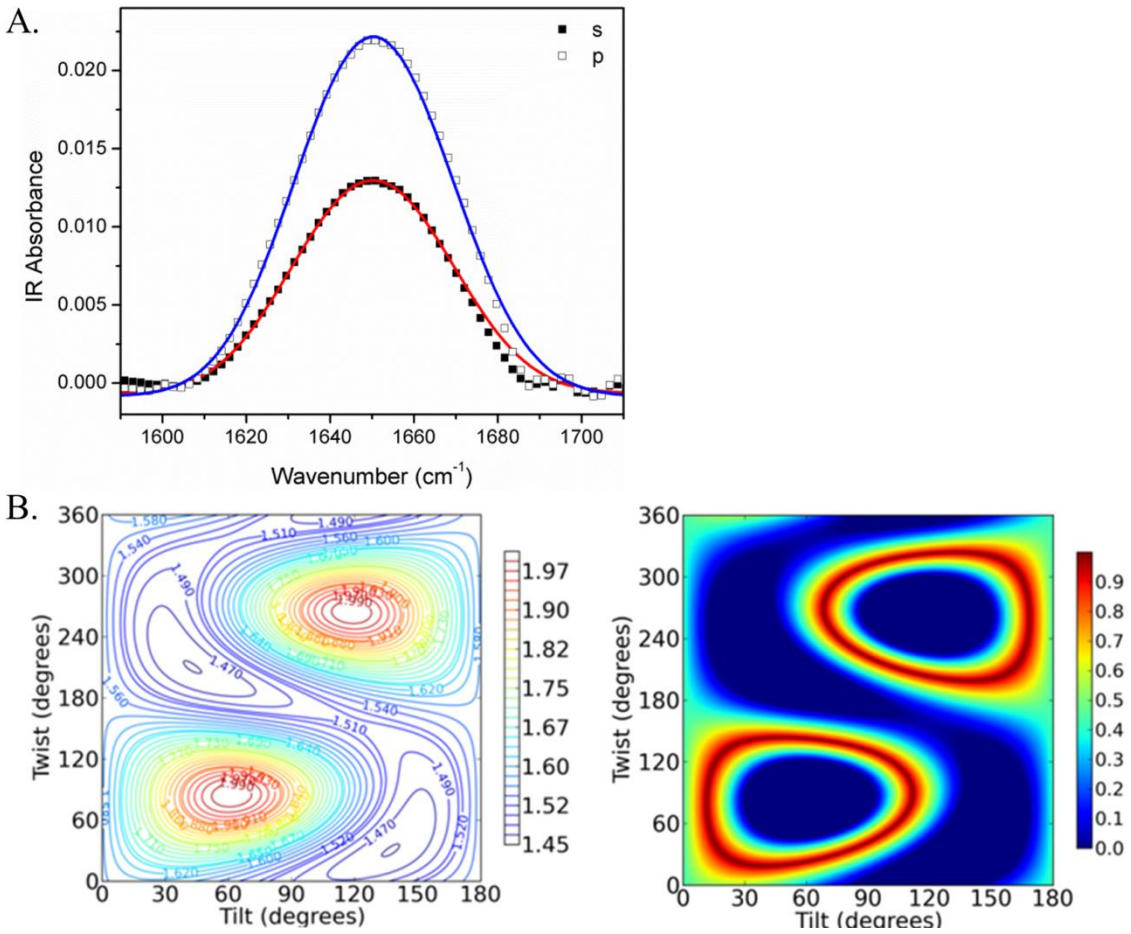

Figure 4.5 A: ATR–FTIR spectra collected from the immobilized β-Gal-V152C at the Mal-EG4 SAM/solution interface using p (blue, open squares) and s (red, filled squares) polarizations. Squares: experimental data; lines: fitting results. B: Dependence of the ATR–FTIR dichroic ratio R^{ATR} on the tilt/twist angles of β-Gal calculated using the newly developed computer package.[56] Right: Possible orientation angle regions deduced based on the experimentally measured R^{ATR} ratio of β-Gal-V152C. Colors indicate the quality of the match (1=exact).

c) Combining orientational constraint from SFG and ATR-FTIR

By overlapping the possible orientation angle regions deduced using SFG and ATR-FTIR measurements (Figure 4.6) it can be seen that there are only six regions in which the possible orientation angle combinations can satisfy both SFG and ATR-FTIR measurements. Furthermore, because the cysteine residue in β-Gal must be in contact with the SAM surface, we could exclude the possible orientations with tilt angles larger than 90 degrees. If we choose the best matches between the experimentally measured data and the calculated orientations, for the regions with tilt angles smaller than 90^o, we have one large area (an arc) with possible tilt angles ranging from 15^o to 30^o while twist angles ranging from 60^o to 130^o, along with a very small region of tilt angle of around 75^o and twist angle of around 30^o (Figure 4.6, right plot). We plot two representative orientations from the first arc region and one orientation from the latter small angle region in Figure 4.7, along with other three representative orientations with tilt angles bigger than 90^o. We believe that the orientations shown in Figues 4.7a and 4.7b are the most likely orientations because they are consistent with the intended orientation that would arise by chemical immobilization between the enzyme cysteine side chain and the surafce maleimide groups. As shown in Figure 4.6, the possible angle region corresponding to the orientations shown in Figures 4.7a and 4.7b is much larger than the one corresponding to the orientation shown in Figure 4.7c, which also implies that the possibility of the protein adopting similar orientations as shown in Figures 4.7a and 4.7b is much higher than that shown in Figure 4.7c.

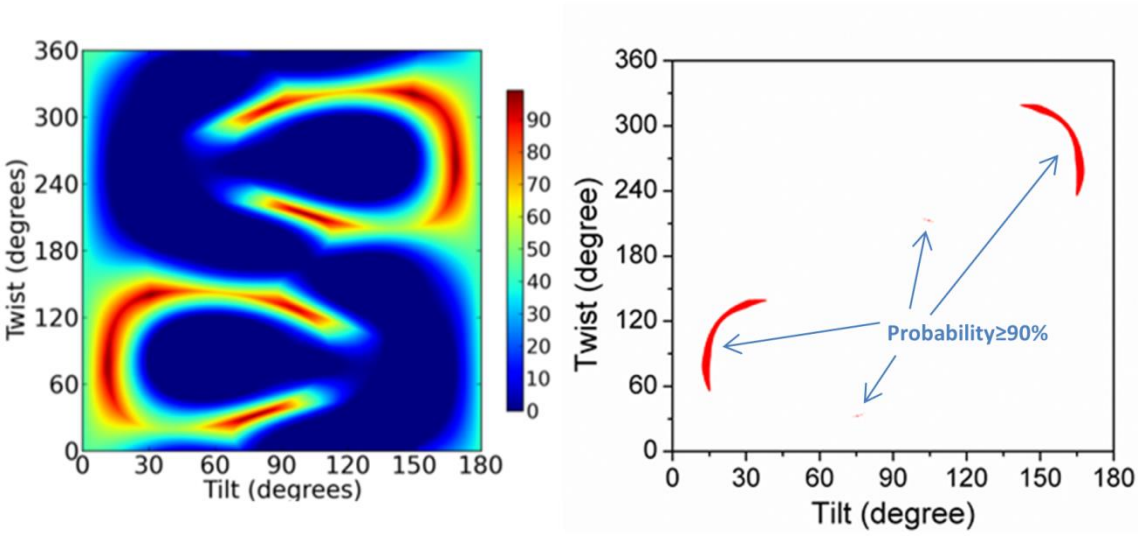

Figure 4.6 Possible orientation angle regions deduced based on both the SFG and ATR–FTIR measurements. Colors indicate the quality of the match (100%=exact). The right figure plotted the possible orientation angles with probability ≥ 90% in red.

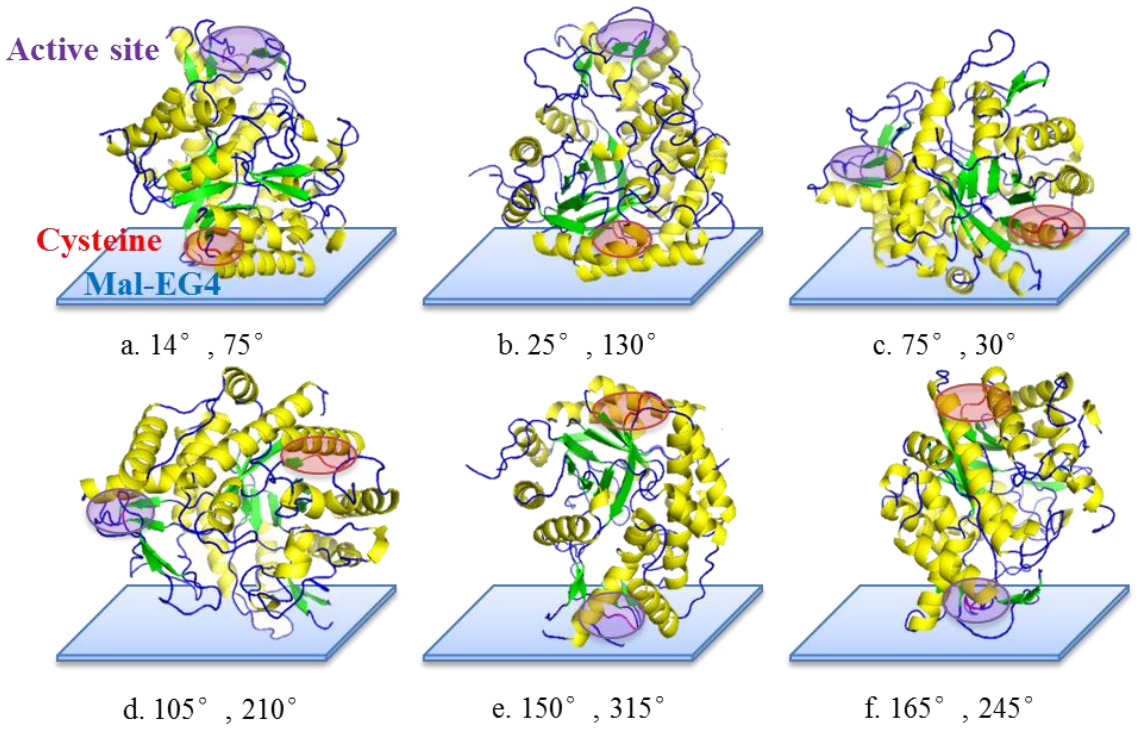

Figure 4.7 Possible orientations of immobilized β-Gal shown in format of (tilt angle, twist angle). The most likely orientations are a. (14°, 75°) and b. (25°, 130°) because they are well correlated to the designed orientations.

4.3.2.4 SFG studies on β-Gal on OTS SAM

SFG ssp spectra in the amide I frequency region were collected from the interface between OTS SAM and the buffer solution before and after the addition of β-Gal into the buffer solution (Figure 4.8). Before the introduction of β-Gal, no signal was detected. The increase of the SFG signal in the amide I spectral region after the introduction of β-Gal into the buffer solution was attributed to β-Gal that was adsorbed at the OTS SAM/buffer interface. Additional peaks contributed from side chains (1600 cm^{-1} and 1710 cm^{-1}), random structures (1644 cm^{-1}) and β-sheets (1680 cm^{-1}) showed up. The appearance of these side chains and secondary structures of β-Gal on OTS SAM is most likely caused by partially unfolding of the enzyme to expose hydrophobic residues that physically adsorb on the hydrophobic OTS SAM surface through hydrophobic interactions.[48, 78] Similar SFG spectra were detected at OTS/β-Gal solution interface for the "no cysteine" and β-Gal V152C enzymes (not shown) indicating that the cysteine does not greatly alter the physical adsorption on the OTS surface. SFG spectra were also collected after washing the surface with pure buffer solution (Figure 4.8). The spectral intensity decreased, showing that some loosely adsorbed proteins can be washed off the OTS SAM surface. As discussed below, the physically adsorbed β-Gal has much reduced activity compared to the chemically immobilized enzyme.

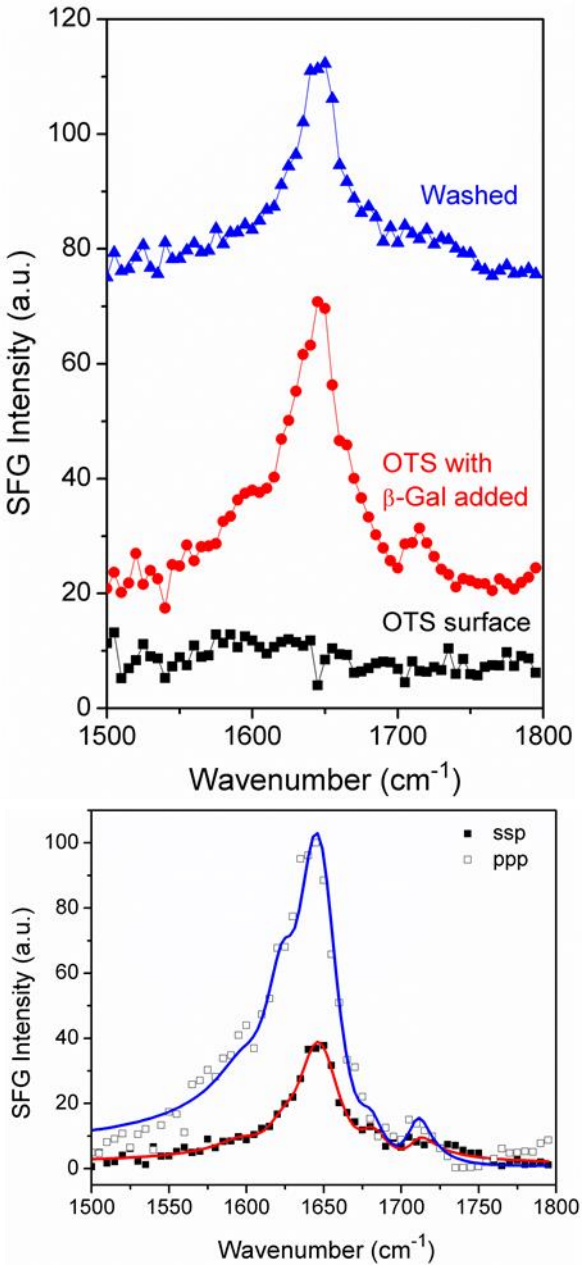

Figure 4.8 Top: SFG spectra collected from the OTS SAM/buffer solution before (black) and after (red) the addition of β-Gal-V152C to the buffer. After washing, SFG signal (blue) decreased, showing some loosely adsorbed enzyme molecules were washed off. Bottom: ssp (red, filled squares) and ppp (blue, open squares) SFG spectra collected from the OTS SAM/buffer solution after the addition of β-Gal-V152C to the buffer. Squares: experimental data; lines: fitting results.

4.3.3 Activity of Surface-immobilized β-Gal

This work was performed by collaborators from Professor Marsh group. Although β-Gal has favorable structural features for determining its surface orientation by SFG, the enzyme was not sufficiently active that we could directly measure β-Gal activity on the prism surfaces used for SFG measurements. To enhance the sensitivity, we attached the enzyme to glass beads coated with either Mal-EG4 SAM or OTS SAM. On a microscopic level, the SAMs on the bead surface should be chemically identical to that of the SFG prisms, but the overall surface area is greatly increased. To increase sensitivity further the fluorogenic substrate fluorescein-β-di-galactopyranoside (FDG) was used to measure activity.

Using this substrate, the specific activity of β-Gal-V152C in free solution was 1.1 $nmol.min^{-1}mg^{-1}$ (Figure 4.9). The specific activity of β-Gal-V152C immobilized on Mal-EG4 derivatized glass beads was 1.08 $nmol.min^{-1}mg^{-1}$ which is identical, within error, to the enzyme in free solution. In contrast the specific activity of β-Gal-V152C physically adsorbed on OTS-derivatized beads was 0.35 $nmol.min^{-1}mg^{-1}$, which is only one third that of the enzyme in free solution.

To determine the specific activities of immobilized and free enzyme, the amount of enzyme attached to the glass beads was quantified by reaction with bicinchoninic acid. This allowed us to compare the loading of the beads with that expected for an ideal monolayer. Based on a bead diameter of 75 μm, and assuming a footprint of ~100 nm^2 for β-Gal, monolayer coverage would result in a loading of ~ 0.27 pmol enzyme/mg of beads. The experimentally determined protein loading for β-Gal-V152C immobilized through Mal-EG4 linker was 0.14 pmol/mg of beads, suggesting that the specifically

tethered enzyme is likely attached as a monolayer with few or no non-covalent interactions between enzyme molecules. For enzyme physically adsorbed on OTS-derivatized beads, the loading was 1.0 pmol/mg of beads, which is much larger than the concentration expected for a monolayer. This suggests that protein-protein interactions between physically adsorbed enzyme molecules are likely to occur and this may be part of the reason that the activity of the physically adsorbed enzyme is much lower.

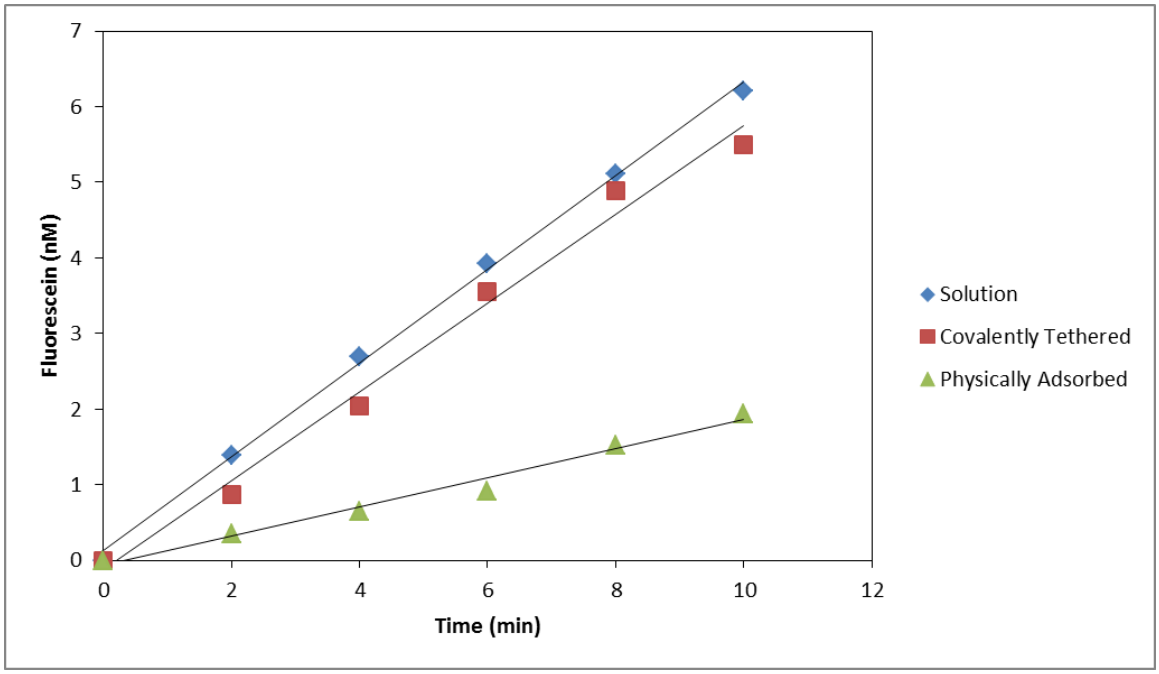

Figure 4.9 Activity of the β-Gal free in solution (blue), covalently tethered to the EG4-Mal SAM via the single engineered cysteine at position 153 (red), and physically adsorbed to the hydrophobic OTS SAM (green). In each case, 10 pmol of β-Gal-V152C was added to 1 mL of solution.

It is interesting to observe stronger SFG signal intensity for β-Gal-V152C immobilized through Mal-EG4 linker compared to that physically adsorbed on OTS even though the surface coverage of the latter is higher. SFG signal intensity is related to the surface coverage and orientation of functional groups or molecules (under the fixed

visible and IR input beam energies). For the chemical immobilization, the enzyme molecules more or less adopt a similar orientation (with the cysteine group facing the surface for immobilization), therefore the signal can be stronger. The signal should be proportional to the square of the surface coverage (assuming orientation is coverage independent, which is likely for chemical immobilization). For the physically adsorbed enzyme molecules, the orientation distribution can be much broader. Therefore SFG signals from enzyme molecules with different orientations can be canceled in some degrees. As a result, the detected SFG signal can be smaller even when the enzyme surface coverage is higher.

4.3.4 Variation of Immobilization Sites on Enzyme Structure and Orientation

4.3.4.1 Effect of secondary structure of the tethering site

To investigate the effect of secondary structure of the tethering site, a β-Gal mutant with a cysteine at glutamic acid-147 (denoted as β-Gal-E147C, structure shown in Figure 4.13 left) was synthesized and immobilized on Mal-EG4 SAM. β-Gal-E147C, compared to β-Gal-V152C whose cysteine is located in a loop region, has the cysteine residue located within a helical structure. The orientation analysis was carried out similarly to the previous section by employing both SFG and ATR-FTIR spectroscopies.

SFG results are shown in Figure 4.10, left plot. Both ssp and ppp spectra are dominated by a peak at ~1650 cm^{-1} which is contributed by the α-helical components and a peak at ~1635 cm^{-1} which is contributed by the β-sheet components in β-Gal immobilized at the SAM/protein solution interface. Fitting the spectra gave a ratio of 1.71 for χ_{ppp}/χ_{ssp} at 1650 cm^{-1}. After correcting for the Fresnel coefficients, a χ_{zzz}/χ_{xxz} ratio of

1.92 was used for possible orientation determination. The tilt and twist angles that satisfy this experimentally measured value are shown in Figure 4.10, right plot.

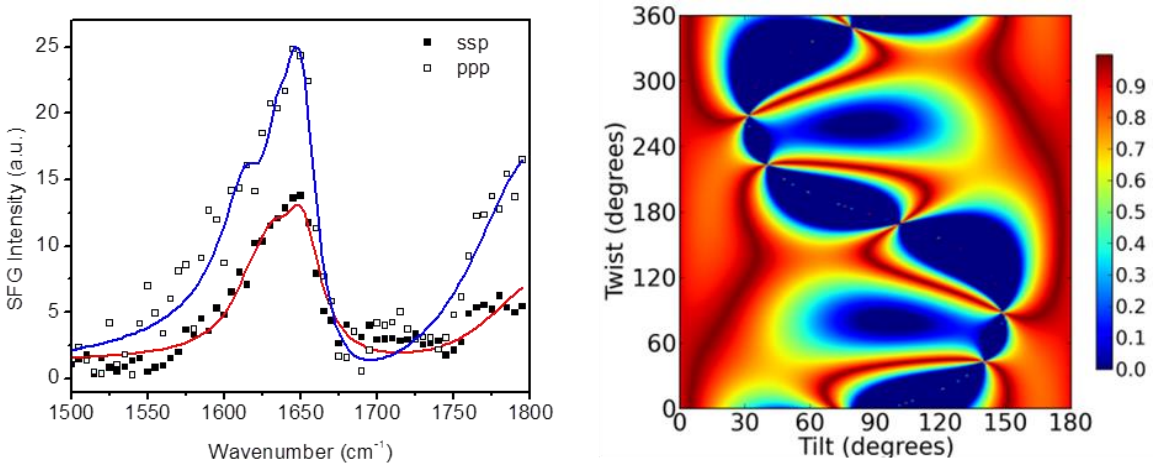

Figure 4.10 Left: SFG ssp (red, filled squares) and ppp (blue, open squares) spectra collected from the immobilized β-Gal-E147C at the Mal-EG4 SAM/solution interface. Squares: experimental data; lines: fitting results. Right: Possible orientation angle regions deduced based on the experimentally measured χ_{zzz}/χ_{xxz} ratio of β-Gal-E147C. Colors indicate the quality of the match (1=exact).

The ATR-FTIR spectra are shown in Figure 4.11, left plot. Both s and p polarized spectra were fitted and the dichroic ratio was deduced for the signal at ~1655 cm^{-1} which is attributed to α-helical components of β-Gal. The dichroic ratio was calculated to be 1.76 after fitting the spectra and this value was used for further analysis. The tilt and twist angles that satisfy measured R^{ATR} value are shown in Figure 4.11, right plot. By overlapping the possible orientation angle regions deduced using SFG and ATR-FTIR spectroscopies, the regions that satisfy both measurements are shown in Figure 4.12. Again, the orientations with tilt angles larger than 90 °were excluded for analysis.

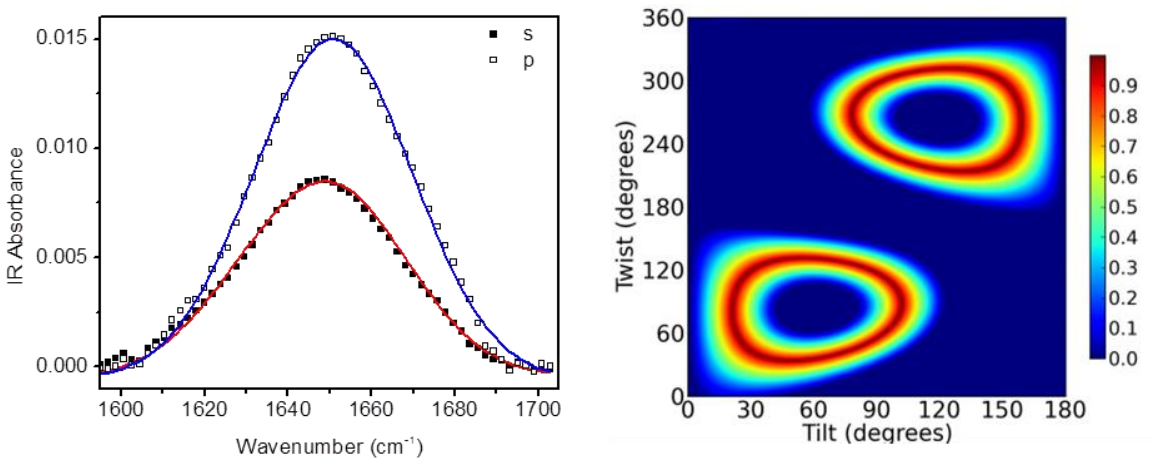

Figure 4.11 Left: ATR–FTIR spectra collected from the immobilized β-Gal-E147C at the Mal-EG4 SAM/solution interface using p (blue, open squares) and s (red, filled squares) polarizations. Squares: experimental data; lines: fitting results. Right: Possible orientation angle regions deduced based on the experimentally measured R^{ATR} ratio of β-Gal-E152C. Colors indicate the quality of the match (1=exact).

Comparing with immobilized β-Gal-V152C, β-Gal-E147C has similar possible orientations in the arc region but does not have the very small region of tilt angle around 75^{o} and twist angle around 30^{o}. This suggests that β-Gal-V152C is more likely to come into contact with the surface than β-Gal-E147C as shown by the higher possibility in the region with tilt angle closer to 90^{o}. This difference can be explained by the flexibility of a loop residue versus a helical residue. When immobilizing to the surface, the attachment via a more flexible point like a cysteine in the loop region, gives the enzyme molecules more rotation freedom than that of a rigid attachment point like a cysteine in a helical structure. As a result, the enzyme has a higher chance to interact with the surface with larger tilt angles. This however, may lead to less stability of β-Gal on surface for V152C than for E147C.

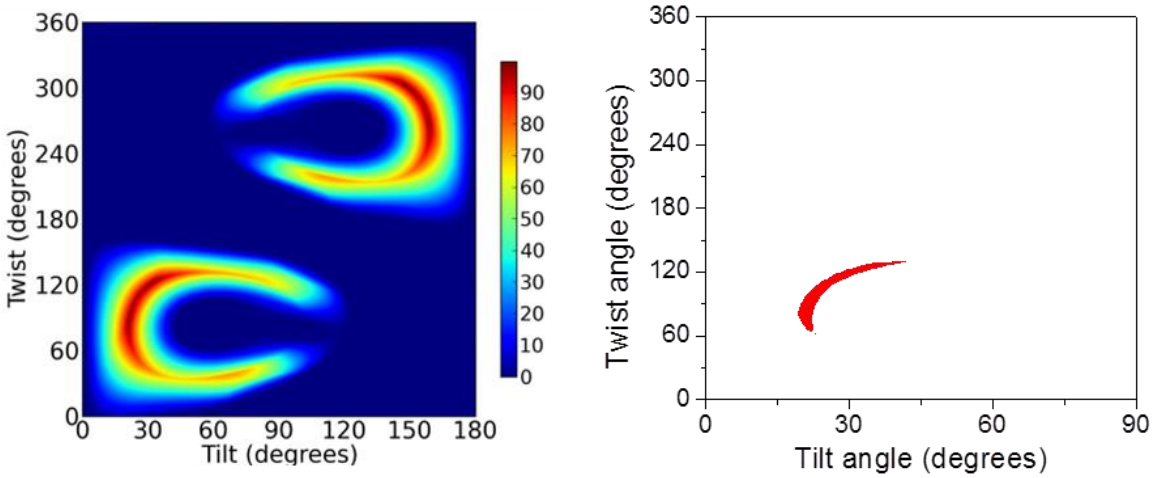

Figure 4.12 Possible orientation angle regions deduced based on both the SFG and ATR–FTIR measurements for β-Gal-E147C. Colors indicate the quality of the match (100%=exact). The right figure plotted the possible orientation angles with probability ≥ 90% in red.

4.3.4.2 Effect of location of the tethering site

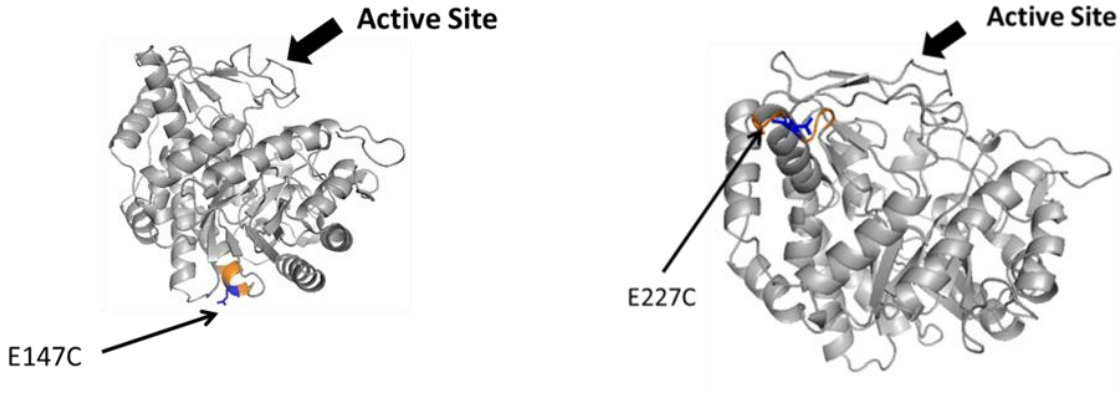

Figure 4.13 Crystal structure of β-Gal-E147C on the left and β-Gal-E227C on the right

Another β-Gal mutant with cysteine at glutamic acid-227 (denoted as a β-Gal-E227C, structure shown in Figure 4.13 right) was engineered by our collaborators from Professor Marsh group and immobilized on Mal-EG4 SAM. The cysteinyl residue in β-Gal-E227C

is located near the active site of the enzyme. SFG studies were performed on the immobilized β-Gal-E227C as shown in Figure 4.14.

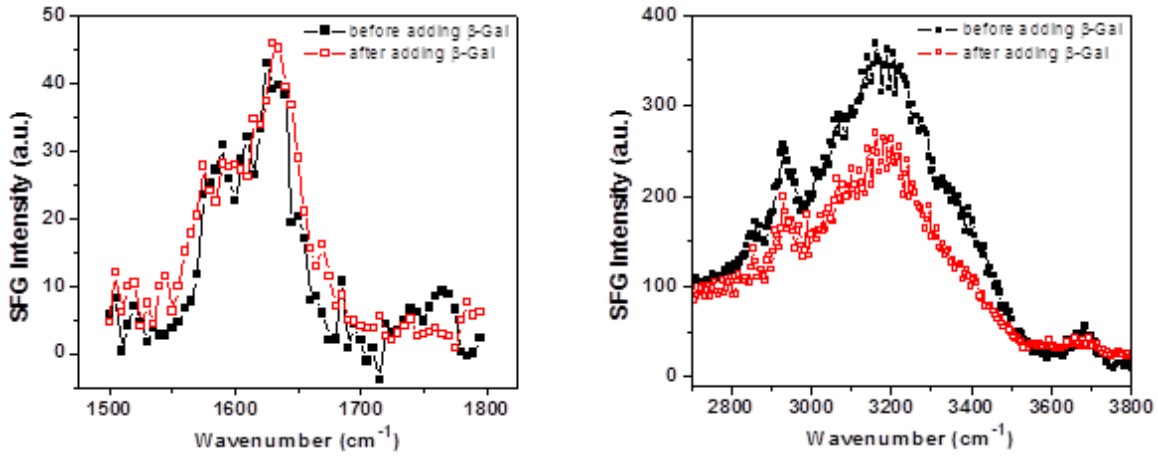

Figure 4.14 SFG ssp spectra collected from the Mal-EG4/PB solution interface before (black, filled squares) and after (red, open squares) introducing β-Gal-E227C to the buffer solution in the amide I (left) and C-H/O-H stretching frequency regions.

SFG spectra were collected from the Mal-EG4/PB interface before and after the introduction of the enzyme solution to the subphase in both amide I and C-H, O-H stretching regions. Different from the case shown in **4.3.1.1.1** where β-Gal containing no cysteinyl residues showed no spectral changes in either frequency region, here the SFG spectra collected from β-Gal-E227C showed no change in amide I region but it showed a decrease in signals in the C-H and O-H stretching frequency region. This difference illustrates that unlike the "no cysteine" β-Gal control sample, β-Gal-E227C did attach to the Mal-EG4 surface, replacing the interfacial water molecules and led to a decrease for the water O-H stretching peak. We speculated that the minimal signal from β-Gal-E227C in amide I region was due to its orientation on the surface. To validate this hypothesis, an SFG intensity map for χ_{xxz} relative to tilt and twist angles was generated using the same software package as shown in Figure 4.15 left (Red indicates a higher intensity while

blue indicates a lower intensity). This map shows us the relative signal intensities for enzyme molecules having different tilt or twist angles. For example, the determined possible orientations for β-Gal-V152C overlay on the relatively high intensity areas (red/orange). If we assume that β-Gal-E227C is immobilized onto the maleimide terminated SAM, it should adopt an orientation with cysteinyl residues face the surface maleimide groups (Figure 4.15). In thi case, the generated SFG amide I signal should be located in a low intensity area (blue/violet) as shown in the figure. This assumption is well correlated to our experimental results. As we indicated above, the SFG signal for the immobilized β-Gal-E227C could not be detected. We therefore believe that the above assumption is valid. For this enzyme orientation, the active sites are buried, facing the prism instead of the solution. Consequently, the enzyme would have minimal activity after being immobilized because the active sites are not readily accessible by the enzymatic substrate molecules. Indeed, the activity of the immobilized β-Gal-E227C was tested and showed a 23% activity compared to β-Gal in solution. This was further proved by an MD simulation performed by our collaborator in Professor Charles Brooks lab. The simulation showed similar possible orientations as proposed from SFG results (Figure 4.16).

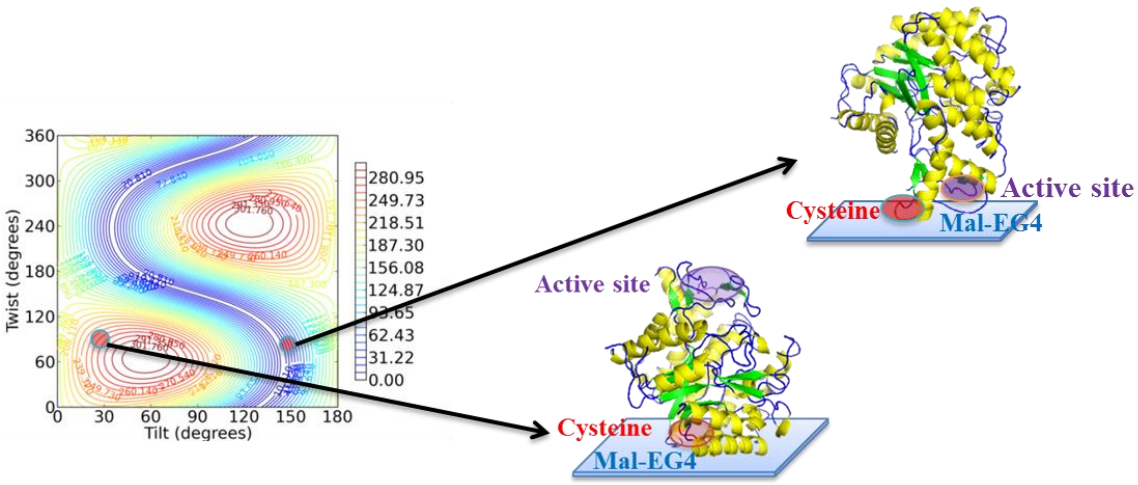

Figure 4.15 Left plot shows the dependence of the SFG χ_{xxz} on the tilt/twist angles of β-Gal calculated using the computer package.[56] Two representative orientations of β-Gal that would generate different SFG intensities are shown on the right. The top enzyme is β-Gal-E227C, the lower enzyme is β-Gal-E147C.

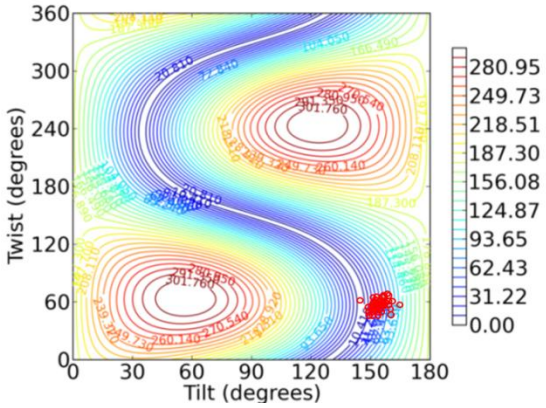

Figure 4.16 Red circles show the possible orientations calculated by MD simulation for β-Gal-E227C which is in agreement with our SFG analysis.

4.4 SUMMARY

In this chapter, specific immobilization of 6-phospho-β-galactosidase through a unique cysteinyl residue was achieved on SAMs containing maleimide end groups and oligo ethyleneglycol spacer segments. The possible orientations of the immobilized β-Gal were determined by combining measurements using two independent vibrational

spectroscopic techniques. The activity of the immobilized enzyme was also tested which was in agreement with the orientation deduced from combined SFG and ATR-FTIR measurements. On the other hand, 6-phospho-β-galactosidase non-specifically adsorbed onto hydrophobic octadecyl SAMs, appeared to be partially denatured and exhibited significantly reduced activity. As we discussed above, in our SFG and ATR-FTIR studies, we assume that the specifically immobilized enzymes do not significantly change their structures. Since the activity of the chemically immobilized β-Gal is similar to that in solution, and the enzyme orientation determined spectroscopically is reasonable, we believe that this assumption is valid in this case. Following the same methodology, the effect of the secondary structure of the attachment point and the location of the attachment point were both investigated and justified by molecular dynamics simulations.

This research demonstrated that the desired orientation of surface immobilized enzymes can be achieved by site specific engineering and surface tethering. A detailed correlation between the directly measured orientations and activity of a surface-attached enzyme has seldom been previously reported. This work provides a systematic means to characterize interfacial orientation of immobilized enzymes, leading to fundamental knowledge regarding which properties of an enzyme may be altered by tethering without compromising its function. This, in the future, will impact the development of an increasingly wide range of devices that use surface-immobilized enzymes as integral components with improved functions, better sensitivity, enhanced stability, and longer shelf-life.

4.5 REFERENCES

(1) Brady, D.; Jordaan, J., Advances in Enzyme Immobilisation. *Biotechnol. Lett.* **2009,** *31*, 1639-1650.

(2) Cao, L. Q., Immobilised Enzymes: Science or Art? *Curr. Opin. Chem. Biol.* **2005,** *9*, 217-226.

(3) Hanefeld, U.; Gardossi, L.; Magner, E., Understanding Enzyme Immobilisation. *Chem. Soc. Rev.* **2009,** *38*, 453-468.

(4) Tischer, W.; Wedekind, F., Immobilized Enzymes: Methods and Applications. *Top. Curr. Chem.* **1999,** *200*, 95-126.

(5) Ansari, S. A.; Husain, Q., Potential Applications of Enzymes Immobilized on/in Nano Materials: A Review. *Biotechnol. Adv.* **2012,** *30*, 512-523.

(6) Cordeiro, A. L.; Hippius, C.; Werner, C., Immobilized Enzymes Affect Biofilm Formation. *Biotechnol. Lett.* **2011,** *33*, 1897-1904.

(7) Frasconi, M.; Mazzei, F.; Ferri, T., Protein Immobilization at Gold-Thiol Surfaces and Potential for Biosensing. *Anal. Bioanal. Chem.* **2010,** *398*, 1545-1564.

(8) Jonkheijm, P.; Weinrich, D.; Schroder, H.; Niemeyer, C. M.; Waldmann, H., Chemical Strategies for Generating Protein Biochips. *Angew. Chem. Int. Ed.* **2008,** *47*, 9618-9647.

(9) Kristensen, J. B.; Meyer, R. L.; Laursen, B. S.; Shipovskov, S.; Besenbacher, F.; Poulsen, C. H., Antifouling Enzymes and the Biochemistry of Marine Settlement. *Biotechnol. Adv.* **2008,** *26*, 471-481.

(10) Lee, S. Y.; Lee, J.; Chang, J. H.; Lee, J. H., Inorganic Nanomaterial-Based Biocatalysts. *BMB Rep.* **2011,** *44*, 77-86.

(11) Noah, N. M.; Omole, M.; Stern, S.; Zhang, S. Y.; Sadik, O. A.; Hess, E. H.; Martinovic, J.; Baker, P. G. L.; Iwuoha, E. I., Conducting Polyamic Acid Membranes for Sensing and Site-Directed Immobilization of Proteins. *Anal. Biochem.* **2012,** *428*, 54-63.

(12) Olsen, S. M.; Pedersen, L. T.; Laursen, M. H.; Kiil, S.; Dam-Johansen, K., Enzyme-Based Antifouling Coatings: A Review. *Biofouling* **2007,** *23*, 369-383.

(13) Rodrigues, R. C.; Berenguer-Murcia, A.; Fernandez-Lafuente, R., Coupling Chemical Modification and Immobilization to Improve the Catalytic Performance of Enzymes. *Adv. Synth. Catal.* **2011,** *353*, 2216-2238.

(14) Tasso, M.; Pettitt, M. E.; Cordeiro, A. L.; Callow, M. E.; Callow, J. A.; Werner, C., Antifouling Potential of Subtilisin a Immobilized onto Maleic Anhydride Copolymer Thin Films. *Biofouling* **2009,** *25*, 505-516.

(15) Veluchamy, P.; Sivakumar, P. M.; Doble, M., Immobilization of Subtilisin on Polycaprolactam for Antimicrobial Food Packaging Applications. *J. Agric. Food. Chem.* **2011,** *59*, 10869-10878.

(16) Halamkova, L.; Halamek, J.; Bocharova, V.; Szczupak, A.; Alfonta, L.; Katz, E., Implanted Biofuel Cell Operating in a Living Snail. *J. Am. Chem. Soc.* **2012,** *134*, 5040-5043.

(17) Sassolas, A.; Blum, L. J.; Leca-Bouvier, B. D., Immobilization Strategies to Develop Enzymatic Biosensors. *Biotechnol. Adv.* **2012,** *30*, 489-511.

(18) Tasso, M.; Conlan, S. L.; Clare, A. S.; Werner, C., Active Enzyme Nanocoatings Affect Settlement of Balanus Amphitrite Barnacle Cyprids. *Adv. Funct. Mater.* **2012,** *22*, 39-47.

(19) Wang, Z. G.; Wan, L. S.; Liu, Z. M.; Huang, X. J.; Xu, Z. K., Enzyme Immobilization on Electrospun Polymer Nanofibers: An Overview. *J. Mol. Catal. B: Enzym.* **2009,** *56*, 189-195.

(20) Klein, M. P.; Nunes, M. R.; Rodrigues, R. C.; Benvenutti, E. V.; Costa, T. M. H.; Hertz, P. F.; Ninow, J. L., Effect of the Support Size on the Properties of Beta-Galactosidase Immobilized on Chitosan: Advantages and Disadvantages of Macro and Nanoparticles. *Biomacromolecules* **2012,** *13*, 2456-2464.
(21) Garcia-Galan, C.; Berenguer-Murcia, A.; Fernandez-Lafuente, R.; Rodrigues, R. C., Potential of Different Enzyme Immobilization Strategies to Improve Enzyme Performance. *Adv. Synth. Catal.* **2011,** *353*, 2885-2904.
(22) Butler, J. E., Solid Supports in Enzyme-Linked Immunosorbent Assay and Other Solid-Phase Immunoassays. *Methods* **2000,** *22*, 4-23.
(23) You, C. C.; De, M.; Han, G.; Rotello, V. M., Tunable Inhibition and Denaturation of Alpha-Chymotrypsin with Amino Acid-Functionalized Gold Nanoparticles. *J. Am. Chem. Soc.* **2005,** *127*, 12873-12881.
(24) Talbert, J. N.; Goddard, J. M., Enzymes on Material Surfaces. *Colloids Surf., B* **2012,** *93*, 8-19.
(25) Shen, Y. R., Surface Properties Probed by Second-Harmonic and Sum-Frequency Generation. *Nature* **1989,** *337*, 519-525.
(26) Eisenthal, K. B., Liquid Interfaces Probed by Second-Harmonic and Sum-Frequency Spectroscopy. *Chem. Rev.* **1996,** *96*, 1343-1360.
(27) Richmond, G. L., Molecular Bonding and Interactions at Aqueous Surfaces as Probed by Vibrational Sum Frequency Spectroscopy. *Chem. Rev.* **2002,** *102*, 2693-2724.
(28) Liu, J.; Conboy, J. C., Direct Measurement of the Transbilayer Movement of Phospholipids by Sum-Frequency Vibrational Spectroscopy. *J. Am. Chem. Soc.* **2004,** *126*, 8376-8377.
(29) Ye, H. K.; Abu-Akeel, A.; Huang, J.; Katz, H. E.; Gracias, D. H., Probing Organic Field Effect Transistors in situ During Operation Using SFG. *J. Am. Chem. Soc.* **2006,** *128*, 6528-6529.
(30) Chen, X.; Yang, T.; Kataoka, S.; Cremer, P. S., Specific Ion Effects on Interfacial Water Structure near Macromolecules. *J. Am. Chem. Soc.* **2007,** *129*, 12272-12279.
(31) Li, Q. F.; Kuo, C. W.; Yang, Z.; Chen, P. L.; Chou, K. C., Surface-Enhanced IR-Visible Sum Frequency Generation Vibrational Spectroscopy. *PCCP* **2009,** *11*, 3436-3442.
(32) Yang, Z.; Li, Q. F.; Gray, M. R.; Chou, K. C., Structures of Water Molecules at Solvent/Silica Interfaces. *Langmuir* **2010,** *26*, 16397-16400.
(33) Humbert, C.; Busson, B., Chapter 10 - Sum-Frequency Generation Spectroscopy of Biointerfaces. In *Biointerface Characterization by Advanced IR Spectroscopy*, Pradier, C. M.; Chabal, Y. J., Eds. Elsevier: Amsterdam, 2011; pp 279-321.
(34) Chen, X.; Wang, J.; Sniadecki, J. J.; Even, M. A.; Chen, Z., Probing Alpha-Helical and Beta-Sheet Structures of Peptides at Solid/Liquid Interfaces with SFG. *Langmuir* **2005,** *21*, 2662-2664.
(35) Wang, J.; Chen, X.; Clarke, M. L.; Chen, Z., Detection of Chiral Sum Frequency Generation Vibrational Spectra of Proteins and Peptides at Interfaces in Situ. *Proc. Natl. Acad. Sci. USA* **2005,** *102*, 4978-4983.
(36) Chen, X.; Chen, Z., SFG Studies on Interactions between Antimicrobial Peptides and Supported Lipid Bilayers. *BBA-Biomembranes* **2006,** *1758*, 1257-1273.
(37) Chen, X.; Tang, H. Z.; Even, M. A.; Wang, J.; Tew, G. N.; Chen, Z., Observing a Molecular Knife at Work. *J. Am. Chem. Soc.* **2006,** *128*, 2711-2714.
(38) Chen, X.; Boughton, A. P.; Tesmer, J. J. G.; Chen, Z., In Situ Investigation of Heterotrimeric G Protein Beta Gamma Subunit Binding and Orientation on Membrane Bilayers. *J. Am. Chem. Soc.* **2007,** *129*, 12658-12659.

(39) Ye, S. J.; Nguyen, K. T.; Le Clair, S. V.; Chen, Z., In Situ Molecular Level Studies on Membrane Related Peptides and Proteins in Real Time Using Sum Frequency Generation Vibrational Spectroscopy. *J. Struct. Biol.* **2009,** *168*, 61-77.
(40) Nguyen, K. T.; King, J. T.; Chen, Z., Orientation Determination of Interfacial Beta-Sheet Structures in Situ. *J. Phys. Chem. B* **2010,** *114*, 8291-8300.
(41) Boughton, A. P.; Yang, P.; Tesmer, V. M.; Ding, B.; Tesmer, J. J. G.; Chen, Z., Heterotrimeric G Protein Beta(1)Gamma(2) Subunits Change Orientation Upon Complex Formation with G Protein-Coupled Receptor Kinase 2 (Grk2) on a Model Membrane. *Proc. Natl. Acad. Sci. USA* **2011,** *108*, E667-E673.
(42) Liu, Y.; Jasensky, J.; Chen, Z., Molecular Interactions of Proteins and Peptides at Interfaces Studied by Sum Frequency Generation Vibrational Spectroscopy. *Langmuir* **2012,** *28*, 2113-2121.
(43) Baugh, L.; Weidner, T.; Baio, J. E.; Nguyen, P.-C. T.; Gamble, L. J.; Stayton, P. S.; Castner, D. G., Probing the Orientation of Surface-Immobilized Protein G B1 Using Tof-Sims, Sum Frequency Generation, and NEXAFS Spectroscopy. *Langmuir* **2010,** *26*, 16434-16441.
(44) Fu, L.; Ma, G.; Yan, E. C. Y., In Situ Misfolding of Human Islet Amyloid Polypeptide at Interfaces Probed by Vibrational Sum Frequency Generation. *J. Am. Chem. Soc.* **2010,** *132*, 5405-5412.
(45) Fu, L.; Liu, J.; Yan, E. C. Y., Chiral Sum Frequency Generation Spectroscopy for Characterizing Protein Secondary Structures at Interfaces. *J. Am. Chem. Soc.* **2011,** *133*, 8094-8097.
(46) Chen, X.; Sagle, L. B.; Cremer, P. S., Urea Orientation at Protein Surfaces. *J. Am. Chem. Soc.* **2007,** *129*, 15104-15105.
(47) Kim, J.; Cremer, P. S., Elucidating Changes in Interfacial Water Structure Upon Protein Adsorption. *ChemPhysChem* **2001,** *2*, 543-+.
(48) Kim, J.; Somorjai, G. A., Molecular Packing of Lysozyme, Fibrinogen, and Bovine Serum Albumin on Hydrophilic and Hydrophobic Surfaces Studied by Infrared-Visible Sum Frequency Generation and Fluorescence Microscopy. *J. Am. Chem. Soc.* **2003,** *125*, 3150-3158.
(49) Weidner, T.; Breen, N. F.; Li, K.; Drobny, G. P.; Castner, D. G., Sum Frequency Generation and Solid-State NMR Study of the Structure, Orientation, and Dynamics of Polystyrene-Adsorbed Peptides. *Proc. Natl. Acad. Sci. USA* **2010,** *107*, 13288-13293.
(50) Baio, J. E.; Weidner, T.; Baugh, L.; Gamble, L. J.; Stayton, P. S.; Castner, D. G., Probing the Orientation of Electrostatically Immobilized Protein G B1 by Time-of-Flight Secondary Ion Spectrometry, Sum Frequency Generation, and near-Edge X-Ray Adsorption Fine Structure Spectroscopy. *Langmuir* **2012,** *28*, 2107-2112.
(51) Tatulian, S. A.; Jones, L. R.; Reddy, L. G.; Stokes, D. L.; Tamm, L. K., Secondary Structure and Orientation of Phospholamban Reconstituted in Supported Bilayers from Polarized Attenuated Total-Reflection FTIR Spectroscopy. *Biochemistry* **1995,** *34*, 4448-4456.
(52) Cerf, E.; Sarroukh, R.; Tamamizu-Kato, S.; Breydo, L.; Derclaye, S.; Dufrêne, Y. F.; Narayanaswami, V.; Goormaghtigh, E.; Ruysschaert, J. M.; Raussens, V., Antiparallel B-Sheet: A Signature Structure of the Oligomeric Amyloid B-Peptide. *Biochem. J* **2009,** *421*, 415-423.
(53) Ye, S. J.; Li, H.; Wei, F.; Jasensky, J.; Boughton, A. P.; Yang, P.; Chen, Z., Observing a Model Ion Channel Gating Action in Model Cell Membranes in Real Time in Situ: Membrane Potential Change Induced Alamethicin Orientation Change. *J. Am. Chem. Soc.* **2012,** *134*, 6237-6243.
(54) Barlow, D. E.; Wahl, K. J., Optical Spectroscopy of Marine Bioadhesive Interfaces. *Annu. Rev. Anal. Chem.* **2012,** *5*, 229-251.

(55) Wang, J.; Paszti, Z.; Clarke, M. L.; Chen, X.; Chen, Z., Deduction of Structural Information of Interfacial Proteins by Combined Vibrational Spectroscopic Methods. *J. Phys. Chem. B* **2007,** *111*, 6088-6095.
(56) Yang, P.; Boughton, A.; Homan, K.; Tesmer, J.; Chen, Z., Membrane Orientation of Gαiβ1γ2 and Gβ1γ2 Determined Via Combined Vibrational Spectroscopic Studies. *J. Am. Chem. Soc.* **2013,** *135*, 5044-5051.
(57) Ding, B.; Chen, Z., Molecular Interactions between Cell Penetrating Peptide Pep-1 and Model Cell Membranes. *J. Phys. Chem. B* **2012,** *116*, 2545-2552.
(58) Wiesmann, C.; Hengstenberg, W.; Schulz, G. E., Crystal Structures and Mechanism of 6-Phospho-Beta-Galactosidase from Lactococcus Lactis. *J. Mol. Biol.* **1997,** *269*, 851-860.
(59) Chaki, N. K.; Vijayamohanan, K., Self-Assembled Monolayers as a Tunable Platform for Biosensor Applications. *Biosens. Bioelectron.* **2002,** *17*, 1-12.
(60) Houseman, B. T.; Gawalt, E. S.; Mrksich, M., Maleimide-Functionalized Self-Assembled Monolayers for the Preparation of Peptide and Carbohydrate Biochips. *Langmuir* **2003,** *19*, 1522-1531.
(61) Uzarski, J. R.; Mello, C. M., Detection and Classification of Related Lipopolysaccharides Via a Small Array of Immobilized Antimicrobial Peptides. *Anal. Chem.* **2012,** *84*, 7359-7366.
(62) Chen, X.; Wang, J.; Boughton, A. P.; Kristalyn, C. B.; Chen, Z., Multiple Orientation of Melittin inside a Single Lipid Bilayer Determined by Combined Vibrational Spectroscopic Studies. *J. Am. Chem. Soc.* **2007,** *129*, 1420-1427.
(63) Nguyen, K. T.; Le Clair, S. V.; Ye, S. J.; Chen, Z., Molecular Interactions between Magainin 2 and Model Membranes in Situ. *J. Phys. Chem. B* **2009,** *113*, 12358-12363.
(64) Nguyen, K. T.; Le Clair, S. V.; Ye, S. J.; Chen, Z., Orientation Determination of Protein Helical Secondary Structures Using Linear and Nonlinear Vibrational Spectroscopy. *J. Phys. Chem. B* **2009,** *113*, 12169-12180.
(65) Yang, P.; Ramamoorthy, A.; Chen, Z., Membrane Orientation of MSI-78 Measured by Sum Frequency Generation Vibrational Spectroscopy. *Langmuir* **2011,** *27*, 7760-7767.
(66) Bayramoglu, G.; Tunali, Y.; Arica, M. Y., Immobilization of Beta-Galactosidase onto Magnetic Poly(Gma-MMA) Beads for Hydrolysis of Lactose in Bed Reactor. *Catal. Commun.* **2007,** *8*, 1094-1101.
(67) Eldin, M. S. M.; Elaassar, M. R.; Elzatahry, A. A.; Al-Sabah, M. M. B.; Hassan, E. A., Covalent Immobilization of Beta-Galactosidase onto Amino-Functionalized PVC Microspheres. *J. Appl. Polym. Sci.* **2012,** *125*, 1724-1735.
(68) Elnashar, M. M. M.; Yassin, M. A., Covalent Immobilization of Beta-Galactosidase on Carrageenan Coated with Chitosan. *J. Appl. Polym. Sci.* **2009,** *114*, 17-24.
(69) Lopez-Gallego, F.; Betancor, L.; Hidalgo, A.; Alonso, N.; Fernandez-Lorente, G.; Guisan, J. M.; Fernandez-Lafuente, R., Preparation of a Robust Biocatalyst of D-Amino Acid Oxidase on Sepabeads Supports Using the Glutaraldehyde Crosslinking Method. *Enzyme Microb. Technol.* **2005,** *37*, 750-756.
(70) Lopez-Gallego, F.; Betancor, L.; Mateo, C.; Hidalgo, A.; Alonso-Morales, N.; Dellamora-Ortiz, G.; Guisan, J. M.; Fernandez-Lafuente, R., Enzyme Stabilization by Glutaraldehyde Crosslinking of Adsorbed Proteins on Aminated Supports. *J. Biotechnol.* **2005,** *119*, 70-75.
(71) Grosova, Z.; Rosenberg, M.; Rebros, M.; Sipocz, M.; Sedlackova, B., Entrapment of Beta-Galactosidase in Polyvinylalcohol Hydrogel. *Biotechnol. Lett.* **2008,** *30*, 763-767.
(72) Taqieddin, E.; Amiji, M., Enzyme Immobilization in Novel Alginate-Chitosan Core-Shell Microcapsules. *Biomaterials* **2004,** *25*, 1937-1945.

(73) Herrwerth, S.; Eck, W.; Reinhardt, S.; Grunze, M., Factors That Determine the Protein Resistance of Oligoether Self-Assembled Monolayers - Internal Hydrophilicity, Terminal Hydrophilicity, and Lateral Packing Density. *J. Am. Chem. Soc.* **2003,** *125*, 9359-9366.
(74) Hoffmann, C.; Tovar, G. E. M., Mixed Self-Assembled Monolayers (Sams) Consisting of Methoxy-Tri(Ethylene Glycol)-Terminated and Alkyl-Terminated Dimethylchlorosilanes Control the Non-Specific Adsorption of Proteins at Oxidic Surfaces. *J. Colloid Interface Sci.* **2006,** *295*, 427-435.
(75) Zheng, J.; Li, L. Y.; Chen, S. F.; Jiang, S. Y., Molecular Simulation Study of Water Interactions with Oligo (Ethylene Glycol)-Terminated Alkanethiol Self-Assembled Monolayers. *Langmuir* **2004,** *20*, 8931-8938.
(76) Li, L. Y.; Chen, S. F.; Zheng, J.; Ratner, B. D.; Jiang, S. Y., Protein Adsorption on Oligo(Ethylene Glycol)-Terminated Alkanethiolate Self-Assembled Monolayers: The Molecular Basis for Nonfouling Behavior. *J. Phys. Chem. B* **2005,** *109*, 2934-2941.
(77) Stein, M. J.; Weidner, T.; McCrea, K.; Castner, D. G.; Ratner, B. D., Hydration of Sulphobetaine and Tetra(Ethylene Glycol)-Terminated Self-Assembled Monolayers Studied by Sum Frequency Generation Vibrational Spectroscopy. *J. Phys. Chem. B* **2009,** *113*, 11550-11556.
(78) Meadows, P. Y.; Walker, G. C., Force Microscopy Studies of Fibronectin Adsorption and Subsequent Cellular Adhesion to Substrates with Well-Defined Surface Chemistries. *Langmuir* **2005,** *21*, 4096-4107.

CHAPTER 5

CONCLUSIONS AND OUTLOOK

Bioactive materials have found a multitude of applications in fields ranging from antibiofouling coatings, tissue engineering to biosensing devices. The increasing demand of different bioactive materials has imposed great need for materials with improved functions, better sensitivity, enhanced stability, and longer life times. However, the working mechanisms of these materials remain unclear, making the rational design and development of these materials truly difficult. By investigating on the structural and orientation perspectives of bioactive components in these materials in biologically relevant environments, this dissertation seeks to offer understanding on the correlations between interfacial molecular structures of these bioactive materials and their functionalities, which can be used optimize the design strategies for improved materials.

Current research using various surface analytical techniques such as SPR, SIMS, XPS, ATR-FTIR and SERS, has provided some important knowledge about the surface structures of different bioactive materials. However, none of the above-mentioned techniques can provide detailed, molecular-level information about interfaces involving these materials *in situ*, limiting their applicability to answer many critical questions. In the research presented in this dissertation, the nonlinear optical technique SFG has been used to study three different biomaterial systems, intending to elucidate structure-function relationships of various bioactive components involved in the materials. These SFG studies have provided detailed, molecular-level information of urface and interfacial

structures of these biomaterials, which can be used to correlate to the activities or properties measured for these materials to comprehend their working. The work presented in this dissertation attempts to extend the knowledge obtained from prior studies accomplished in our group by adding variations to previous systems, generalizing conclusions, optimizing platforms and developing methodologies for complex systems. Altogether, this dissertation illustrates that SFG is a powerful technique for analyzing surface and interfacial structure of bioactive materials, enabling elucidation of structure-function correlation and aiding in the design and optimization of advanced materials.

Three bioactive material systems were investigated using SFG as the main analytical technique. In Chapter 2, PDMS with incorporation of QAS biocide moieties which impart additional anti-biofouling properties to PDMS-based FR coatings was examined. The molecular surface structures of two different types of QAS-incorporated PDMS systems were investigated in different chemical environments using SFG. Specifically, a series of PDMS coatings containing either a QAS with a single ammonium salt group per molecule or quaternary ammonium-functionalized polyhedral oligomeric silsesquioxane (Q-POSS) were measured with SFG in air, water, and artificial sea water (ASW) to investigate the relationships between the interfacial surface structures of these materials and their antifouling properties. Although previous studies have shown that the above-mentioned materials are promising contact-active antifouling coatings, slight variations of the QAS structure can lead to substantial differences in antifouling performance. Indeed, the SFG results presented here indicated that the surface structures of these materials depend on several factors, such as the extent of quaternization, the molecular weight of the PDMS component, and the functional groups of the QAS used for incorporation into

the PDMS matrix. It was concluded that in aqueous environments, a lower extent of POSS quaternization and the use of ethoxy (instead of methoxy) functional groups for QAS incorporating facilitated the extension of the alkyl chains away from the nitrogen atom of the QAS on the surface. The SFG results correlated well to the antifouling activity studies which indicated that the coatings that exhibit a lower concentration of longer alkyl chains protruding out from the surface can neutralize microorganisms more effectively, ultimately leading to better antifouling performance. Furthermore, the results of this study provide additional evidence that incorporated QAS exert their antimicrobial activity through a two-step interaction. The first step is the adsorption of the bacteria on the surface due to the electrostatic attraction between the negatively charged microorganisms and the positively charged QAS nitrogen atoms on the surface. The second step is the disruption of the cell membranes by the penetration of the long, extended alkyl chains of QAS. This study also demonstrates that the best activity comes from the surface with long alkyl chains of QAS protruding out, which can be used as a design rule for PDMS-QAS coatings in the future.

Chapter 3 focused on surface immobilization of peptide molecules. Peptide-immobilized surfaces are important in many applications such as biosensors, implant devices and nanofabrication. To control the functions and activities of immobilized peptides, it is crucial to investigate the structures of these peptides. In this study, SFG was applied to the investigation of peptide immobilization on a maleimide-functionalized polymer PS-MA surface as a function of time and peptide conformation. Cecropin A (1-8)-melittin (1-18) hybrid and sheep myeloid antimicrobial peptide (SMAP) were used as models to understand the time dependent immobilization behavior *in situ* and in real time

to generalize the understanding of peptide immobilization onto PS-MA surface. Peptide concentration and solvent hydrophobicity were varied to study the response of the immobilized peptides. The orientation of immobilized peptides on PS-MA surface was determined using polarized SFG spectra. It has been found that the peptide solution concentration and solvent composition both influence the immobilization process and the final orientation of the immobilized peptides. To improve the functionality and durability of the maleimide solid platform, a Mal-EG4 SAM was constructed and finally, a maleimide functionalized CVD polymer surface was created for peptide immobilization. Model peptide CP1 was immobilized through either N- or C-terminus to examine the effect of the attachment point on the conformation and orientation of immobilized peptide. It was concluded that both the tethering position and the interaction between AMPs and surfaces greatly alter the activity of the immobilized AMPs. Moreover, the AMP sequence/structure with inherently rigidity proposed by MD simulations was immobilized onto the CVD surface and the rigidity was confirmed by SFG studies. This research indicates that using SFG experimental results and MD simulation prediction, we can design peptides with optimized sequences to minimize surface-peptide interactions to ensure that the immobilized peptides adopt desired structure and the highest activity.

Chapter 4 further studied surface immobilization, but on enzyme molecules. Surface enzyme-immobilized materials are widely used in many applications including biosensors, antifouling coatings, food packaging materials and biofuel cells. Enzymes tend to lose their activity when in contact with a support surface, a phenomenon that has been attributed to unfavorable orientation and (partial) unfolding. In this work, cysteinyl residues were intentionally introduced to a desired site of the enzyme and specific

immobilization of β-Gal through the unique cysteinyl residue was achieved on Mal-EG4 SAM. A systematic means to characterize interfacial orientation of immobilized enzymes was developed using combined studies with SFG and ATR-FTIR. The possible orientations of the immobilized β-Gal through different cysteinyl locations were determined, which were well correlated to the tested activity of β-Gal. The placement of the cysteinyl residues unveiled the effect of secondary structure as well as the location of the attachment on the conformation and orientation of the immobilized β-Gal. It was shown that activity and stability of enzyme-immobilized materials highly depends on the structure and orientation of the enzyme molecules after immobilization. This research successfully developed systematic methodology to control the orientation of surface immobilized enzymes by enzyme engineering to maximize the activity.

In summary, experimental platforms and theoretical calculation methodologies have been developed to study surface/interfacial structures of various bioactive materials *in situ* for three different systems including marine antifouling materials, antimicrobial materials and biosensing materials. These studies have revealed that structural differences are directly related to the difference in the biofunctionality of the materials. Based on the structure-function relationships found strategies for optimizing the performance of different bioactive materials have also been proposed. This dissertation demonstrates that SFG, an intrinsically surface/interface sensitive technique, is a powerful and unique tool to help understand the interfacial interaction mechanisms of bioactive materials. The components of the materials, the composition of the contacting media, and the construct of the biomolecules incorporated can all be varied in order to optimize biological

molecule-surface interaction. In this work, the biofunctionality tests of all the materials were performed separately from SFG experiments.

In the future, various optical spectroscopy/microscopy can be employed and incorporated with SFG spectroscopy in order to test the biofunctionality of these materials simultaneously (e.g., using fluorescence) while the SFG experiments are being conducted. This way, any deviations resulting from different experimental conditions or sample geometries will be eliminated. In addition, the methodology developed in this dissertation can be further employed to investigate on bioactive components of various applications such as nitroreductases with environmental, biotechnological and clinical importance, and dehydrogeneses used for biofuel production. Besides this methodology development and application, future studies can be focused on peptides/proteins with different secondary structures. In this dissertation, α-helical structure was mainly studied because it is the predominant secondary structure found in peptides and proteins. However, other secondary structures can play important roles in regulating biological activities. For example, β-sheet structure has found to participate in formation of protein aggregates and fibrils that lead to many human diseases.